# Structural states associated with the power stroke of myosin heads in muscle: a 2D-X-ray diffraction study

Von der Naturwissenschaftlichen Fakultät der

Gottfried Wilhelm Leibniz Universität Hannover

zur Erlangung des Grades

Doktor der Naturwissenschaften

Dr. rer. nat.

genehmigte Dissertation

von

Dipl.-Phys. Ante Radocaj

geboren am 18.05.1962 in Sibenik, Kroatien

**2007**

Referent: Prof. Dr. Walter Müller

Koreferent: Prof. Dr. Bernhard Brenner

Tag der Promotion: 19. Februar 2007

# Table of contents

# Summary

Muscle contraction is driven by the cyclic interaction of myosin heads with actin filaments due to the hydrolysis of ATP. Isometric force is generated by elastic distortion of myosin heads when they change from their states of weak binding to actin to the strongly attached form. During a length release of activated muscle fibers, further structural changes become favored as myosin heads go forward in their working cycle. The power stroke of each myosin head comprises a series of states while the myosin head is strongly bound to actin. The last state of the power stroke is the nucleotide-free, rigor state of the myosin head. After this, the myosin head detaches from actin while binding a new ATP molecule.

In order to explore the structure and function of states occurring later in the power stroke, we applied small ramp-shaped releases to isometrically contracting muscle fibers from rabbit psoas muscle. The accumulation of these later states was monitored by fiber tension recorded during the ramp-shaped releases. Before and during the ramp-shaped releases diffraction patterns from the fibers were recorded using high-brilliance synchrotron radiation at the ESRF in Grenoble and the RAPID detector developed at the SRS in Daresbury. This allowed us to record "snapshots" within very short time frames of 2 to 4 ms. For comparison, diffraction patterns were taken from the same fibers in relaxing as well as in rigor condition. Features that are sensitive to the rigor or rigor-like structure of the myosin head were analyzed in the time-resolved diffraction patterns recorded at the ESRF in Grenoble as well as in static diffraction patterns that were recorded at the SRS in Daresbury from fibers incubated in the presence of different concentrations of MgATPγS. The latter diffraction patterns served as a model for the behavior of features on the diffraction patterns when different proportions of myosin heads are in rigor while the other myosin heads are weakly attached to actin.

Our data show that a redistribution of myosin heads occurs during the ramp-shaped release. States that occur later in the power stroke are thereby populated with a larger number of myosin heads, while the total number of myosin heads stereospecifically attached to actin remains constant. Even though later states were increasingly populated, no accumulation of rigor-like states was detectable. Model calculations show that the intensity distribution along the sixth actin layer line is sensitive to structural changes within the myosin head. We demonstrated that the distinct profile of the sixth actin layer line observed after increasing the population of later states in the power stroke by

application of a ramp-shaped release can not result from changes in a mixture of myosin heads in rigor and in states of weak binding to actin. Our data indicate that myosin heads are accumulated in a state, which has to be substantially different from the rigor-like structure of the myosin head. This state of the myosin head has not been structurally characterized yet. It could correspond to a state before or shortly after the release of inorganic phosphate ($P_i$) from its binding site in the myosin head, as other later states in the power stroke show rigor features in diffraction patterns.

# Zusammenfassung

Muskelkontraktion wird durch die zyklische Interaktion von Myosinköpfen mit Aktinfilamenten als Folge der Hydrolyse von ATP generiert. Isometrische Kraft entsteht durch die elastische Verformung der Myosinköpfe beim Übergang von Zuständen mit schwacher Bindung an Aktin zu stark gebundenen Zuständen. Während einer Verkürzung von aktivierten Muskelfasern werden weitere strukturelle Änderungen bevorzugt während die Myosinköpfe in ihrem Arbeitszyklus voranschreiten. Der Kraftschlag eines jeden Myosinkopfs besteht aus einer Serie von Zuständen, während welcher der Myosinkopf stark an Aktin gebunden ist. Der letzte Zustand des Kraftschlags ist der nukleotidfreie Rigor-Zustand des Myosinkopfs. Danach löst sich der Myosinkopf von Aktin, während er ein neues ATP-Molekül bindet.

Um die Struktur und Funktion von Zuständen zu erforschen, die später im Kraftschlag auftreten, ließen wir kleine, rampenförmige Verkürzungen Muskelfasern aus dem Psoasmuskel des Kaninchens in isometrischer Kontraktion zu. Die Anhäufung von diesen späteren Zuständen wurde über die Spannung der Fasern während der rampenförmigen Verkürzungen verfolgt. Vor und während der rampenförmigen Verkürzungen wurden Beugungsbilder der Fasern mit hochintensiver Synchrotronstrahlung am ESRF Grenoble mittels des am SRS Daresbury entwickelten RAPID-Detektors aufgenommen. Dadurch war es uns möglich "Schnappschüsse" in sehr kurzen Zeitabschnitten von 2 bis 4 ms aufzunehmen. Zum Vergleich wurden Beugungsbilder der gleichen Fasern unter Relaxations- und Rigor-Bedingungen aufgenommen. Merkmale, die für Rigor- oder rigorähnliche Strukturen empfindlich sind, wurden sowohl auf den am ESRF Grenoble aufgenommenen zeitaufgelösten Beugungsbildern als auch auf den am SRS Daresbury aufgenommenen statischen Beugungsbildern von Fasern, die unter verschiedenen Konzentrationen von MgATPγS inkubiert wurden, analysiert. Die letzteren Beugungsbilder dienten als Model für das Verhalten von Merkmalen auf den Beugungsbildern, wenn sich unterschiedlich viele Myosinköpfe im Rigor befinden, während die restlichen Myosinköpfe schwach an Aktin gebunden sind.

Unsere Ergebnisse zeigen, daß es während der rampenförmigen Verkürzung zu einer Umverteilung der Myosinköpfe kommt. Zustände, die später im Kraftschlag auftreten, werden dabei mit einer größeren Anzahl an Myosinköpfen bevölkert, wobei die

Gesamtzahl der stereospezifisch an Aktin gebundenen Myosinköpfe konstant bleibt. Obwohl spätere Zustände stärker bevölkert wurden, konnte keine Anhäufung von rigorähnlichen Zuständen festgestellt werden. Modelrechnungen zeigen, daß die Intensitätsverteilung entlang der sechsten Aktinschichtlinie auf strukturelle Änderungen innerhalb des Myosinkopfs empfindlich ist. Wir zeigten, daß das individuelle Profil der sechsten Aktinschichtlinie, das nach Anhäufung von späteren Zuständen im Kraftschlag mittels rampenförmiger Verkürzung registriert wurde, nicht durch Änderungen in der Mischung von Myosinköpfen im Rigor und in schwach an Aktin gebundenen Zuständen entstehen konnte. Unsere Resultate zeigen auf, daß Myosinköpfe in einem Zustand angehäuft werden, der sich von der rigorähnlichen Struktur des Myosinkopfs wesentlich unterscheiden muß. Dieser Zustand des Myosinkopfs wurde bisher noch nicht strukturell charakterisiert. Er könnte einem Zustand vor oder kurz nach Abgabe von anorganischem Phosphat ($P_i$) von seiner Bindungsstelle am Myosinkopf entsprechen, da andere spätere Zustände im Kraftschlag Rigor-Merkmale auf den Beugungsbildern zeigen.

# Keywords / Stichworte

Muscle contraction, cross-bridge, power stroke

Muskelkontraktion, Querbrücke, Kraftschlag

# List of abbreviations

| | |
|---|---|
| A | actin |
| ADP | adenosine-5'-diphosphate |
| AEBSF | 4-(2aminoethyl)-benzylsulfonyl-fluoride |
| AlF$_4$ | aluminum fluoride |
| ALL1 | first actin layer line |
| ALL5 | fifth actin layer line |
| ALL6 | sixth actin layer line |
| ALL7 | seventh actin layer line |
| AM | actomyosin complex |
| Ap$_5$A | P1, P5-(di-adenosine 5')-pentaphosphate |
| ATP | adenosine-5'-triphosphate |
| ATPase | adenosine-5'-triphosphatase |
| ATPγS | adenosine-5'-O-(3-thiotriphosphate) |
| a.u. | arbitrary units |
| DTT | DL-dithiothreitol |
| E64 | N-(trans-epoxylsuccinyl-L-leucine-4-guanidinobutylamide) |
| EDTA | ethylene diamine-N, N, N', N'-tetra acetic acid |
| EGTA | ethylene glycol-bis(-aminoethylether)-N,N,N',N'-tetra acetic acid |
| EM | electron microscopy |
| ESRF | European Synchrotron Radiation Facility |
| F-actin | filamentous actin (polymer) |
| G-actin | globular actin (monomer) |
| h.s. | half sarcomere |
| $I_{1,1}/I_{1,0}$ | ratio of equatorial 1,1 and 1,0 intensities |
| LMM | light meromyosin |
| M | myosin |
| M3 | third myosin layer line (meridional reflection) |
| MgATP | magnesium-adenosine-5'-triphosphate |
| MgATPγS | magnesium-adenosine-5'-O-(3-thiotriphosphate) |
| MLL1 | first myosin layer line |
| mM | millimolar |

| | |
|---|---|
| $P_i$ | inorganic phosphate |
| pCa | negative decadic logarithm of $Ca^{++}$ ion concentration in molar |
| pH | negative decadic logarithm of $H^+$ ion concentration in molar |
| SAXS | small angle X-ray scattering |
| SRS | Synchrotron Radiation Source |
| U | unit |

# Introduction

Muscle function is part of our life. It defines us as entities moving in the dimensions of space and time. Since the antique times different biophysical models explaining the function of muscle have been developed. But it is not until the 1940s that the proteins that are mainly responsible for the contractile system have been identified (Straub, 1942; Banga and Szent-Gyorgyi, 1942; Szent-Gyorgyi, 1944). It was then established that it is the interaction of the macromolecular proteins actin and myosin that generates force and contraction in muscle. The exact course of this interaction is still a vivid topic of research.

To prepare the ground for further explanations about the known muscle function, let me first present an overview of the microscopic structure of muscle. As shown in figure 1 a whole muscle is structurally divided into bundles of muscle fibers, which in turn consist of myofibrils arranged in parallel. In skeletal and heart muscle a striation is visible by light microscopy and was described using the terms A-bands, I-bands, Z-lines, H-zones, as shown in the figure. In microscopy with polarized light the region of the A-bands appears as anisotropic structures and the region of the I-bands as isotropic structures. The term Z-line comes from the German "Zwischenscheibe". The section of the myofibril ranging from one Z-line to the next is called a sarcomere. It forms the structural and functional unit of the muscle. Its length is about 2.4 μm in resting muscle. Finer structures within the sarcomere cannot be resolved by normal light microscopy. Suitable methods for higher resolution are, for example, electron microscopy, X-ray diffraction and neutron diffraction, as they provide shorter wavelengths than visible light.
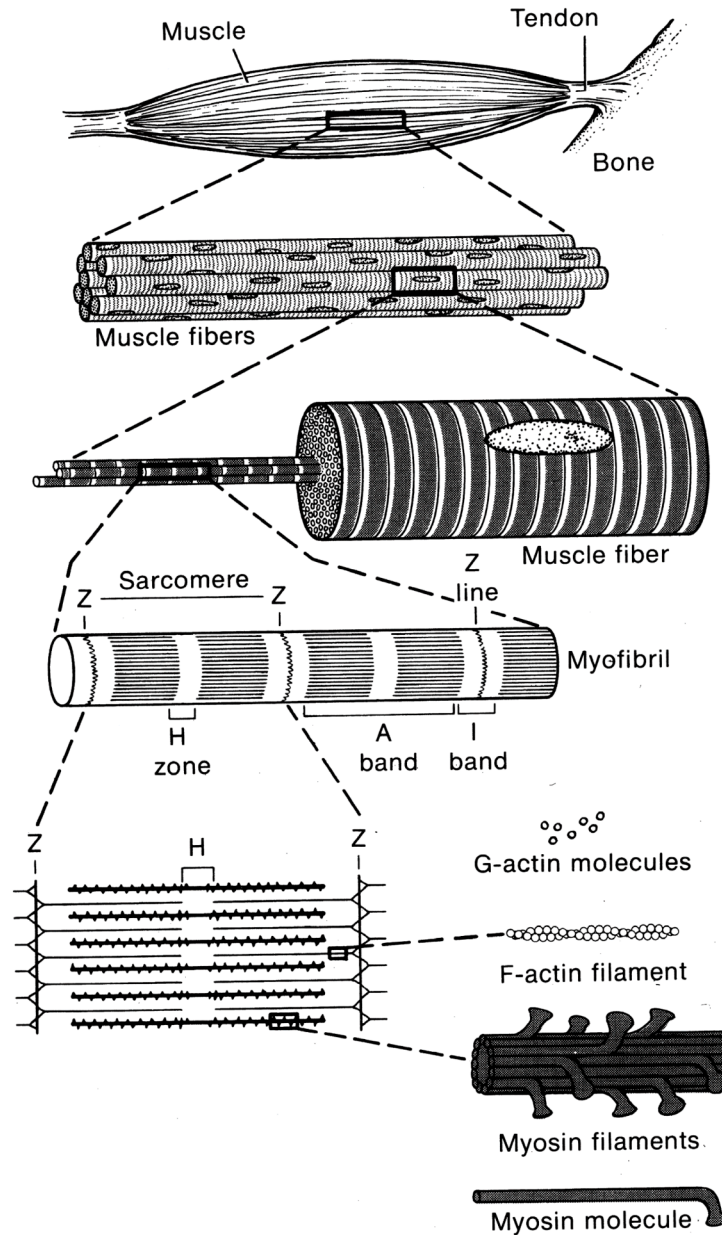
*Fig. 1: Structural elements of muscle showing the organization from the macroscopic to the microscopic and molecular structures. From Bloom and Fawcett, 1968. The structure of the actin and myosin filaments has been better resolved recently, but the shown scheme remains generally correct.*

## *The sliding filament model of muscle contraction*

Early X-ray diffraction studies (Huxley, 1953b; Hanson and Huxley, 1953) indicated that within the sarcomere the contractile proteins actin and myosin are organized in the form of interdigitating thin and thick filaments. The thick filaments (myosin filaments)

are located at hexagonal lattice positions within the A-band and the thin filaments (actin filaments) are at the trigonal lattice points between the thick filaments. For a schematic cross-section see figure 10, which is discussed later in a different context. As no change in the axial periodicities of diffraction images has been observed when the muscle was lengthened, it was concluded that the lengths of the filaments do not change during contraction. Muscle contraction must therefore be accomplished by sliding of the thin and thick filaments past each other (Huxley and Niedergerke, 1954; Huxley and Hanson, 1954), and the sliding force must be produced in the overlap zone of the two types of filaments. It was proposed that molecular structures (cross-bridges) connecting the two types of filaments have to change their conformation to enable sliding and force production (Huxley and Niedergerke, 1954). By electron microscopy it was confirmed that such cross-bridges actually consist of myosin heads protruding from the thick filaments (Huxley, 1953a; Huxley, 1957).

The thick filaments are located in the middle of the sarcomere, forming the A-band, and are constituted of myosin molecules arranged with their rod-like part in the backbone of the filament, while the other ends (the heads of the myosin molecules) protrude out of the filament. The myosin molecules in each thick filament are arranged in opposite directions in the two halves of the filament, making the thick filament bipolar. The thin filaments are tethered at intermittent positions to the Z-line. The longitudinal structure of the sarcomere and the sliding of the filaments are illustrated in figure 2.

Biochemical studies have revealed that the thin filaments consist not only of filamentous strands (F-actin) formed from globular actin monomers (G-actin), but thin filaments also contain regulatory proteins. These are the proteins Troponin and Tropomyosin and serve, as the term regulatory proteins implies, for the regulation of the contractile function of the muscle.
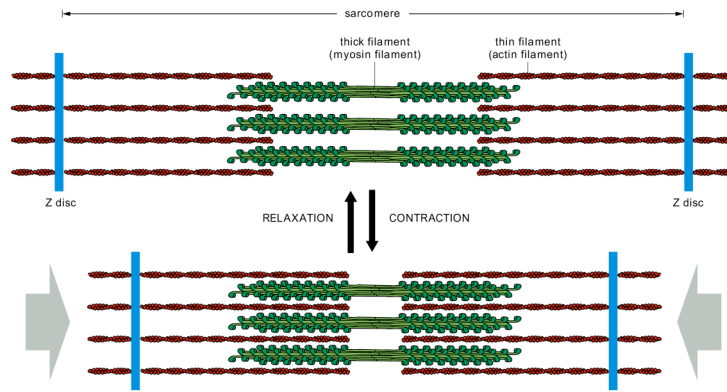
*Fig. 2: The sarcomere. Contraction and relaxation of the muscle is realized by the sliding of the interdigitating thick and thin filaments past each other. The lengths of the filaments remain essentially the same during both processes. From Alberts et al., 2002.*

## *Transitions between different structural states of the cross-bridge*

As it is clear that the contractile force has to be produced within the overlap zone of the thick and thin filaments, structural changes of the cross-bridges have to be responsible for force development. Length change experiments (Huxley and Simmons, 1971) led to the proposal that the structural change of the cross-bridge is composed of multiple steps responsible for maintaining force and for shortening of the sarcomere. The quick tension recovery after a sudden step-wise shortening of the muscle fiber (see figure 3) was interpreted as the signature of the structural changes responsible for force generation during muscle contraction. In this concept, isometric force is maintained by elastic distortion of the cross-bridge, while during shortening the elastically stored free energy is converted into sliding movement. According to this model perception, the cross-bridge has to be able to achieve different structural conformations, with several of these states being capable of bearing force. Since cross-bridges act asynchronously, the whole population of cross-bridges in a muscle fiber is distributed between the different force-bearing and non-force-bearing structural states. An individual cross-bridge passes dynamically through its cycle of different states. A synchronized transition of a large number of cross-bridges into different structural states can be achieved by mechanical maneuvers applied to the muscle fiber, as, for example, in the step-wise length change experiments performed by A. F. Huxley and Simmons.
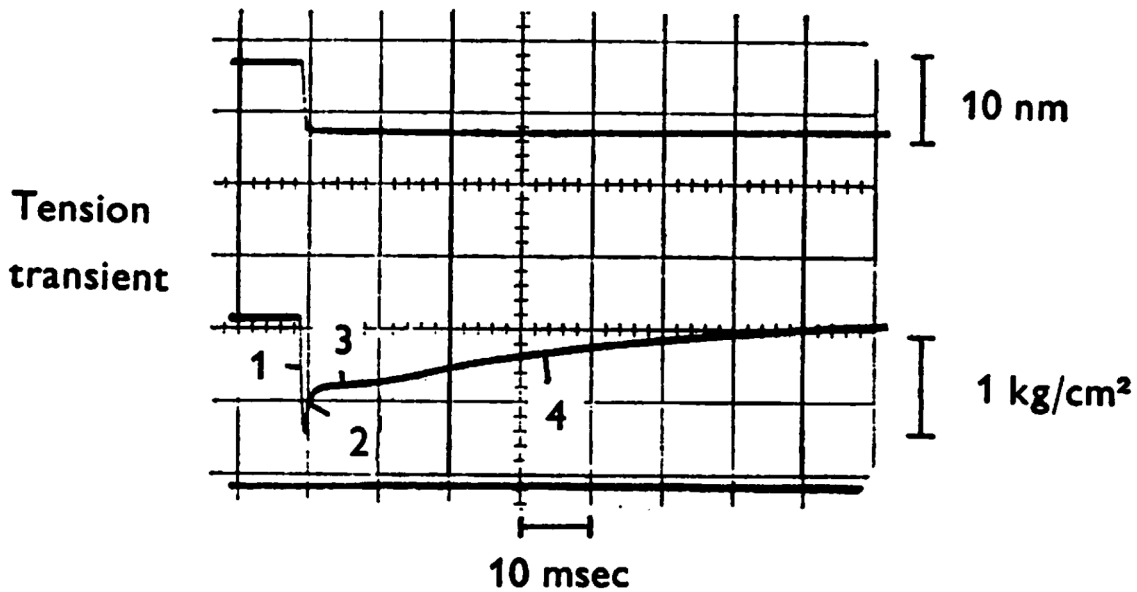
*Fig. 3: The figure shows a recording of the tension transient upon a step-wise shortening of isolated frog muscle fibers during tetanic stimulation. The upper trace is the time course of the lengths of the muscle fibers. The numbers attached to the middle trace indicate parts of the tension trace corresponding to Huxley-Simmons-phases 1 to 4, whereby phase 2 is the rapid early tension recovery interpreted as the transition to subsequent conformational states (conformations 2 and 3 in figure 4), whereas phases 3 and 4 are accounted for by detachment and re-attachment of cross-bridges. The bottom trace is the tension base line. From Huxley, 1974.*

The mechanical model proposed by A. F. Huxley and Simmons (1971) describes two or more conformations of the cross-bridge as shown in figure 4. In each subsequent conformation the myosin head has a stronger binding to actin than in the previous one and the elastic component of the cross-bridge is more stretched. This elastic deformation accounts for the force maintained in the cross-bridge. Force is accordingly built up on transition from conformation 1 to subsequent conformations. A. F. Huxley and Simmons (1971) interpreted this transition as the mechanism underlying the early tension recovery (phase 2 in figure 3) and also responsible for generating and maintaining force during isometric contraction. That means that isometric force in a muscle fiber would be maintained by a certain percentage of cross-bridges that already made the transition into conformation 2 or subsequent conformations.
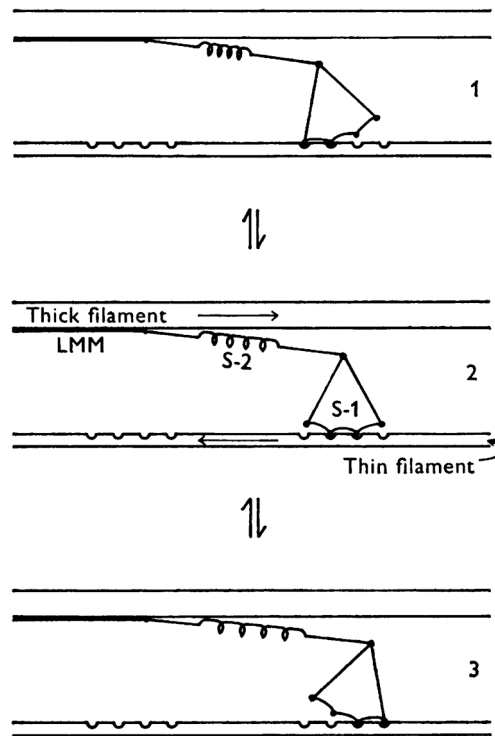
*Fig. 4: Mechanical model proposed by A. F. Huxley and Simmons (1971) describing the mechanism of force development capable of explaining the tension transients obtained in response to step-wise shortening of activated muscle fibers. From Huxley, 1974.*

Brenner, 1991, and Brenner et al., 1995, found that the above described concept of A. F. Huxley and Simmons cannot be correct. If during isometric steady-state contraction a proportion of cross-bridges would be in conformation 2 or subsequent conformations, a step-wise stretch should produce a tension trace similar to the one in figure 3 but flipped upside-down. This, however, was not recorded. By applying small ramp-shaped releases to isometrically contracting muscle fibers, Brenner, 1991, was able to differentiate the transition between different conformations from other effects, such as attachment and detachment of cross-bridges. Even though, an inversion of the tension transients recorded during a release could not be achieved during a stretch of isometrically contracting fibers. From this Brenner et al., 1995, concluded that force generation does not occur only in conformation 2 or subsequent conformations. Instead, isometric force obviously is already generated by conformation 1.

## *ATP-hydrolysis and the cross-bridge cycle*

When the muscle contracts, mechanical work is exerted. Chemical energy is converted into mechanical work. From early viscosity studies of extracted myosin and actin (Banga and Szent-Gyorgyi, 1942; Szent-Gyorgyi, 1942) and birefringence studies (Needham et al., 1942) it was concluded that ATP is the energy source of muscle contraction. It was established that myosin has ATPase activity when it is combined with actin to form actomyosin, and that ATP induces shortening of actomyosin threads. The conformational changes of the cross-bridges, which drive muscle contraction, are therefore coupled to the ATPase activity of the myosin head domain, and lead to the conversion of ATP to ADP and inorganic phosphate ($P_i$). For a single cross-bridge going through one cycle of conformational changes, one ATP molecule is hydrolyzed. A simple scheme of the cycle coupling the biochemical with the conformational states of the cross-bridge has been developed by Lymn and Taylor, 1971 (see Fig. 5). The cycle consists of four basic steps. The cross-bridge is formed by the myosin head, which is attached to actin when neither ATP, nor ADP or phosphate is bound to myosin. This is the AM state, panel 1 in the figure. With the binding of ATP the myosin head detaches from actin (M.ATP state, panel 2). In the next step, ATP is hydrolyzed but the hydrolysis products are not yet released from the active site of the myosin head (M.ADP.$P_i$ state, panel 3), the myosin head, however, becomes "cocked" to a position that primes it for attachment to actin. At the transition to state 4 the head attaches again to actin (AM.ADP.$P_i$ state). While in the next step the hydrolysis products $P_i$ and ADP are released, forming the AM state (the rigor state - panel 1) the myosin undergoes a conformational change by which the attached myosin head becomes strained. This last transition is called the power stroke or working stroke. If the filaments are allowed to slide past each other, the strain generated by the power stroke can be released and leads to shortening of the muscle. If the filaments are held at a fixed position (isometric contraction), the strain is maintained and is observed as active force.
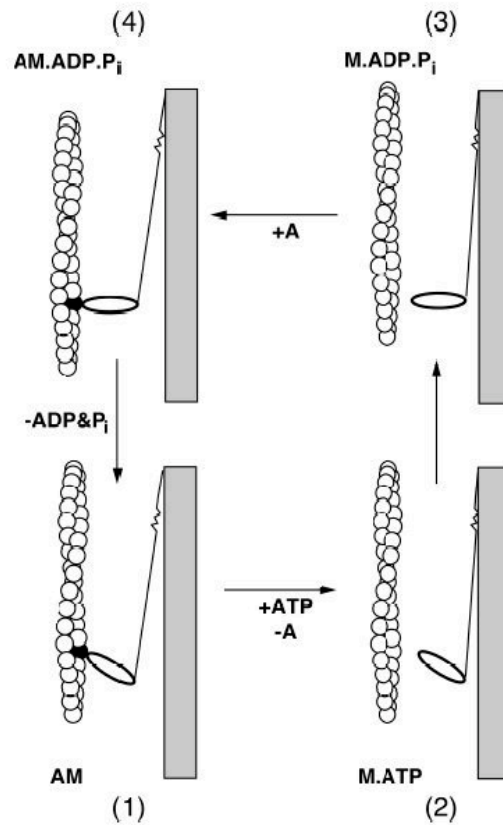
*Fig. 5: The Lymn-Taylor-Cycle. The gray bar stands for the backbone of the myosin filament. The actin filament is depicted as the helix on the left side and the cross-bridge, in this model, consists of the oval head and the rod-like tail. From Geeves and Holmes, 1999.*

This simple scheme depicts the basic mechanism of force production in a single cross-bridge. This concept is still valid, although some significant modifications were integrated which will be described in a later section of the introduction. Our main point of interest, though, are the conformational changes occurring during the power stroke, i.e. during the transition between state 4 and state 1 in the Lymn-Taylor scheme (Fig. 5). As we will see, this transition, however, is quite more complex than assumed in the Lymn-Taylor scheme.

## *Suitable methods to elucidate conformational changes of the cross-bridge*

As we are not able to directly see and feel the interactions between the proteins in muscle, we have to employ different methods of measurement to gain deeper

understanding of the structures, structural changes and molecular mechanisms. A number of different methods are applicable in order to study the structure and function of the cross-bridge. Each of these methods has its specific advantages and disadvantages. Thus, a combined application of different approaches seems to be most promising.

The two general methods of imaging and non-imaging techniques have to be distinguished. The reason why we cannot see molecular structures with light microscopy is that the resolution of microscopes is limited by their aperture and the wavelength of the applied light. Even if the magnification is increased, after a certain point the image remains blurred and finer structures cannot be resolved further. This limitation is governed by the rules of optics. A point source is actually projected as an airy disc due to diffraction of the circular aperture of the microscope. The images of two points cannot be distinguished any more when the intensity maximum of one airy disc coincides with the first intensity minimum of the other. The smallest resolvable distance (r) between two points is described by the Rayleigh criterion:

$$r = 0.61 \, \lambda \, / \, NA$$

where $\lambda$ is the wavelength of the light and NA is the numerical aperture:

$$NA = n \sin \theta$$

where n is the refractive index of the immersion medium and $\theta$ is the half-angle of the maximum cone of light that can enter or exit the objective lens.

As the wavelength for visible light is from about 400 to 700 nm and the numerical aperture may achieve values up to 1.4, the theoretical best resolution for visible light is therefore about 200 nm, which is not sufficient to resolve changes in the cross-bridge structure during muscle contraction that are expected to be in the range of a few nanometers.

**Mechanical experiments**

Mechanical experiments generally allow measurements of force-length relationships or the time course of force and/or length after sudden changes in length or load of single muscle fibers, myofibrils, fiber assemblies or whole muscle. Environmental conditions of the investigated samples can be influenced by the chemical composition and temperature of the solution the sample is immersed in. Conclusions concerning the underlying molecular structures and their mechanical properties are made from

measured force or stiffness values. The mechanics of the cross-bridge action can be "sensed" by mechanical experiments, although it cannot be seen directly.

From force transients after step-wise shortening and lengthening of activated muscle fibers Huxley and Simmons (1971) concluded that the cross-bridge changes between at least two conformational states while it is attached to the actin filament. The complete ensemble of attached cross-bridges is distributed between these different states. The population of the different states is governed by the rate constants pertaining to the transitions between the different conformational states. The rate constants between attached states of the cross-bridge are dependent on the strain of the cross-bridge (Hill, 1974). Thus, when an attached cross-bridge that has not yet completed the power stroke is strained in the direction of the power stroke, the likelihood of transiting into later states of the power stroke by changing its conformation appropriately increases. The adequate opposite is valid, of course, in the other direction, when the cross-bridge is strained in the direction opposing its movement during the power stroke.

Thus, by adequate mechanical maneuvers the rate constants between the different states of the cross-bridge can be changed and a coordinated action of cross-bridges can be provoked, whereby various conformational states are populated or depopulated. During a short release of an activated fiber, the thick and thin filaments slide past each other and exert strain on the attached cross-bridges, changing the rate constants of the transitions between various conformational states of the power stroke and favoring later states of the power stroke.

As we are interested in the mechanism of the power stroke, this coordinated transition is worthwhile to be investigated. Instead of applying Huxley-Simmons type rapid shortening steps (Huxley and Simmons, 1971), an accumulation of late states in the power stroke can also be accomplished by a ramp shaped release, a shortening maneuver with constant speed, corresponding to a series of infinitesimal shortening steps (Kuhn et al., 1979; Ford et al., 1977; Brenner, 1991; Brenner et al., 1995). To gain a comprehensive understanding of the investigated mechanisms, it is opportune to combine mechanical experiments with imaging techniques. Three imaging techniques will be discussed in the following section.

**Protein X-ray-crystallography**

The mechanical and chemical function of a protein is strongly influenced by the particular folding of the protein. The three-dimensional structure can be investigated by

crystallographic means. The macromolecules, though, have to be in an appropriate shape to be able to agglomerate to crystals. Therefore, the method is not applicable to every macromolecule.

As explained before, light (electromagnetic waves) of a wavelength much shorter than that of the visible light has to be employed to resolve structures on the molecular level. Coherent X-ray radiation is applicable for this purpose. For a suitable compromise between resolution and absorption, a wavelength of 1.54 Å was usually used in laboratory sources (Cu Kα line). The applied radiation is mostly produced in X-ray tubes with cooled rotating anodes, necessary because of the high electron flux impacting the anode. Wavelength selectivity is achieved by the characteristic emission of the anode material (e.g. copper - Cu Kα line).

Diffraction images produced by Bragg reflections of an X-ray beam directed at the crystalline sample are used for resolving the structure. But, for being able to calculate the structure from the diffraction image, the phase problem has to be solved. The recorded diffraction patterns only contain the intensity information of the reflected light but not the phase information. Therefore, the structure of the diffracting matter cannot be calculated straightforwardly by Fourier synthesis.

The phase problem can be solved by isomorphous replacement, a method developed by Max Perutz (Green et al., 1954), in which a light atom in the macromolecule is replaced by a heavy atom (e.g. mercury) and the diffraction pattern of the derivatized protein is compared to that of the underivatized protein. This method is widely applicable even today.

In 1958 Max Perutz determined the three-dimensional crystal structure of hemoglobin to a 0.55 nm resolution and John Kendrew determined the structure of myoglobin. The crystal structure of monomeric actin (G-actin) was solved first by Kabsch et al., 1990, while the structure of myosin subfragment 1 (S1), the head of the myosin molecule containing the actin and the nucleotide binding site, was solved by Rayment et al., 1993b. No crystal structure, however, was obtained yet for the actomyosin complex. So, conclusions about conformational changes of the myosin head during the power stroke, i.e. while it is bound to the actin filament, can only be drawn from other imaging methods, using the known crystal structures of S1 or S1 constructs.

**Electron microscopy**

A preferred method to derive structural information from complexes of different proteins that cannot be co-crystallized is the fitting of the crystal structure of the individual proteins into electron micrographs of the complex. In the case of actin-myosin interaction, the known crystal structures of the actin filament and the S1 or S1 fragments are fitted into reconstructions of cryo electron microscopy data of actin filaments decorated with myosin heads (S1) or S1 fragments.

Electron microscopy (EM) offers a resolution in the order of 1 nm. From early electron micrographs of longitudinal thin sections of muscle fibers the existence of cross-bridges between the thick and thin filaments has been demonstrated (Huxley, 1957). They appear as a ladder-like structure and show diverse angular orientations (Reedy et al., 1965). As the thick and thin filaments themselves do not change their length significantly during contraction, it was proposed that the cross-bridges between them are responsible for force development and shortening of the muscle (Huxley and Niedergerke, 1954). Their orientations represent different structural conformations (Reedy et al., 1965).

In cryo electron microscopy, specimens are rapidly frozen at liquid nitrogen temperature and cut into films thinner than 500 nm, to prevent multiple scattering of the electrons. Three-dimensional images of the specimen are reconstructed from layers of two-dimensional recordings. Apart from the high resolution, cryo EM offers the advantage of being able to capture the structure of the sample in a defined condition. Thus further insight in the structural changes occurring during contraction can be gained (Milligan and Flicker, 1987; Milligan et al., 1990).

The disadvantage - at least for our kind of interest - is that cryo EM, as well as other sample preparations for electron microscopy, investigates a non-functional sample. Also, the preparation method is very sensitive and may produce artifacts.

**X-ray fiber diffraction**

Unlike electron microscopy, X-ray diffraction allows to investigate living muscular tissue (Huxley and Brown, 1967; Huxley, 1968). By limiting the irradiation of the sample, it remains functional and structurally undamaged. The method permits to apply definable mechanical and chemical conditions to the sample. Therefore, it appears appropriate as an imaging technique accompanying the earlier described mechanical maneuvers.

The method has to meet a couple of requirements. To be principally able to achieve the resolution necessary for resolving changes in the macromolecular structure during muscle contraction, the used light (electromagnetic radiation) has to have a wavelength of the same order of magnitude as the investigated structure. The brilliance of the light source has to be sufficient to be able to record images on a time-resolved millisecond basis. Only this allows to record diffraction images during length changes of the fibers, which are applied in very short time intervals, e.g. a few milliseconds.

We used synchrotron radiation to meet these requirements. Intense electromagnetic radiation is produced as braking radiation ("Bremsstrahlung") when the electron beam in the storage ring is led through so called insertion devices, undulators or wigglers. The wavelength is fixed to 0.1 nm at beamline ID02 of the ESRF Grenoble and 0.154 nm at beamline 2.1 of the SRS Daresbury, where we performed our experiments. The X-ray beam was focused by monochromators and mirrors in both facilities. Monochromators are asymmetrically cut germanium crystals or silicon crystals at Daresbury and Grenoble, respectively. Specific Bragg-reflections from the crystals are used to achieve high wavelength selectivity, and by controlled bending of the crystals, the X-ray beam is focused in one direction.

The coherent light directed to the sample is scattered from it, whereby the amount of scattering from each structural unit depends on its electron density. As muscle fibers contain a regular molecular structure, they act similar to a crystal and produce a scattering image having distinct peaks of intensity. Light waves scattered from different units interfere with each other. Depending on the relative phases between the scattered waves, in some directions they interfere constructively, whereas in some other directions they interfere destructively. In these later directions no light from the sample is recorded. The interference process of scattered light is called diffraction. An image-detecting device placed behind the sample records the intensity distribution, i.e. the diffraction pattern, which depends on the structure of the scattering sample. For technical details and further illustrations the interested reader is referred to the appendix "X-ray diffraction in a nutshell", which was the handout for a seminar I held in front of our lab group in October 2004.

Muscle does not behave as a perfect crystal. There is a certain degree of disorder in the structure. Therefore, the recorded two-dimensional diffraction patterns exhibit broad peaks of light intensity on a background of differently scattered light. Nevertheless, the patterns reflect information about the macromolecular structure of the scattering

structural elements within the muscle fibers and can be analyzed accordingly. When the scattering structure within the muscle fibers changes, e.g. due to changes of the physical or chemical environment, recorded peaks on the diffraction pattern change their intensity distribution and position.

The helical arrangement of masses on the thick and thin filaments in muscle fibers produces typical reflections on the 2D X-ray diffraction patterns (Squire, 1981; Harford and Squire, 1997). The reflections are categorized into equatorial, meridional and off-meridional reflections (see figure 6, where the typical features of diffraction patterns from muscle fibers are explained). Basics of X-ray diffraction are also described in the appendix "X-ray diffraction in a nutshell".

As known from general diffraction theory the distances on the image are inversely proportional to the size of the periodicities of structural elements that produce the reflections. A tighter grating produces larger distances between reflections, i.e. a wider diffraction pattern, and vice-versa. According to this, the space the image is projected on is also referred to as reciprocal space and distances in reciprocal space are described in reciprocal length units.

From a given structure the diffraction image in reciprocal space can be calculated using the Fourier-transform

$$G(\mathbf{S}) \ = \ \int_V \rho(\mathbf{r}) \, e^{2\pi i \, \mathbf{r} \bullet \mathbf{S}} \, dV,$$

where $G(\mathbf{S})$ is the diffraction (containing the amplitude and phase information of the diffracted light) at a point in space described by the vector $\mathbf{S}$ (in units of $1/\lambda$), $\rho(\mathbf{r})$ is the scattering power (electron density) at a point in the sample described by the vector $\mathbf{r}$. From a known $G(\mathbf{S})$ the electron density distribution $\rho(\mathbf{r})$ can be reconstructed using the inverse function of the Fourier-transform, the Fourier-synthesis. On the two-dimensional area of the detector only the intensity is recorded, i.e. the value proportional to $|G(\mathbf{S})|^2$ with the values of $\mathbf{S}$ restricted to the two-dimensional plane. Because the phase information contained in $G(\mathbf{S})$ is lost in this case, the electron density distribution cannot be reconstructed straightforwardly.

One possible approach to the interpretation of recorded two-dimensional X-ray diffraction patterns is therefore modeling of the molecular structure of the sample and calculation of the resulting pattern from the thus defined electron density distribution. Thereby the electron density distribution can be varied to optimally fit recorded

diffraction patterns. Simple models presenting filamentous actin (F-actin) as a discontinuous helix with the periodicity of its density distribution already yield the typical actin layer lines in the diffraction patterns, although their intensity distribution does not match recorded diffraction patterns. The same is valid for the myosin filament and reflections resulting from its helical density arrangement (Knupp and Squire, 2004; Squire and Knupp, 2004).

Actin and myosin filaments are formed by helical arrangement of actin monomers and myosin monomers, respectively. Their electron density along the helical path is therefore not continuous but rather more discrete. Such "discontinuous" helices produce diffraction patterns with repeating meridional reflections, having a spacing inversely proportional to the subunit translation on the helix. The off-meridional reflections are lying on so-called helix crosses originating from the meridional reflections. Their position is also governed by the repeat, the pitch and the diameter of the helix (Vainstein, 1966; Squire, 1981).

To find a good fit of the calculated diffraction pattern to the measured one, density distributions from know crystal structures of actin (Kabsch et al., 1990; Holmes et al., 1990; Lorenz et al., 1993) and myosin (Rayment et al., 1993b) have to be included in the modeling. Approximation of structural details by spheres of the same size permits reduction of the continuous Fourier-integral to a Fourier-series and thus easy computation of the transform. The form of the spheres then modulates the resulting pattern with the diffraction of a single sphere (an airy disk), according to the convolution theorem (Vainstein, 1966).

By taking into account the mismatch of the periodicities of the actin and myosin filament the distribution of attached cross-bridges in the overlap region of the two filaments can be modeled (Gu et al., 2002). The distribution is modulated by the repeat of the actin filament (~ 36 nm) and by the distance between the crowns on the myosin filament (~ 14.3 nm). Gu et al., 2002, introduced a number of degrees of freedom within the myosin heads, their origins on the myosin backbone and their binding positions on the actin filament to construct the attached cross-bridges. The parameters pertaining to these degrees of freedom are varied to achieve an optimal fit to measured reflections on the diffraction pattern. Although this model reveals information about the possible distortions and orientations of the myosin head when it is strongly attached to actin and makes predictions about the influence of the second, unattached myosin head, it is not

able to appropriately model the intensity distributions of the lower index actin and myosin layer lines.

The intensities of these layer lines are also modulated by the regular arrangement of actin and myosin filaments in the hexagonal lattice of the contractile apparatus. This intensity modulation is called "lattice sampling". The sampling of these layer lines, however, is not only produced by the regular transversal lattice of the actin and myosin filaments. Influences of axial and transversal disorder have also to be taken into account. Adequate modeling of lattice sampling is of huge importance for us, as we are interested in the role of the rigor conformation of the cross-bridges that produces diffraction patterns with very prominent lattice sampling. An example of a two-dimensional diffraction pattern of fibers, where all cross-bridges are in this rigor conformation is shown in figure 7.
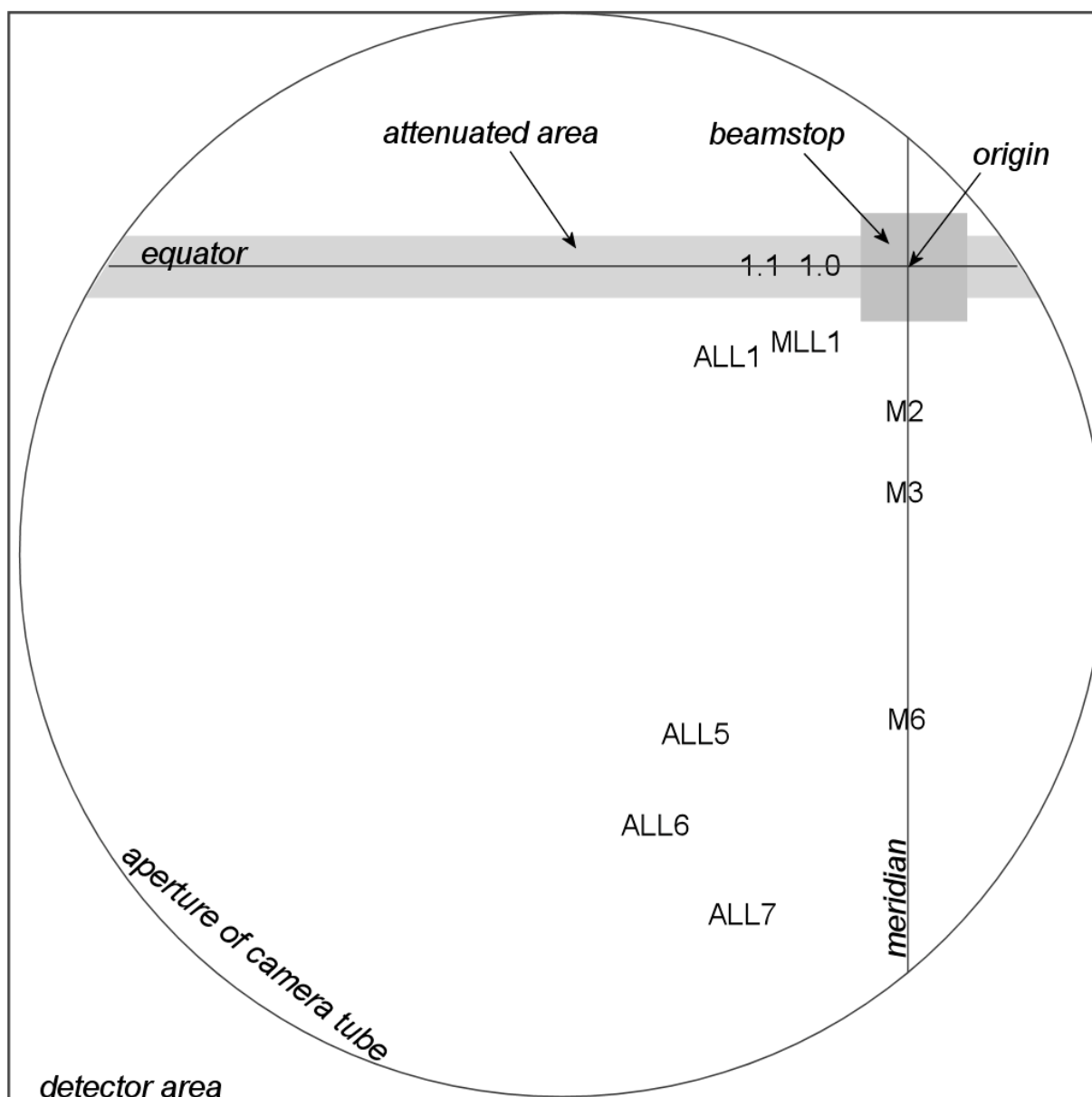
*Fig. 6: Scheme explaining the diffraction pattern in figure 7. The diffraction pattern was recorded at the ESRF in Grenoble. The image was recorded on the RAPID detector with an active size of 200 mm x 200 mm and 1024 x 1024 pixels. Intensity is recorded in a circular disk produced by the aperture of the camera tube. Only few, scattered photons were recorded outside this area. The origin is in the upper right part of the image. It corresponds to the position of the non-scattered X-ray beam, which is inhibited from hitting the detector directly (and damaging it) by a square peace of lead, the beamstop. The horizontal direction crossing the origin is called the equator and the vertical the meridian. The region around the equator was attenuated about 3.5-fold by a strip of lead to diminish artifacts of the detector response produced by high-intensity peaks. Intensity peaks on the equator correspond (figure legend continues)*

*(figure legend continued) to the arrangement of the filaments in the hexagonal lattice structure of the contractile apparatus, i.e., the arrangement of diffractive mass in the fibers projected on a plane perpendicular to the fiber axis. As a reference see figure 10, where the influence of mass distribution between thick and thin filaments on the intensities of the 1,0 and 1,1 equatorial reflections is explained. The meridional reflections correspond to periodically repeating structures along the axis of the filaments. They are indicated by M2, M3 and M6. M3, for example, corresponds to the axial translation of the myosin heads in the myosin filaments, i.e., the distance of one crown of heads to the other, which is about 14.3 nm. The off-meridional reflections, MLL1, ALL1, ALL5, ALL6, ALL7, are layer lines produced by the helical arrangement of masses on the myosin (MLLs) and actin (ALLs) filaments, respectively. Their position is governed by the pitch and repeat of the helical arrangement of myosin heads and actin monomers, respectively. Details are explained in the appendix. The positions of the reflections on the diffraction pattern are mapped according to the reciprocal values of the corresponding periodic distances in the sample. The diffraction image is therefore referred to as reciprocal space. According to this, ALL6 is also called the 59-Å-layer line and ALL7 the 51-Å-layer line.*
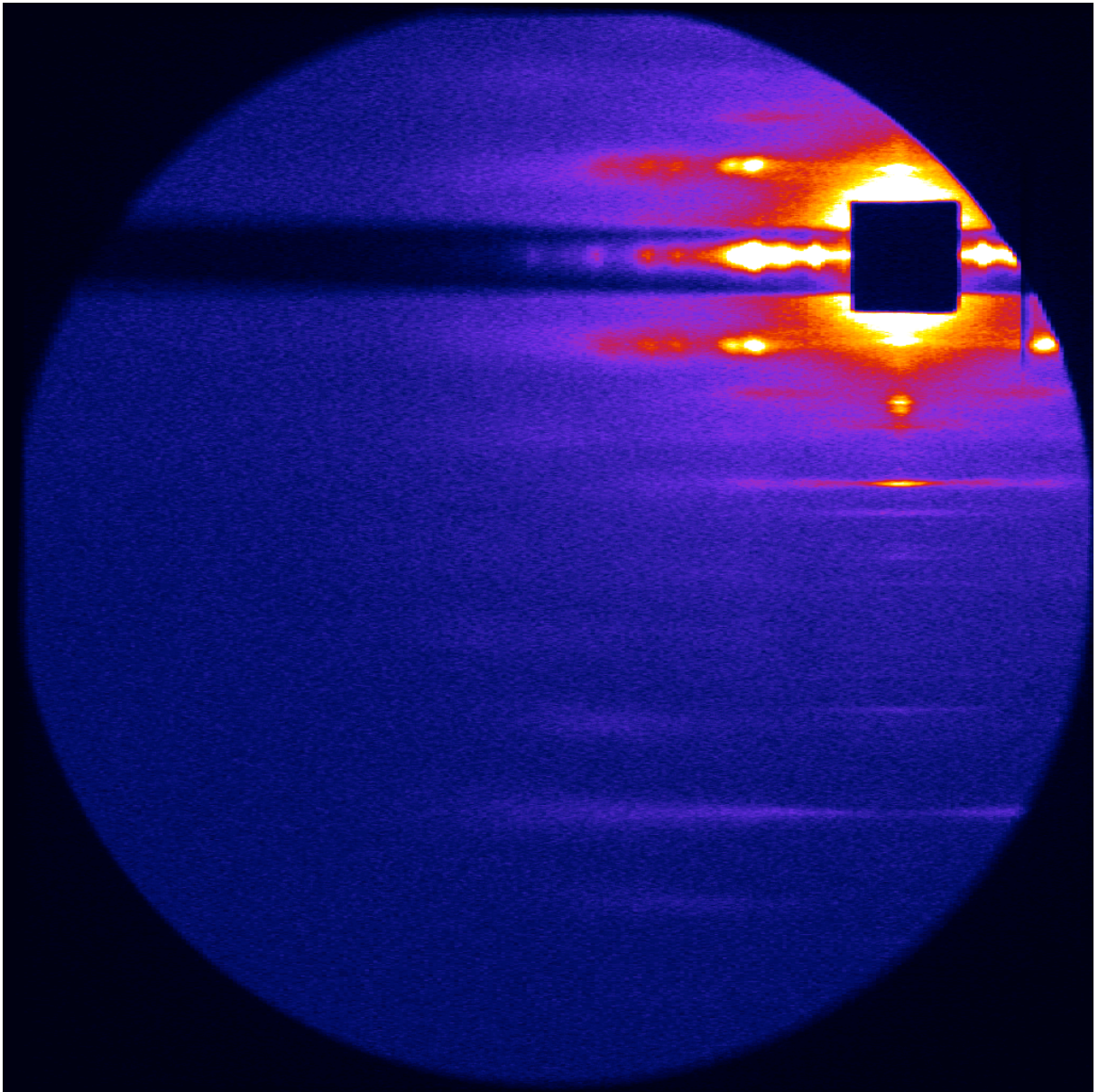
Color gradient:
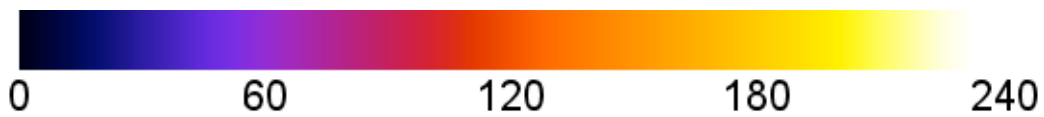
Fig. 7: 2D-X-ray diffraction pattern of muscle fibers in rigor condition recorded with the RAPID detector. The image is displayed in pseudo colors. Typical rigor features are visible, most prominently, on the first actin layer line (ALL1), which shows the characteristic lattice sampling. Intense actin layer lines are produced by the labeling of the actin filaments with stereospecifically attached myosin heads. The image also shows an intense 1,1 equatorial reflection.

In skeletal muscle of higher vertebrates actin and myosin filaments form a super-lattice, as the myosin filaments have two possible orientations. Therefore, a unit cell, which comprises the repeating elements of the diffracting material, has to include at least one myosin filament of each orientation. If the diffracting structure can be divided in repeating unit cells, it generally suffices to calculate the Fourier-transform of one unit cell and account for the complete structure using the convolution theorem (Vainstein, 1966).
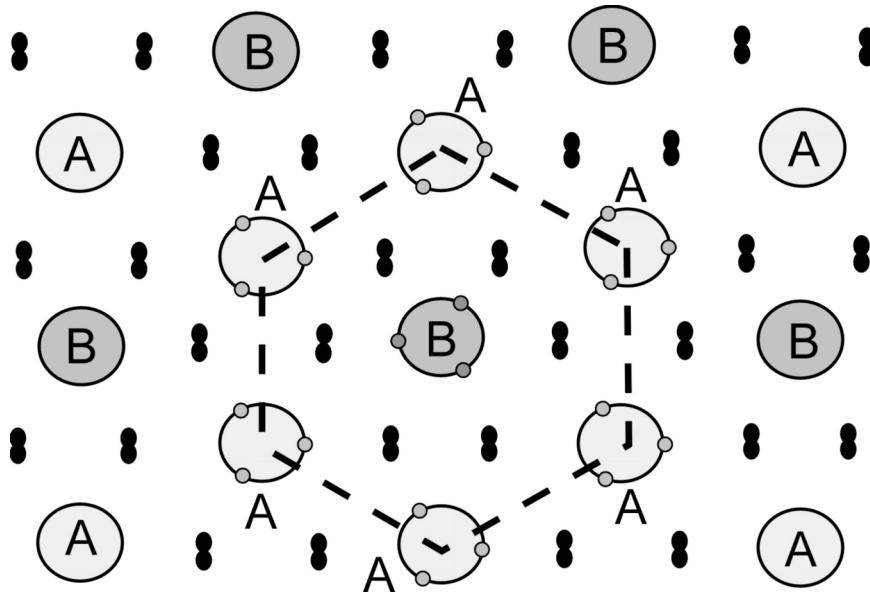


*Fig. 8: Transversal lattice of myosin and actin filaments in the overlap zone. The scheme depicts a transversal cut through the A-band of the muscle fiber. The big gray circles represent the myosin filaments and the small circles on their circumference the positions of the origins of the myosin heads on the myosin backbone. The small black double circles are the actin filaments. In vertebrate skeletal muscle the myosin filaments have two possible orientations marked by the letters A and B, which are distinguished by the arrangement of the origins of the myosin heads. This lattice is called the superlattice, whereas in a simple lattice, as for example in bony fish muscle, only one orientation of the myosin filaments is present. A constructed unit cell, that comprises the smallest repeating part of the superlattice, therefore, has to contain myosin filaments of both orientations. In their model, Koubassova and Tsaturyan, 2002, defined the dashed hexagon the unit cell. From Koubassova and Tsaturyan, 2002.*

In the model presented by Koubassova and Tsaturyan, 2002, a hexagonal unit cell is defined, which contains six actin and three myosin filaments, whereby the central one

has a different orientation from the other myosin filaments (Fig. 8). By introducing disorder in the form of deviations of axial and transversal positions within the unit cell and between neighboring unit cells, typical lattice sampling on the low index layer lines was modeled, while in the same time there is no visible lattice sampling on the fifth, sixth and seventh actin layer line. The modeled profiles of the layer lines thus fit the experimental data nicely, although the ratios of total intensities of the actin layer lines could not be approximated to experimental data sufficiently. According to the authors, this could be due to the lack of troponin and tropomyosin in the model. Nevertheless, this model is highly useful for us, because it yields information about the intensity distributions along the layer lines depending on the number and labeling pattern of attached myosin heads, as well as different types of disorder.

Vainstein, 1966, distinguishes mainly two types of disorder: disorder of the first kind and disorder of the second kind. The first is induced by Brownian motion and random movements resulting, for example, from cross-bridge action. The second is propagated by elastic neighbor-to-neighbor interactions. Koubassova and Tsaturyan, 2002, approximated disorder of the first kind by axial and transversal deviations within the unit cell, and disorder of the second kind by deviations between unit cells.

Of major consequence for the interpretation of our own results are the following conclusions derived from the Koubassova and Tsaturyan model:

(i) The intensity distribution along the first actin layer line (ALL1) is highly sensitive to transversal disorder, both of first and second kind. With decreasing transversal disorder lattice sampling gets more pronounced, whereas for increasing transversal disorder the sampled profile gets smoother.

(ii) The intensity distribution along the ALL1 is practically independent of axial disorder and of the molecular structure, the conformation of various domains, and the orientation of the cross-bridges.

(iii) The total off-meridional intensity of ALL1 depends solely on the number of stereospecifically attached myosin heads.

(iv) The intensity distribution along the sixth actin layer line (ALL6) is independent of the distribution pattern of attached myosin heads.

(v) Lattice sampling on ALL6 is negligible, what coincides with our own experimental results in various conditions.

(vi) The total intensity and the intensity distribution along the ALL6 is highly sensitive to the structure, conformation, and orientation of the cross-bridges. Even minor

structural changes or bending of the light chain domain of the myosin heads produce significant changes both in the profile and total intensity of ALL6.

Concerning point (iii) it has to be noted that the intensity of layer lines generally increases with the number of diffractors. The intensity, though, does not quite follow the square law introduced by Haselgrove, 1975, stating that the intensity is proportional to the square of the number of diffractors. It is rather found to increase linearly for small numbers of diffractors (Tamura et al., 2004).

Based on the model of Koubassova and Tsaturyan, 2002, recorded changes on the first actin layer line during applied mechanical maneuvers can, therefore, be interpreted in the following way. An overall increase in ALL1 is associated with an increase in the number of diffractors, i.e. an increase in the number of myosin heads stereospecifically attached to actin. An increase in the sampled maxima of ALL1 alone, i.e., without an increase in total intensity, is associated with increased transversal order within the muscle fiber.

Changes in the shape of the sixth actin layer line indicate structural changes within the attached cross-bridges. These changes include possible density shifts within the myosin head as it takes up another conformation, or as domains of the myosin head are tilted or bent, or as the myosin head itself is tilted or bent as a whole. Thus, changes on the sixth actin layer line that occur during mechanical maneuvers at time-points crucial for force-development, give us information about structural changes of the cross-bridge during its power stroke or during force-development.
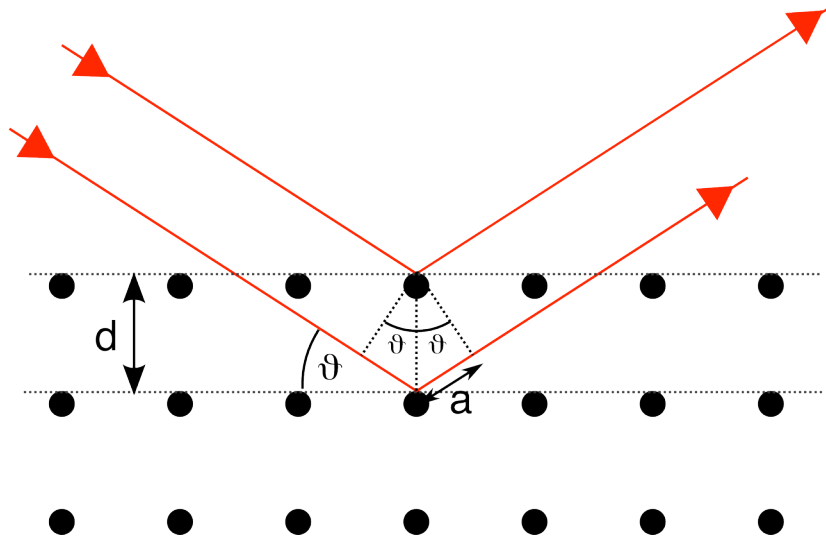
*Fig. 9: Schematic illustration of Bragg's law. Incident light (red lines, coming from the left side) is being reflected on the lattice planes. The emerging light beams (right side) are interfering constructively, when the pathlength difference is an integer multiple of the wavelength of the light. The condition for constructive interference is therefore: $2a = n\lambda = 2d\sin\vartheta$, where $2a$ is the pathlength difference, $\lambda$ is the wavelength, d is the lattice spacing, and $\vartheta$ is the angle of incidence of the light.*

The equatorial reflections on the diffraction patterns, the group of most intense reflections in the diffraction pattern, allow to monitor the density distribution in the transversal direction of the muscle fiber. Actin and myosin filaments are arranged in a regular hexagonal array, which diffracts X-rays in a direction perpendicular to the fiber axis.

The positions of the reflections pertaining to lattice planes with a spacing d are described by Bragg's law:

$$n\lambda = 2d\sin\vartheta$$

as illustrated in figure 9. The incident light is deflected by the angle $2\vartheta$. For small angles $\vartheta$, the above equation can be approximated by

$$n\lambda = d\frac{S_n}{L}$$

where $S_n$ is the distance of the n-th order reflection from the origin on the diffraction pattern and L is the camera length, i.e. the distance of the detector from the sample. The positions of the equatorial reflections for each lattice plane in small angle X-ray scattering (SAXS) are therefore determined by

$$S_n = nL\frac{\lambda}{d} \, .$$

The above equation shows the inverse relationship between distances in the sample and on the diffraction pattern, as described earlier when introducing reciprocal space. Figure 10 shows a schematic axial projection of the lattice planes 1,0 and 1,1 in the hexagonal filament array and the 1st order (n=1) equatorial reflections coming from them. The positions of the 1,0 and 1,1 equatorial reflections are determined by the inverse lattice spacing of the 1,0 and 1,1 lattice planes, respectively.

The intensities of the equatorial reflections depend on the scattering densities of the diffractors lying on the corresponding lattice planes. The 1,0 lattice plane includes only myosin filaments, whereas the 1,1 lattice plane includes both myosin and actin filaments. The ratio of the intensities of the reflections ($I_{1,1}/I_{1,0}$) gives a practicable measure for the density distribution between actin and myosin filaments. When diffracting mass shifts from the myosin to the actin filaments, $I_{1,1}/I_{1,0}$ increases accordingly. Figure 10 illustrates this effect. More density on the myosin filaments produces high 1,0 peaks and low 1,1 peaks (left two panels of the figure), and more density on the actin filaments the opposite (right two panels of the figure). Influences of the disorder of the first kind (random disorder), which may change during mechanical maneuvers, are canceled out in the ratio. Only disorder of the second kind (propagating disorder) is affecting $I_{1,1}$ more than $I_{1,0}$ (Vainstein, 1966) and may therefore have an influence on the ratio $I_{1,1}/I_{1,0}$ during mechanical maneuvers.

Two-dimensional X-ray pattern contain many other features that are obviously sensitive to different mechanical and chemical conditions of the muscle sample. For the analysis of our results, though, we picked out only the recorded reflections that are sensitive to cross-bridges in rigor conformation. The third and sixth myosin layer lines, the meridional reflections M3 and M6, respectively, come from the ~14.3 nm translation between the crowns of myosin heads. Therefore these reflections are sensitive only to changes in the myosin heads not attached to actin or to parts of the attached heads that follow the myosin periodicity, e.g. the neck region near the origin on the myosin backbone (Koubassova and Tsaturyan, 2002). Part of the reflection comes also from the myosin backbone itself (Linari et al., 2000). The information obtained from M3 and M6 is therefore quite complex and does not allow unambiguous interpretation of the role of the rigor conformation in the power stroke.

Based on the above explanations, we focus our study on the first and sixth actin layer line and on the equatorial 1,0 and 1,1 reflections.
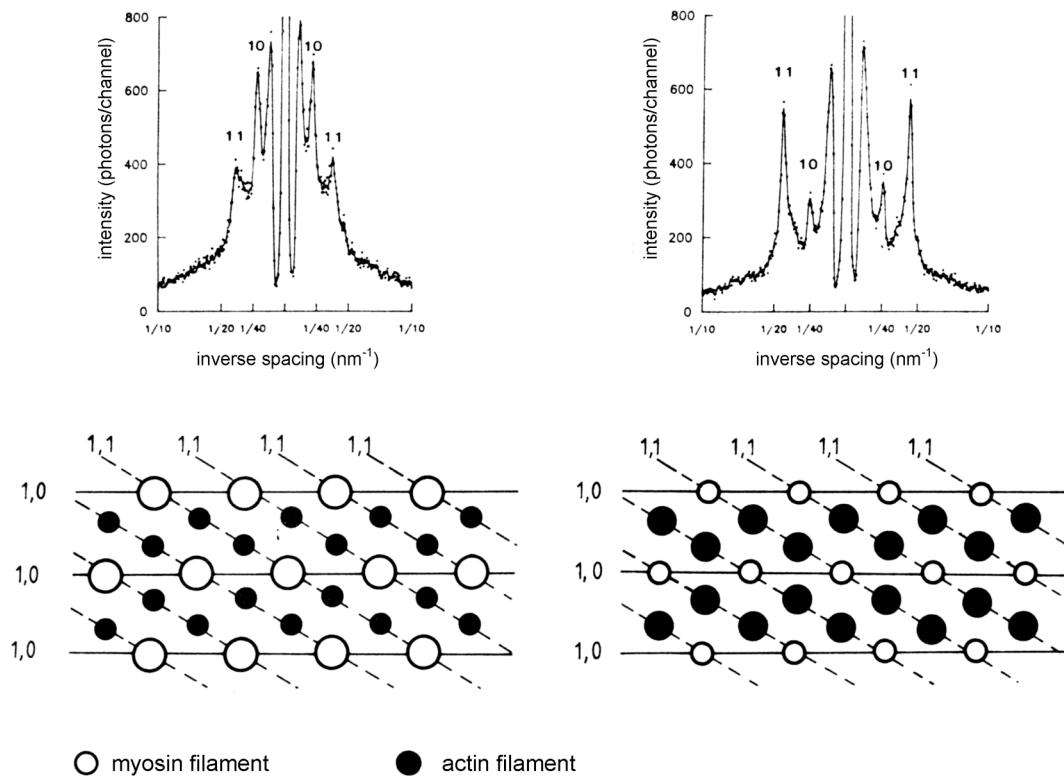


*Fig. 10: Effect of mass shift on equatorial reflections. Two profiles of the equatorial reflections (above) are shown for two different density distributions on the actin and myosin filaments (below). The redistribution of electron density within the transversal lattice of the muscle fiber affects both the 1,0 and the 1,1 equatorial reflections. The 1,0 and 1,1 reflections pertain to densities on the 1,0 and 1,1 lattice plane, respectively. Modified from Brenner, 1986b*

**Other investigative methods**

There are of course other methods capable to explore the structure and function of muscle, such as biochemical experiments, measurement of membrane potentials, single molecule detection techniques, etc., but I am not going to delve into them.

In order to investigate the structural changes occurring during the power stroke and the role of the rigor-like cross-bridge conformation, we applied the method of X-ray diffraction in combination with mechanical maneuvers and controlled chemical environment, because it is a noninvasive method offering information about molecular structures with a spatial resolution of nanometers.

## *Conformational changes of the myosin head*

Conformational changes that occur within the myosin head while it is attached to actin are responsible for the power stroke. The shape of the myosin molecule is described in figure 11. The LMM (light meromyosin) is incorporated into the backbone of the thick filament, whereas HMM (heavy meromyosin) that consists of the subfragments S1 and S2 sticks out of the backbone. The cleavage points between the different fragments are considered hinge regions. Each myosin molecule comprises two heavy chains and thus two myosin heads (subfragments 1 - S1). The S1 fragments retain the ATPase activity even when they are cleaved from the rest of the myosin. It is therefore assumed that the conformational change during the power stroke takes place in this subfragment.
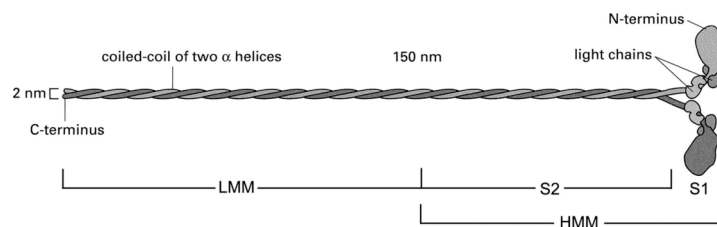


*Fig. 11: The myosin molecule consists of a long coiled-coil region, which is partially incorporated into the backbone of the thick filament (LMM). The other fragment (HMM) consists of a shorter coiled coil (subfragment 2 - S2) and two globular heads subfragment 1 - S1). From Alberts et al., 2002*

The structure of S1 has been solved by protein crystallography (Rayment et al., 1993b, Fig. 12). S1 consists essentially of a head domain that comprises an actin binding site and a nucleotide-binding site and of a neck domain consisting of a long α-helix surrounded by two light chains. By fitting the obtained S1 structure to density images from cryo-electron microscopy Rayment et al., 1993a the structure of the actomyosin complex was reconstructed and associated to the nucleotide-free, rigor state of the cross-bridge (AM). This structural state is, according to this model, the "post-power-stroke" conformation of the cross-bridge.

Further conclusions were drawn from crystallographic data on truncated myosin head domains of Dictyostelium discoideum myosin II. A "pre-power-stroke" conformation was obtained by complexing with ADP-vanadate, a non-hydrolysable ATP analogue (Smith and Rayment, 1996). In this conformation the converter domain is rotated by 70°

compared to Dictyostelium constructs in a "post-power-stroke" conformation (Fisher et al., 1995). This 70° rotation of the converter domain produces a tilt of the neck domain. It is concluded that the neck domain of S1 functions as a lever arm, pulling the motor domain towards the M-line in the sarcomere and thus contributing to the power stroke. In this rotation, the end the lever arm moves about 11 nm.
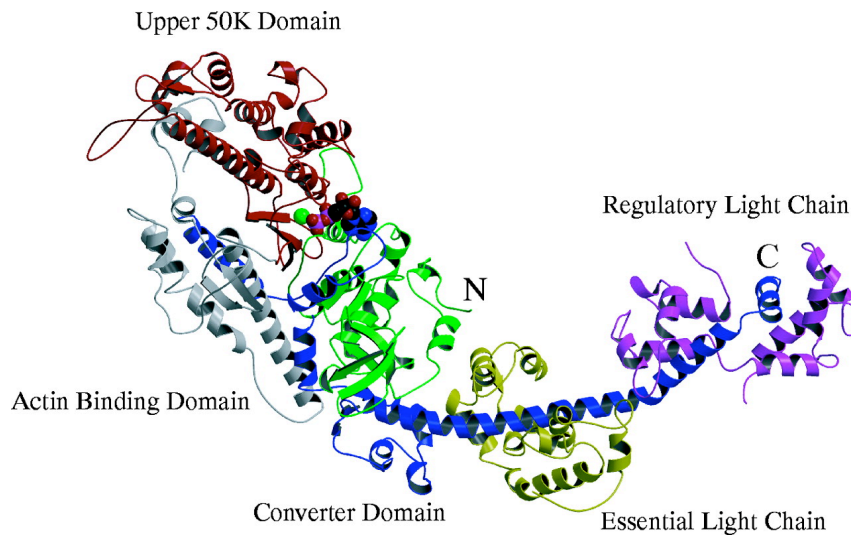


*Fig. 12: Ribbon representation of the structure of chicken skeletal muscle subfragment 1 (S1). S1 consists of an elongated head, containing the upper 50K domain, the actin binding domain and the converter domain, and a tail or neck region, carrying the two light chains. From Geeves and Holmes, 1999.*

Different orientation of cross-bridges in electron micrographs (Reedy et al., 1965) were interpreted to show that reorientation of the myosin head (S1) represents the conformational change that constitutes the power stroke. Earlier fiber diffraction data suggested different orientations of the myosin head, ordered and disordered, with respect to the actin helix (Brenner and Yu, 1993). In addition, protein crystallography of S1 and S1 fragments revealed different orientations of the light chain binding domain for different states of the nucleotide in the active site (Rayment et al., 1993a). From these data it is possible that both reorientation of the attached myosin head relative to the actin helix and reorientation of the lever arm within the S1 fragment contribute to the power stroke (Brenner et al., 1995).

## *Current concepts of the cross-bridge cycle*

Based on the above concept of pre and post power stroke it was proposed (Geeves and Holmes, 1999) that force is generated by the transition between these two conformational states and that force is maintained by a number of cross-bridges which are in the post-power-stoke conformation, specifically, in a structural state like the nucleotide-free, rigor conformation. It was further proposed that this concept is also consistent with the tension recovery experiments performed by A. F. Huxley and Simmons (Huxley and Simmons, 1971), where quick tension recovery was interpreted as an increase in the number of cross-bridges late in the power stroke.

Actually, this theory could not be confirmed by X-ray diffraction methods. Two-dimensional X-ray diffraction images (Huxley and Brown, 1967; Haselgrove, 1975; Huxley et al., 1982, Rapp et al., 1991, Bordas et al., 1993; Kraft et al., 2002) did not show rigor-like features during active contraction, although the fraction of force generating cross-bridges during isometric contraction is thought to be 55-70% (Kraft et al., 2002). Instead, intensities of layer lines on the X-ray diffraction patterns differ substantially from those recorded from muscle fibers in rigor. In addition, mechanical and X-ray experiments (Brenner, 1991; Brenner et al., 1995) showed that very likely isometric force is generated already at the transition from weakly to strongly bound cross-bridges, i.e., before the rigor conformation is reached.

A comprehensive biochemical scheme of the states in the cross-bridge cycle is shown in figure 13. In the weak binding states the cross-bridges attach and detach from actin dynamically with high rates (Stein et al., 1979; Chalovich et al., 1981; Brenner, 1980; Brenner, 1986a). For force generation, though, a transition to strong binding states is required, as only strong binding states can be force bearing.

As no rigor-conformation of cross-bridges was detected during isometric contraction, the question arises, what role states with a rigor conformation may play in force generation. When the power stroke is performed, the cross-bridge transits from weak binding states to strong binding states, while in a first step inorganic phosphate is released followed by release of ADP in a later step. The rigor state is reached as a transient state when ADP is finally released, and the rigor state ends when ATP binds to the active site and the cross-bridge transits to the weakly bound states again.
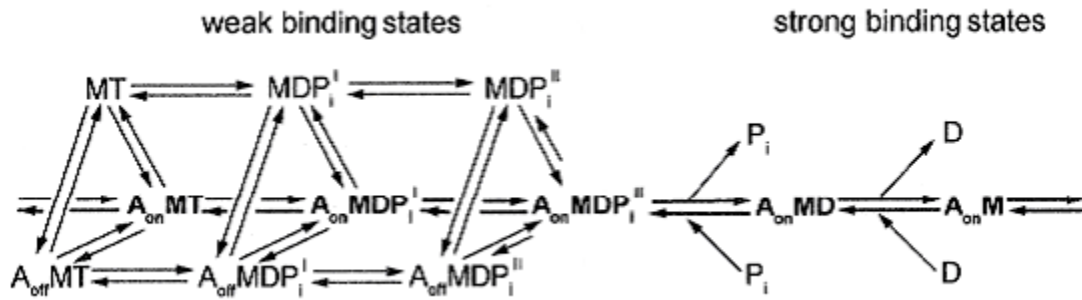
*Fig. 13: Kinetic scheme of the cross-bridge cycle, indicating the different weak and strong binding states. Modified from Brenner and Chalovich, 1999. A = actin, $A_{on}$ = calcium activated actin filament, $A_{off}$ = non-activated actin filament (without calcium), M = myosin, T = MgATP, D = MgADP, $P_i$ = inorganic phosphate. The different lengths of the transition arrows indicate qualitatively the different values of the rate constants of the various reaction steps. Weak binding and strong binding cross-bridge states are distinguished biochemically and mechanically. Weak binding states are characterized by a low binding affinity to actin, even in the presence of calcium when the thin filament is activated (Stein et al., 1979; Chalovich et al., 1981), and by the inability to activate the contractile system (Chalovich et al., 1983). Strong binding states, on the other side, have a high binding affinity to actin. Cross-bridges that are strongly bound to actin can activate the contractile system even in the absence of calcium and undergo the complete cross-bridge cycle (Greene and Eisenberg, 1980).*

## The question at hand

Mechanical events are coupled to the biochemical transitions described in the scheme of the cross-bridge cycle (figure 13). As the power stroke is a multi-step process (Huxley and Simmons, 1971), (i) several of the reaction steps shown in the scheme of figure 13 are associated with structural changes of the attached cross-bridge, and (ii) very likely some of the biochemical states shown in the scheme of figure 13 are associated with several different conformational states. During the power stroke the filaments are driven past each other, or force is maintained while energy is stored in elastic distortion. The power stroke is initiated at the transition from weak to strong binding states and continues through the series of transitions among strong binding states. Most likely isometric force is generated by states early in the power stroke that do not show structural features like rigor cross-bridges. Whether the transition to the rigor state also

contributes to the power stroke is still unclear as is the question whether rigor like states are at all significantly populated during isometric contraction. In this study we therefore investigated the structural changes seen when cross-bridges during force generation are driven to their later states in the power stroke by ramp-shaped releases applied during isometric force generation. We used this approach since this maximizes the probability to detect rigor like cross-bridge states, if their occupancy can become significant at all. Since 2D diffraction patterns bear unique signatures of structural features, especially of rigor and rigor-like cross-bridges, we recorded 2D diffraction patterns as snapshots during ramp-shaped releases applied to muscle fibers during steady state isometric contraction and focused our analysis on the unique signatures of the structural features of rigor and rigor-like cross-bridges.

# Materials and methods

## *Single fiber preparation*

Single fibers were isolated from chemically skinned small bundles of skeletal muscle fibers from rabbit psoas muscle, as described previously (Brenner, 1983; Yu and Brenner, 1989; Kraft et al., 1995; Kraft et al., 2002). For the experiments performed at the SRS in Daresbury, rabbits of the race Californian Giants (about 2 years age and 5 kg weight) were obtained through the animal facility of the University of Keele and were sacrificed according to the procedures established and approved by the University of Keele. At the ESRF in Grenoble we used New Zeeland rabbits of about 4 kg weight. The rabbits were injected with 3 ml Dolethal (Vétoquinol, Lure Cedex, France) and bleed by cutting of the carotid artery. Access to the M. psoas maior was provided by ventral opening the abdomen. After removal of fatty and connective tissue, muscle fiber bundles of 2-3 mm diameter and 8-12 mm length were excised and transferred to a perspex chamber cooled on ice. Without changing their lengths, the bundles were fixed with stainless steel needles on a layer of Sylgard silicone („RTV 615 A+B", Dow Corning Corp., Midland, MI, USA) that covered the bottom of the chamber. The bundles were incubated 30 to 60 minutes at 4°C in skinning solution (for specification see chapter "Solutions") with 0.5 vol. % Triton X-100 (Roche 1332481) as a detergent, in order to dissolve the cytoplasmic membranes. After this first incubation period, the solution was exchanged with skinning solution not containing Triton X-100. In the air-sealed chamber, the bundles could be kept in the skinning solution at 4°C for several days. To avoid ATP depletion the skinning solution was changed daily.

For the preparation of single fibers from the "skinned" fiber bundles, ~3-cm-long sections of the bundles were excised and pinned to the Sylgard coating of a smaller perspex chamber filled with skinning solution. Single fibers were pulled out of the fiber bundles in axial direction using a pair of tweezers (Dumont & Fils, Switzerland, No. 5). The fibers were covered continuously with skinning solution. Overstretched, damaged, inhomogeneous or conical fibers were rejected.

## *Mounting and length control*

Approximately 15 single fibers (for the time-resolved experiments at the ESRF) or 30 (for recording of static patterns at the SRS) were mounted side by side into the x-ray setup (Kraft et al., 1999). For this purpose, consecutively each of the single, previously prepared, fiber was individually attached with silicone glue („RTV 3145", Dow Corning Corp., Midland, MI, USA) to the lever of the linear motor, on one end, and a force transducer, at the other end. Special care was taken, not to overstretch or distort the fibers. After all fibers were attached to motor and force transducer, the fibers were put into rigor by immersion in "quick rinse" solution (composition see below) with ionic strength of 80 mM. After rigor had fully developed, the ends of the fibers were briefly fixed with 5% glutaraldehyde (Sigma, G-5882). Subsequently, the fibers were relaxed in relaxing solution of 120 mM ionic strength. This solution was removed for a very short time (~2 sec.) to stabilize the attachments by application of a surgical glue (Histoacryl Blau, 1050052, Aesculap, Tuttlingen). After polymerization of the surgical glue, the fibers were immersed again in skinning solution. The surgical glue provided a tight and stable connection of the fibers to motor and force transducer.

Arrays of 15 or 30 single skinned fibers instead of natural fiber bundles were used in order to minimize distances for diffusion of substrates into the fibers. Sarcomere lengths were adjusted to 2.4 µm using diffraction of a helium-neon laser beam. Control of overall fiber length was achieved with the linear motor. In addition, sarcomere length could be monitored on a screen showing the diffracted laser light. Sarcomere length was monitored as a control for structural stability of the fiber throughout the experiments, especially during activation.

## *Solutions*

Solutions used to achieve relaxation and rigor condition of the fibers were identical to those described by Kraft et al., 1999.

Composition of the skinning solution used to permeabilize the muscle bundle (incl. 0.5% Triton-X-100) and store the fibers for at most 2 days after isolation:

       5 mM $KH_2PO_4$ (Fluka, 60220)

       5 mM Mg-acetate (M-0631)

       5 mM EGTA (E-4378)

       3 mM ($Na_2$) ATP (A-3377)

50 mM sodium creatine phosphate (P-7936)

8 mM $NaN_3$ (Serva, 30175)

Added protease inhibitors:

0.01 mM leupeptin (L-2884)

0.01 mM antipain (A-6191)

0.01 mM E64 (E-3132)

0.01 mM pepstatin A (P-4265)

0.001 mg/ml aprotinin (A-1153)

1 mM AEBSF (Applichem, A1421)

10 mM glutathione (G-4251)

5 mM DTT (D-0632)

Composition of the relaxing solution used also for preincubation of the fibers before activation:

10 mM imidazole (I-0125)

2 mM $MgCl_2$ (M-1028)

1 mM MgATP (A-3377)

10 mM caffeine (C-0750)

10 mM sodium creatine phosphate (P-7936)

200 U/ml creatine phosphokinase (C-3755)

3 mM EGTA (E-4378)

The composition of the activating solution was the same as for the relaxing solution, except that 3 mM Ca-EGTA was used instead of 3 mM EGTA.

For comparison, static patterns with different MgATPγS concentrations and saturating $Ca^{++}$ concentrations (pCa 4.5) were recorded. The composition of the 20 μM MgATPγS solution was:

10 mM imidazole (I-0125)

2 mM $MgCl_2$ (M-1028)

1 mM Ca-EGTA (C-3881, E-4378)

20 μM MgATPγS (Roche, 102342, purified by ion exchange

chromatography as described in Kraft et al., 1992)

0.25 mM $Ap_5A$ (D-4022)

0.005 U/ml hexokinase (H-5000)

200 mM D- glucose (Merck, 1.08337)

Solutions with 100 µM and 1000 µM MgATPγS were composed accordingly. At 1000 µM MgATPγS 0.01 U/ml instead of 0.005 U/ml hexokinase were used.

The rigor solution contained:

> 10 mM imidazole (I-0125)
>
> 2.5 mM EGTA (E-4378)
>
> 2.5 mM EDTA (ED2SS)

For rapid transition of the fibers into rigor "quick rinse" solution was used. It contained:

> 10 mM imidazole (I-0125)
>
> 2.5 mM EGTA (E-4378)
>
> 7.5 mM EDTA (ED2SS)

The ionic strength of the solutions was adjusted to 80 mM by adding potassium propionate and the experimental temperature was held constant at 5 °C throughout all measurements. All solutions were adjusted to pH 7.0. All solutions used for recording of X-ray diffraction patterns contained 10 mM glutathione (G-4251), 5 mM DTT (D-0632) and 1000 U/ml catalase (C-30) to reduce radiation (beam) damage of the fibers (Kraft et al., 1999). All substances were obtained from Sigma Chemical Co. (St. Louis, MO), except where noted otherwise. The numbers in parentheses are catalogue numbers of the substances.

## *Experimental protocols*

**Time-resolved experiments at the European Synchrotron Radiation Facility (ESRF), Grenoble, France**

**X-ray diffraction**

Two-dimensional, low angle x-ray diffraction patterns of arrays of single skinned fibers of rabbit psoas muscle were recorded at beam-line ID02 of the ESRF in Grenoble, France, using the RAPID detector developed at the SRS in Daresbury, UK (Lewis et al., 1995; Lewis et al., 1997; Lewis et al., 1999). The camera length was 6.2 m. The size of the active area of the detector was 200 mm x 200 mm.

With this camera length only one quadrant of the diffraction patterns, ranging from the area of the beam stop and including the actin based layer lines at inverse spacings 1/5.9 nm$^{-1}$ and 1/5.1 nm$^{-1}$, could be recorded (see figure 7). The equatorial intensities were attenuated about 3.5-fold using a strip of lead. This attenuation was required to diminish the effect of reduced detector signals in rows and columns that include high intensity

peaks. This reduction in detector signals, i.e., sensitivity of the detector, is produced by the dead time of the detector after a photon impact. During a short time period (the dead time), the detector is insensitive to further photon impacts in the same row and column of its detection area.
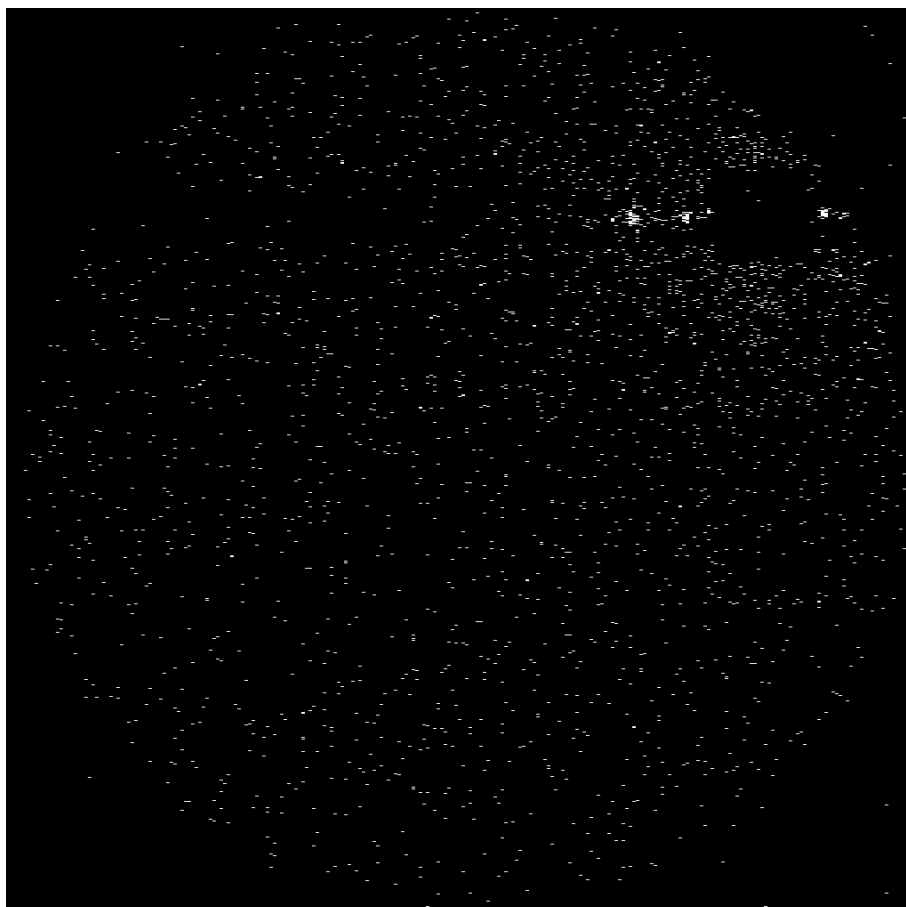


*Fig. 14: Single snapshot of 2 ms exposure time, showing single photons recorded with the RAPID detector.*

The RAPID detector is a two-dimensional position sensitive photon-counting device. It comprises a "wire MicroGap" detector and excels with a very high local count rate of $\sim 10^6$ photons/mm$^2$/s and negligible dark and read-out noise (Lewis et al., 1997). This detector therefore allowed us to record single "snapshots" of the diffraction patterns within very short time frames (2 to 4 ms), which contain only few scattered photons (Fig. 14). Because of the low noise level of the detector, it was possible to pool 560 to 840 snapshots (depending on the number of experiments performed) without noticeable increase of background noise. By accumulation of 560 to 840 snapshots, which is

equivalent to a total accumulation time of 2-3 seconds, diffraction patterns with sufficient intensities even in some of the actin- and myosin-based layer lines were obtained for all time frames (Fig. 15).
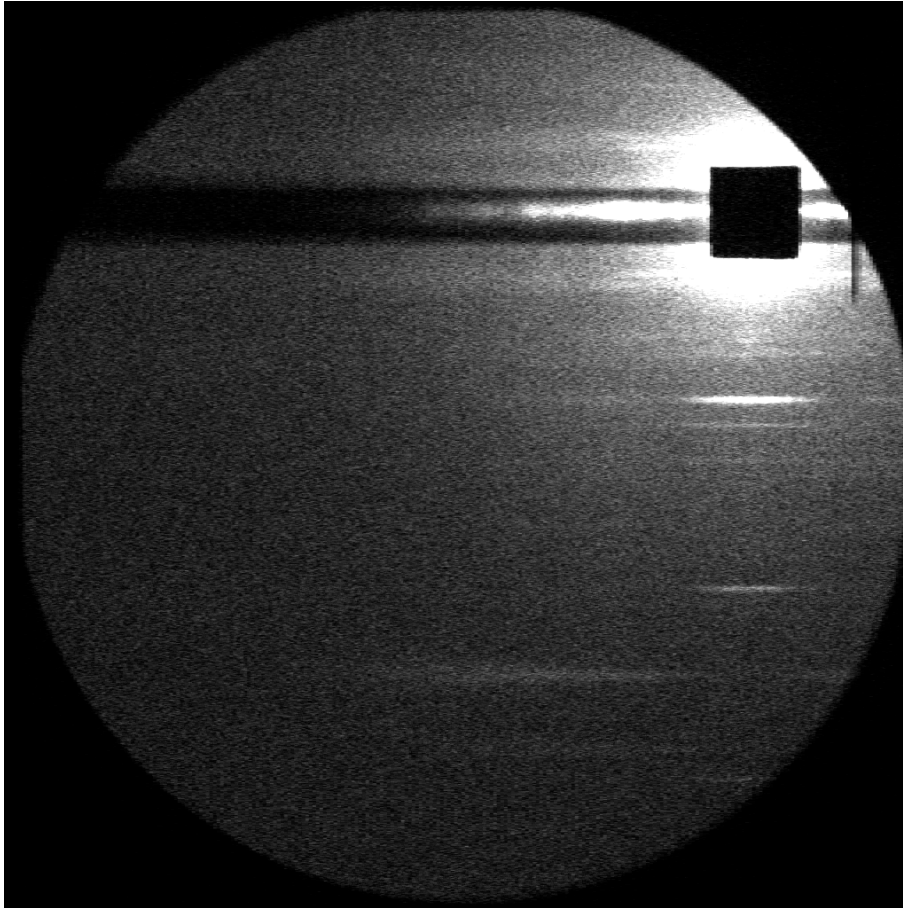


*Fig. 15: Two-dimensional X-ray diffraction pattern obtained by pooling of data of all corresponding time frames of all 6 activated single fiber arrays. The pattern shown here is the pattern taken in the 3 ms frame during isometric contraction (of Fig. 16).*

By recording multiple images at short exposure times and low irradiation of the fibers, it was possible to preserve the structure of the muscle sample. The specific properties of the RAPID detector enabled us to pool sufficient numbers of images. In test trials during previous experiments, such accumulation was not possible with a CCD detector. This was probably due to the high dark noise and read-out noise that generated an unacceptable signal to noise ratio.

**Experimental protocol**

After activated fibers, mounted in our setup, reached isometric steady-state contraction, they were submitted to repeated length changes (ramp shaped releases) where the fibers were allowed to shorten linearly with time and were re-stretched to their original length after each such release. The amplitude of these ramp-shaped releases was 1.6 to 1.7% of the original fiber-length in the isometric steady-state contraction. The maximum amplitude of 1.6 to 1.7% was reached after 20 ms and was followed by a re-stretch to the original fiber-length within 4 ms. These ramp-shaped length changes were repeated after a period of isometric contraction of 0.3 seconds. For the chronology of the releases, see figure 16.

After five such ramp-shaped release/re-stretch cycles, a period of nearly unloaded active shortening was allowed for 100 ms, followed by re-stretch to the original isometric sarcomere length. After a waiting period during which isometric force redeveloped to its steady state level, a new cycle of five ramp-shaped releases was started. The protocol of unloaded shortening and re-stretching after five cycles of ramp-shaped releases and re-stretches was done to stabilize fiber structure and to avoid accumulation of disarray of the sarcomeres during prolonged activation of skinned fibers (Brenner, 1983). The complete procedure (isometric shortening with re-stretch, followed by 5 ramp-shaped releases) was repeated 28 times for each single fiber array, except for some experiments where the procedure was terminated after 14 cycles due to development of fiber instabilities. The overall length of the single fiber array and the signal of the force transducer were recorded throughout the entire experimental protocol. During each of the ramp-shaped releases five X-ray diffraction images were recorded in defined time frames with exposure times ranging from 2 to 4 ms (Fig. 16):

Time frame I - shortly before the start of the release, i.e. at constant length representing isometric steady-state conditions (exposure time 3 ms).

Time frame II - during the first rapid force decline before the force reaches a plateau (exposure time 2 ms).

Time frame III - after the force plateau, i.e. during a second period of force decline (exposure time 3 ms).

Time frame IV - following time frame III with a pause of less than 0.1 ms (exposure time 3 ms).

Time frame V - immediately before the end of the release, exposure time 4 ms.
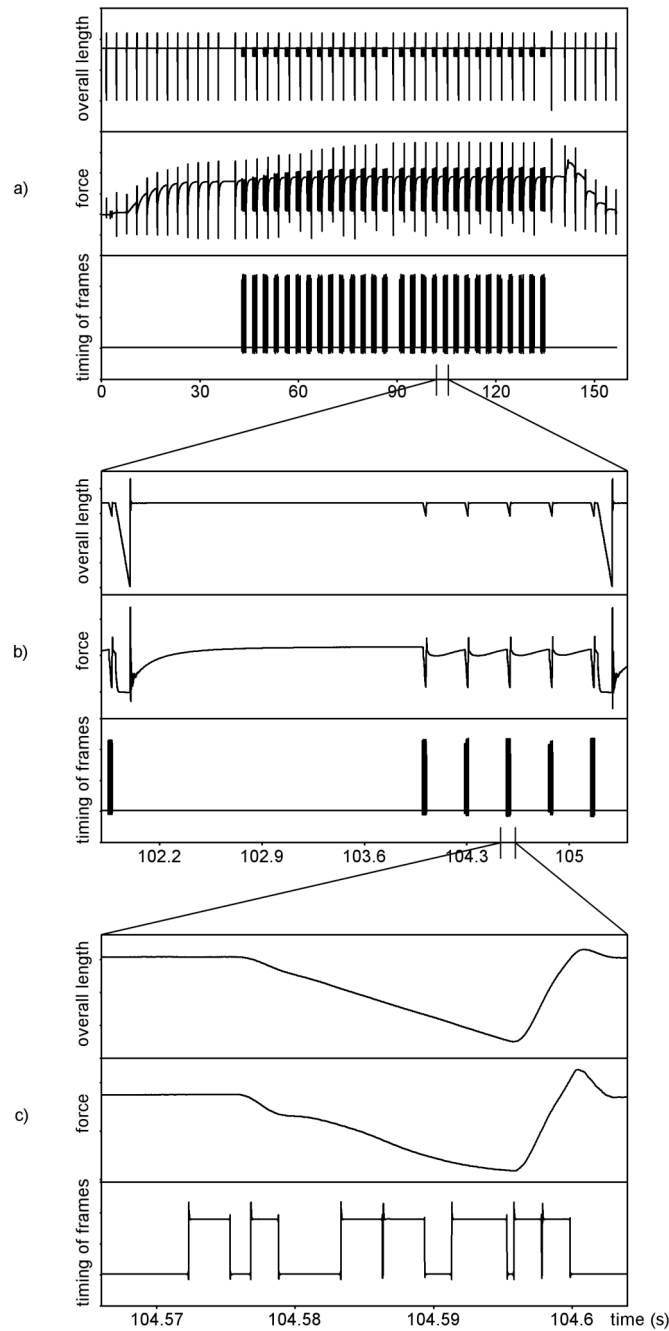
*Fig. 16: Experimental protocol shows the timing of the mechanical maneuvers and collection of diffraction patterns. Panel a) shows the overall length (top trace), force (middle trace) and timing of frames of x-ray patterns (lower trace). The panel shows the whole 160 seconds of the protocol on each single fiber array. Panel b) is the expansion of one cycle of isotonic release, re-stretch with recovery of isometric force and the 5 small ramp-shaped releases imposed after force has reached its steady state level. Panel c) is an expanded view of one small ramp-shaped release followed by re-stretch to starting length.*

**Data reduction and analysis**

X-ray diffraction images recorded in corresponding time frames during each of the 5 x 28 ramp-shaped releases were added up to increase the photon count. The whole protocol was repeated with six activated single fiber arrays and the resulting six images were added up after careful alignment of the individual patterns (see below). Diffraction patterns with the same time frames and the same timing protocol were also recorded from fibers in relaxing (4 experiments) and in rigor solution (5 experiments), but without any length changes imposed on the fiber arrays (no ramp-shaped releases and re-stretches; no large scale releases as for isotonic condition). To obtain comparable intensity levels, the accumulated photon counts were divided by the number of experiments carried out for each condition (activated, relaxed, rigor) and also divided by the shutter open time of each of the fife time frames.

After the initial pooling of corresponding time frames in the single experiments, the resulting images were corrected for dead time of the detector using the routine DTC developed by the SRS (Lewis et al., 1999). Next, uneven sensitivity of the detector was compensated by dividing each image by a flat-field image recorded with the detector while the beam was widely scattered by air upon removal of the evacuated beam pipe between sample position and detector. Finally, each image was carefully rotated and centered before adding up corresponding images of the different fiber arrays. Programs from the CCP13 software suite of the SRS Daresbury were used for this purpose. Signal-to-noise ratio for the first myosin and first actin layer-line was increased by folding the diffraction patterns along the equator, i.e. using the sum of the measured intensity values above and below the equator.

The scale for the inverse spacing in the diffraction patterns was calibrated by assuming that the position of the M3 reflection on the meridian for fibers in rigor condition is $1/14.43$ $nm^{-1}$ (Xu et al., 1997, Huxley and Brown, 1967).

A 1D profile of the equator, including the 1,0 and 1,1 reflections (Fig. 17), was obtained by vertical integration (see Fig. 17 C), using the program BSL from the CCP13 suite.

A rectangular section of the most intense region of the first myosin and first actin based layer line, labeled A in figure 17, was integrated horizontally to obtain a 1D profile of this segment of the two layer lines. The integration covered the region from radial inverse spacing of $0.039$ $nm^{-1}$ to $0.06$ $nm^{-1}$. This range was chosen because (i) the intensity increase of the first actin based layer line during contraction is largest (Bordas et al., 1999) and (ii) actin and myosin components are well separated from the troponin

reflection on the meridian which overlaps with the first actin and first myosin based layer line in the range nearer to the meridian.

The 5.9 and 5.1 nm actin layer lines (ALL6 and ALL7 respectively) were integrated horizontally within a rectangular area containing both layer lines, as shown in figure 17.
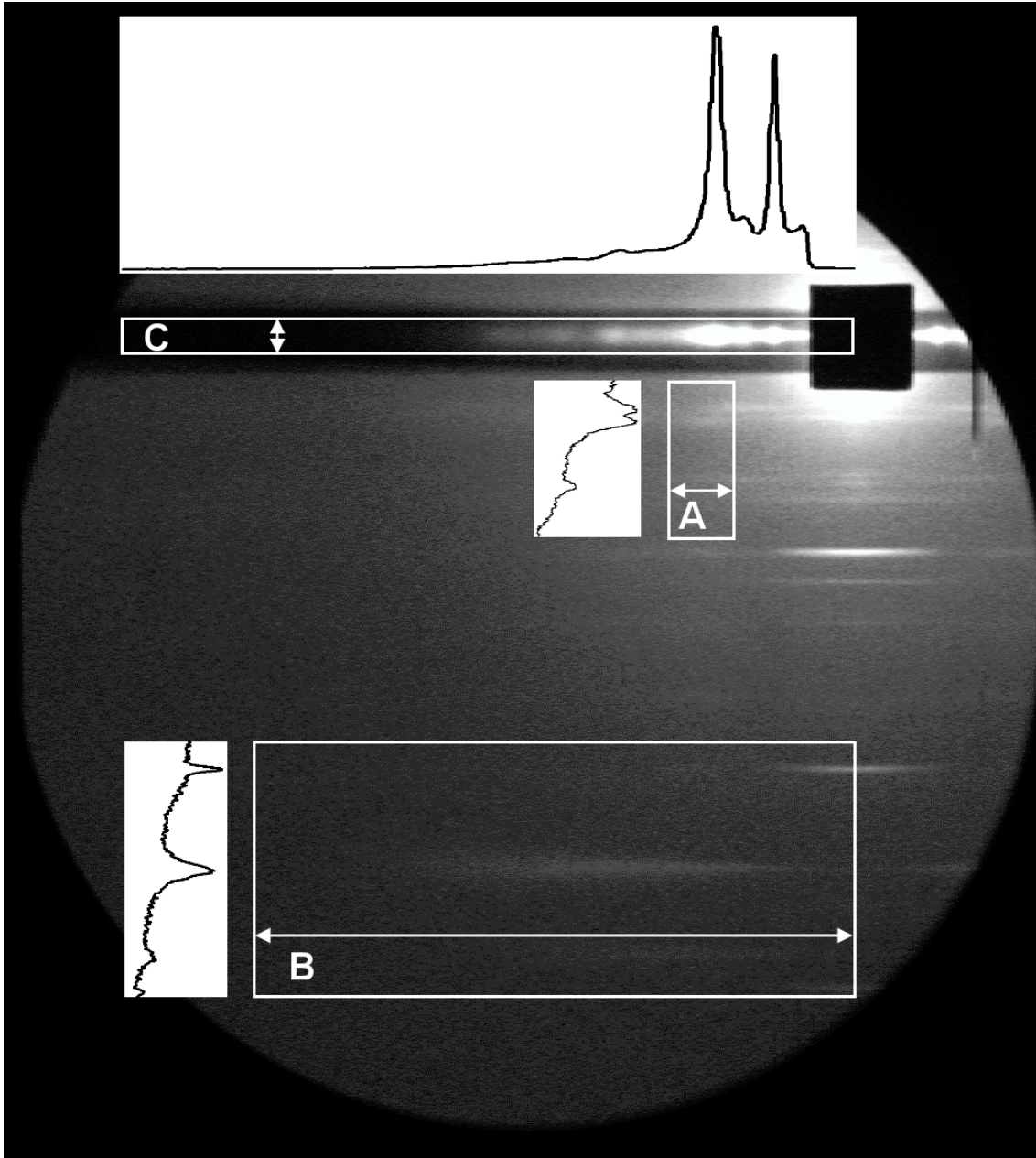


*Fig. 17: Investigated areas. In order to obtain 1D profiles, rectangular areas of interest (A-C) were defined. Within areas of interest, integration was performed by adding up intensity values along a pixel line or row line as indicated by the double arrows, i.e., the intensity profile of the equator was obtained by vertical integration, the other two profiles by horizontal integration.*

A function consisting of the sum of an appropriate number of Gaussian peaks (one for each reflection) and one exponential decay (for the background) was fit to the 1D intensity profiles using the software ORIGIN (OriginLab Corporation, Northampton, MA). The fitting functions and used parameters for profiles with two and profiles with four peaks are described in the appendix. An example for fitting of the first actin and first myosin based layer line (profile A from figure 17) is shown in figure 18. The area of each individual peak was obtained from the least-square fit. As the precise point-spread function of the beam is not known, data were also fit with Lorentz-peaks instead of Gaussian peaks. However, least-square fitting with Lorentz-peaks produced higher chi-square values (data not shown), while the areas obtained with the Gaussian peaks represent fairly well the intensities of the actual reflections (Fig. 18).
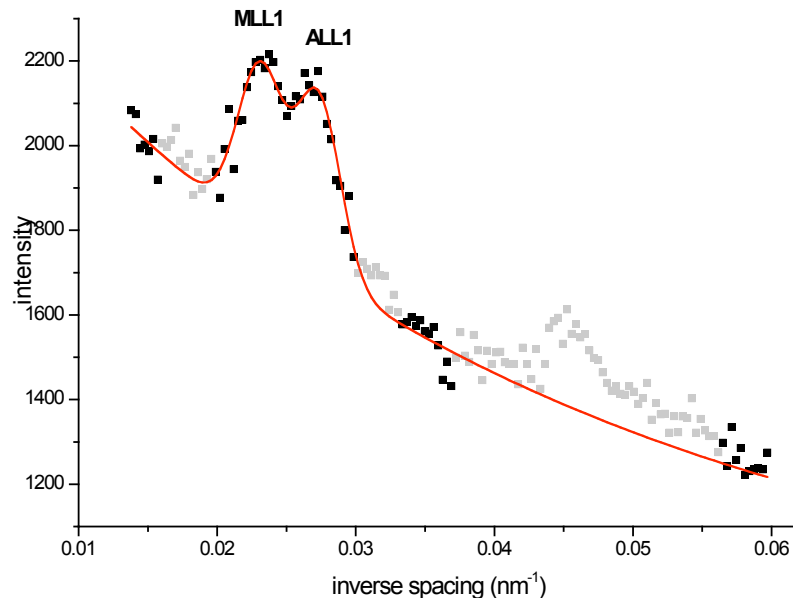


*Fig. 18: One-dimensional intensity profile of MLL1 and ALL1. Profile obtained by horizontal integration of region A defined in figure 17. The black and gray squares represent intensity values for each detector raster line of the integrated profile. The gray dots were suppressed during fitting, as they could be part of other reflections. The ranges of the suppressed dots were kept the same for all analyzed profiles. Continuous line: Fit of MLL1 and ALL1 with a function that consists of the sum of two Gaussian peaks and one exponential decay (for the underlying background).*

The fitting procedure was performed for the five patterns recorded in time frames I to V before and during the ramp-shaped release imposed on the activated fibers. For the patterns recorded under relaxed and rigor conditions, without the mechanical maneuvers, intensity values were obtained from each of the time frames by the same procedure. Since no mechanical maneuvers were imposed, these intensity values were used to calculate mean value and standard deviation for both relaxed and rigor conditions. A weighted mean of the standard deviation for relaxed and rigor intensities was taken as an error estimate for the intensity values obtained from the active fibers in time frame I to V.

## Static patterns recorded at the Synchrotron Radiation Source (SRS), Daresbury, UK

### X-ray diffraction and experimental protocol

Two-dimensional X-ray diffraction patterns of single fiber-arrays were recorded under relaxing conditions, in rigor, and in the presence of 1000, 100 and 20 μM MgATPγS, using a position sensitive multiwire detector at station 2.1 of the SRS at Daresbury, UK, (Kraft et al., 2002). All MgATPγS solutions contained saturating $Ca^{++}$ concentrations (pCa 4.5).

### Data reduction and analysis

The recorded images were corrected for unevenness of the detector using a detector response pattern obtained by irradiation with a radioactive $^{55}Fe$ source. The patterns were then normalized to the intensity of the main beam monitored through a semitransparent beam stop. Camera background including solution scattering was recorded after removal of the muscle fibers, while the solution chamber stayed in place. The background was then subtracted from the recorded diffraction patterns. After rotation and centering, the images were folded along the equator and meridian, i.e. the intensities at corresponding positions in all four quadrants were added up. For each of the investigated states (relaxed, rigor, 1000, 100 and 20 μM MgATPγS) diffraction images from five single fiber arrays were added up to increase signal-to-noise ratio.

One-dimensional profiles of the equator, the first myosin and first actin based layer line, the meridian and the 6th actin based layer line were calculated by integrating corresponding areas at the same inverse spacings as used for the time-resolved patterns

recorded at the ESRF, Grenoble. The intensities and standard errors of the investigated reflections and layer lines were obtained by least-square fitting, as described above.

**Intensity profiles along the sixth actin layer line**

Intensity profiles along the sixth actin layer line (ALL6) were obtained in the following way: It was assumed that sufficiently narrow strips in the middle between the 5th and the 6th and between the 6th and the 7th actin layer lines do not contain any intensities from other layer lines. Accordingly, they should contain only background information. For the static diffraction patterns (recorded in Daresbury) 0.0027 $nm^{-1}$ was chosen as the width of these strips, whereas for the time-resolved patterns (recorded in Grenoble) wider strips of 0.0048 $nm^{-1}$ were necessary because of the higher noise in the patterns (see Fig. 19).

The two thus defined background strips, flanking the sixth actin layer line on both sides, were integrated in the axial direction to obtain radial 1D-profiles. The background profiles were smoothened by calculating a rolling average applied to the sum of the two background strips and stretching over 40 points in the case of the static patterns and 200 points in the case of the time-resolved patterns.

The area lying in-between the background strips, containing the ALL6, was integrated axially to obtain a radial 1D-profile. The width of the integrated strip was in the case of the static patterns 0.028 $nm^{-1}$, and in the case of the time-resolved patterns 0.024 $nm^{-1}$.

For each of the static patterns the background-subtracted profile of ALL6 was obtained by subtracting the appropriate proportion of the background strips from the strip containing the ALL6. Because of the higher recording noise of the time-resolved patterns, the strip containing the ALL6 in each pattern was not subtracted by the background strips from the same pattern (as was the case for the static patterns) but by the average of the background strips from all seven time-resolved patterns recorded in different time frames. This was done assuming that the background did not change substantially throughout the release and re-stretch procedure. Small standard deviations (0.61% of the total intensity, 0.64% of the intensity of the first third, 1.12% of the intensity of the second third) of the background strips from all seven time frames vindicate this assumption. These standard deviations compare well to the standard deviation of the intensity of the most intense 1,0 and 1,1 reflections on the equator (about 1%) recorded under static conditions, where no mechanical maneuvers were performed.

The background-subtracted ALL6 profiles were smoothed by rolling average of 20 and 100 points, for the static and the time-resolved patterns, respectively.
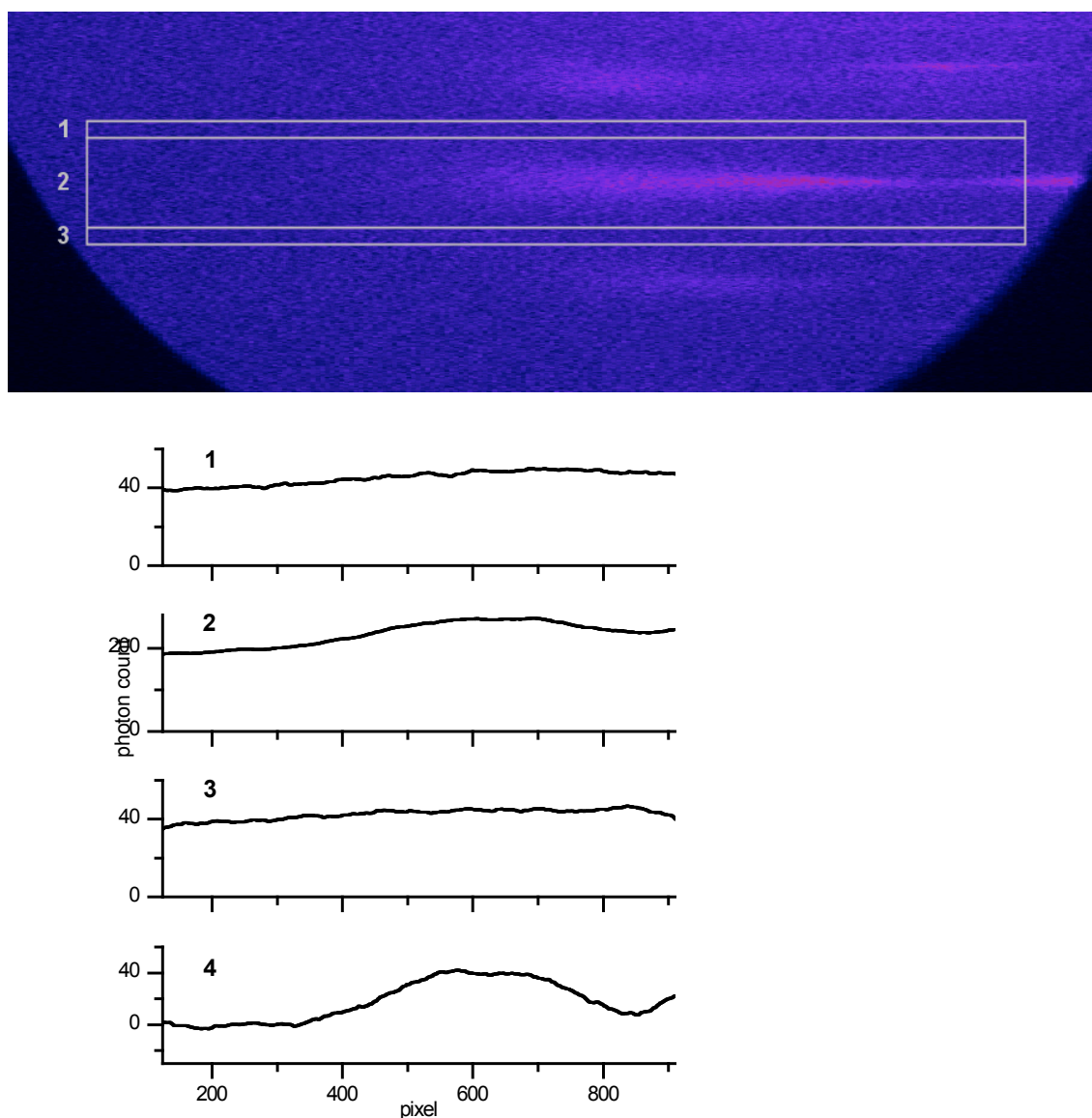


*Fig. 19: Background subtraction for the profile of the sixth actin layer line. The rectangles in the 2D X-ray diffraction pattern enclose the regions taken for the background strips (1 and 3) and the region containing the layer line (2). The profiles along the strips 1 to 3 are shown in the traces 1 to 3 of the diagram. Trace 4 is the profile of the layer line obtained by subtracting trace 1 and 3 from trace 2 divided by appropriate factors corresponding to the widths of the strips.*

# Results

## *Two-dimensional X-ray diffraction patterns*

Diffraction patterns for decreasing MgATPγS concentrations show increasing rigor features (figure 20). Different MgATPγS concentrations seem to produce mixtures between the patterns recorded at rigor and relaxed condition. This correlation is expected from the fact, that with different MgATPγS concentrations different proportions of strongly bound myosin heads in rigor conformation and myosin heads in a weak binding state are generated (Kraft et al., 2002). Features that are obviously sensitive to the proportion of rigor heads are (i) the intensity of the equatorial 1,0 and 1,1 reflections, (ii) the intensity of the first actin layer line (ALL1) and (iii) the extent of lattice sampling on it, and finally (iv) the intensity and radial profile of the sixth actin layer line (ALL6). Patterns recorded in the time resolved experiments under rigor and relaxed condition at the ESRF show the same features as the corresponding ones recorded in the static experiments at the SRS. Due to a much smaller size of the focus at the detector at the ESRF, details of the time-resolved 2D patterns, like width of the layer lines, lattice sampling spots, equatorial reflections etc., are much better resolved at figure 21. From looking at the presented patterns of the time-resolved experiments for activated fibers during time frame I and time frame III no obvious increase in rigor features is visible. However, less obvious changes are possible. i.e., the proportion of the rigor heads might rise minutely from time frame I to time frame III. Therefore, a quantitative analysis and comparison of properly determined describing indicators for rigor features is necessary.

For such a detailed analysis we have chosen the following indicators: (i) the ratio of the equatorial 1,1 and 1,0 intensities ($I_{1,1}/I_{1,0}$), (ii) the intensity of the first actin layer line, (iii) the intensity and profile of the sixth actin layer line.

A: relaxed



D: 20 µM MgATPγS



B: 1000 µM MgATPγS
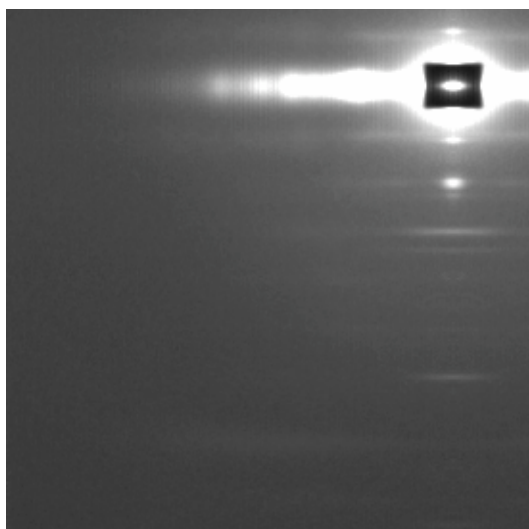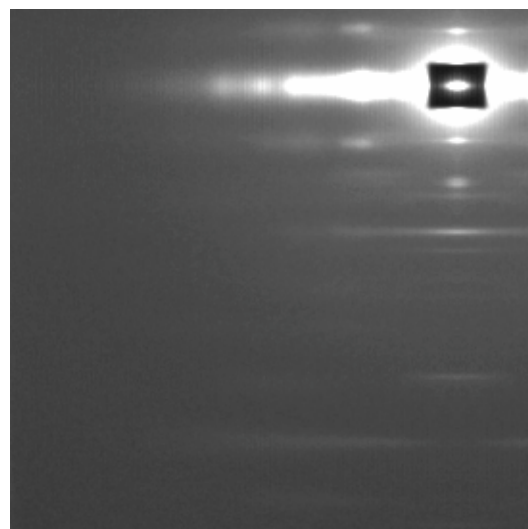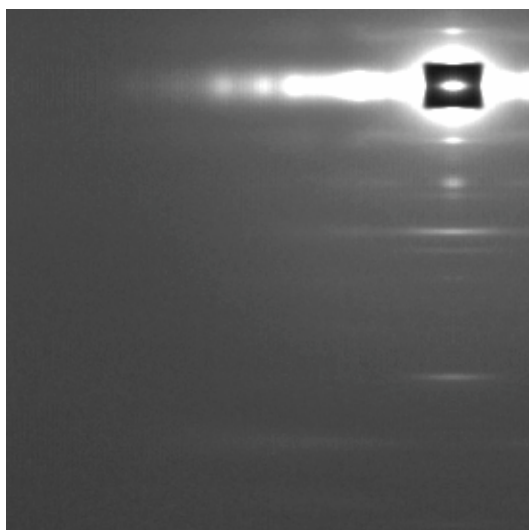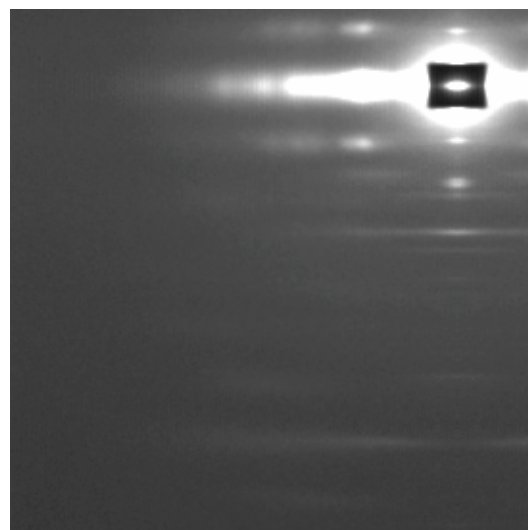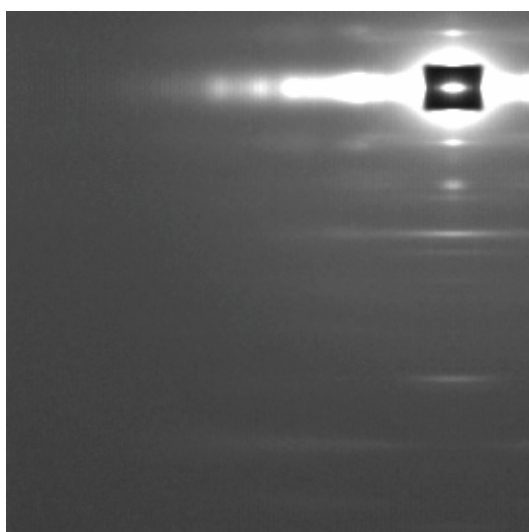


E: rigor

*Fig. 20: 2D X-ray diffraction patterns recorded in the static experiments in relaxing condition (panel A), with different concentrations of MgATPγS (panels B through D) and in rigor (panel E). In the latter the typical rigor features are visible. In panels B to D, the rigor features become increasingly apparent with decreasing MgATPγS concentrations.*



C: 100 µM MgATPγS
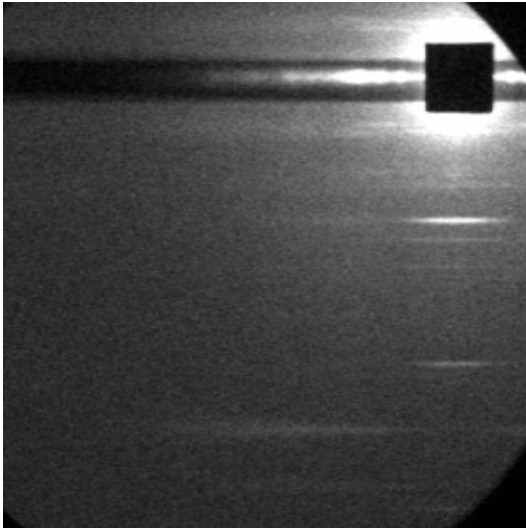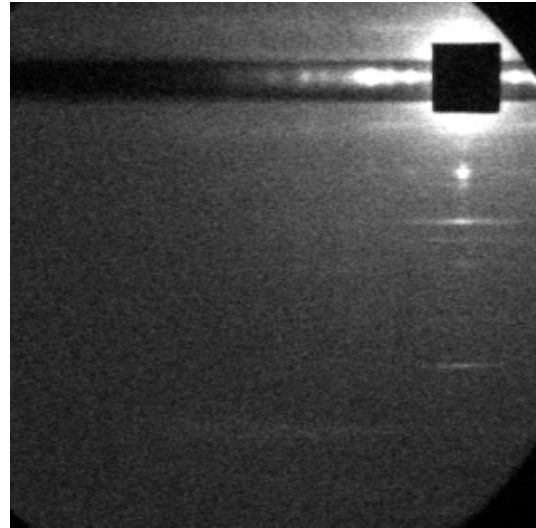
A: time frame I



D: relaxed
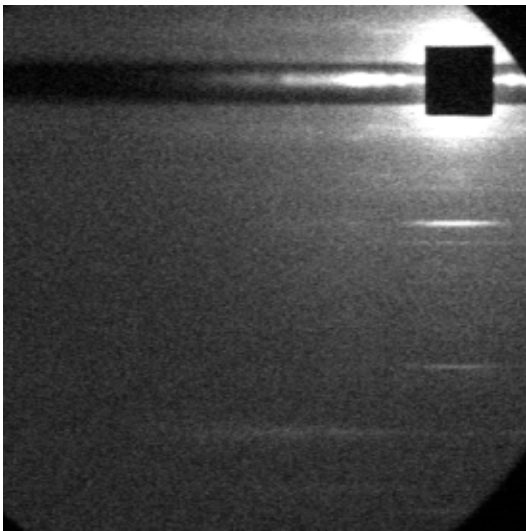


B: time frame II
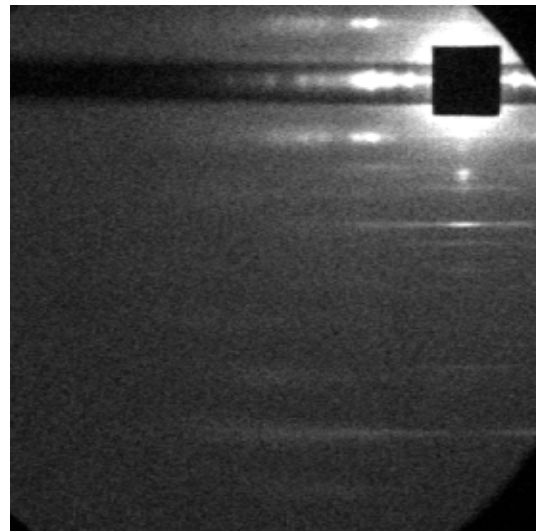


E: rigor
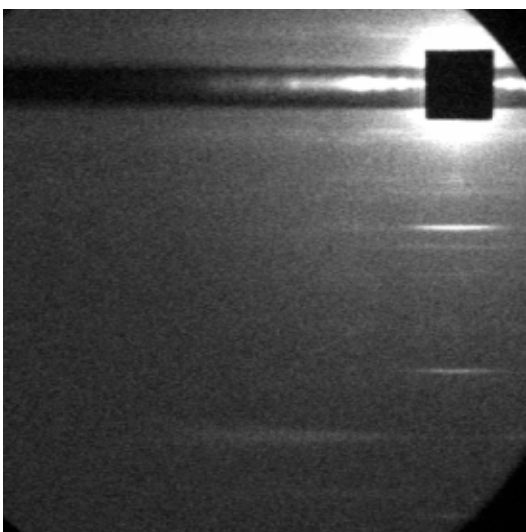


C: time frame III

*Fig. 21: 2D X-ray diffraction patterns recorded in the time-resolved experiments. Panels A, B and C show patterns taken before the start of the ramp-shaped release, early in the release and late in the release, respectively. Panels D and E show patterns of the fibers in relaxing condition and in rigor, respectively. When comparing the patterns in panel A, B and C of this figure with patterns taken during the static experiments and at different concentrations of MgATPγS (Fig. 20), no appearance of rigor features is detectable during the ramp-shaped release.*

## $I_{1,1}/I_{1,0}$

The ratio of the equatorial reflections, $I_{1,1}/I_{1,0}$, was measured to be 2.9 in rigor and 1.1 in relaxing condition (figure 22, a, left) at the ESRF and 2.3 and 1.2 respectively (figure 22, a, right) at the SRS. In the static patterns recorded at the SRS (figure 22, a, right) the measured $I_{1,1}/I_{1,0}$ reflects the different proportions of nucleotide free myosin heads stereospecifically attached to actin at different MgATPγS concentrations. In the time-resolved patterns of the activated fibers recorded at the ESRF (Fig. 22 a, left panel), the $I_{1,1}/I_{1,0}$ values for isometric condition (time frame I) and at the beginning of the ramp-shaped release (time frame II) do not differ significantly. This is followed, though, by a substantial increase at the transition from time frame II to time frame III (black squares in figure 22 a, left panel) from 1.87 to 1.98. The overall changes are small and are resolved more clearly when the data are shown on an expanded scale (inset figure 22 a, left panel). The $I_{1,1}/I_{1,0}$ ratios from static patterns in rigor and under relaxing condition, recorded at the ESRF are shown by the red and green symbols, respectively.

The error estimation for $I_{1,1}/I_{1,0}$ obtained for the activated fibers for time frames I to V was calculated from the scatter of the value for patterns recorded from fibers in rigor and relaxing conditions. As the 1,0 and 1,1 reflections produce a very high signal on the detector, the error associated with the measured intensities is very low. For the ratio $I_{1,1}/I_{1,0}$ it is about 0.7%. It is also much lower than the nearly 6% change in the ratio occurring from time frame II to time frame III.
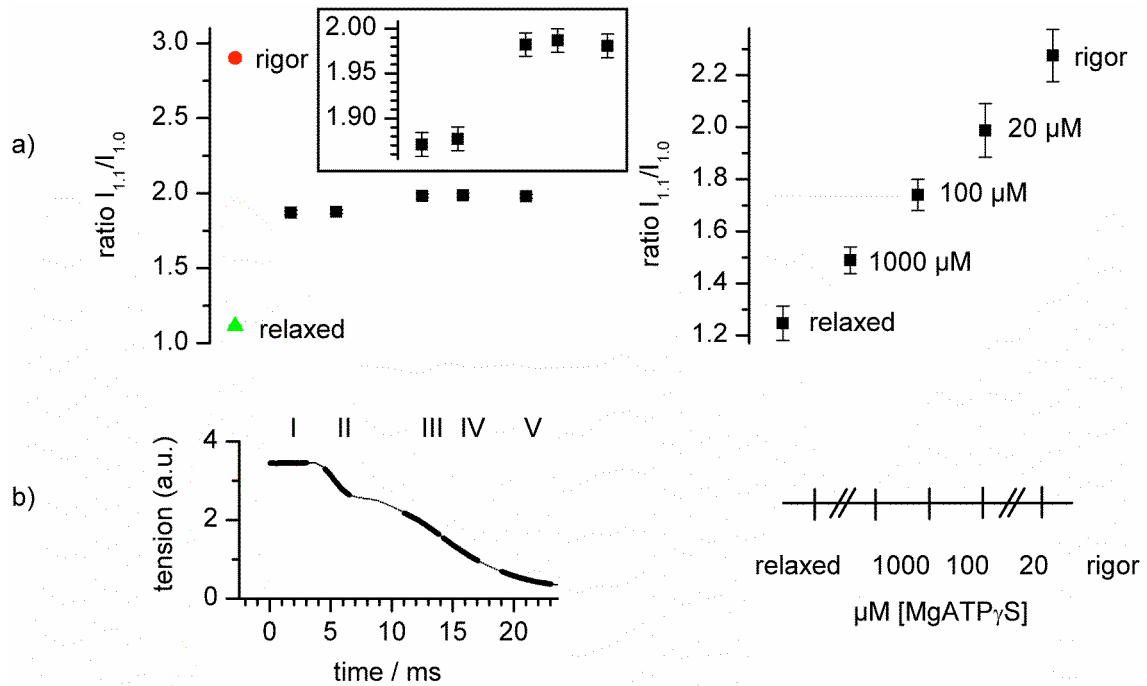
*Fig. 22: Ratio of equatorial 1,1 and 1,0 intensities ($I_{1,1}/I_{1,0}$). Left column: a) Ratio $I_{1,1}/I_{1,0}$ of the time-resolved patterns recorded at the ESRF. Squares represent the ratio $I_{1,1}/I_{1,0}$ for activated fibers before and during the ramp-shaped release. Data-points are plotted above the mid points of the time frames I to V: I - immediately before the release, II - at the beginning of the release, III - early after the force-plateau, IV - later after the force-plateau, V - at the end of the release. Triangles represent mean values obtained from all time frames recorded under relaxing conditions; circles represent mean values recorded under rigor conditions. Error bars are calculated from values at the different time frames in rigor and relaxation where fibers were held at a constant length. The size of the error bars on the squares is the weighted mean of the error of the relaxed and rigor conditions. Error bars are often smaller than the symbol size. In the inset in graph a) the ratio values for the activated fibers in the time frames I to V are shown on an enlarged scale. b) The time course of the fiber tension, shown at the bottom of the left column indicates the timing of the exposure intervals (time frames I to V), during which the five patterns were recorded. The time frames are illustrated by the solid segments of the force trace. Right column: Ratio $I_{1,1}/I_{1,0}$ of the static patterns recorded under (from left to right) relaxing conditions, with 1000 μM MgATPγS, 100 μM MgATPγS, 20 μM MgATPγS, and in rigor. Error bars represent the standard error of the fit, calculated by the fitting software.*

## *ALL1*

For the static patterns recorded at the SRS, the intensity distributions along the first actin layer line (ALL1) (figure 23, upper panel) show a continuous increase in the intensities of the maxima reflecting lattice sampling. The intensity maxima are lowest under relaxing conditions and become more and more prominent from 1000 µM MgATPγS through 100 and 20 µM to 0 µM, i.e., rigor condition. The increase of ALL1 intensity after subtraction of background is associated with an increasing number of nucleotide free, rigor cross-bridges. However, for the patterns recorded during isometric contraction and the ramp-shaped release (frames I to V of the time resolved experiments, figure 23, lower panel), no larger change in the peak intensities is visible. Only the profile of the rigor condition shows the same typical shape as seen in the static experiments. Note, however, the better details in the patterns recorded at the ESRF. This is due to the much sharper focus at the ESRF beam line. Thus, various parts of the lattice sampling are less "smeared out" and more distinct than in the data from the beam line 2.1 of the SRS.
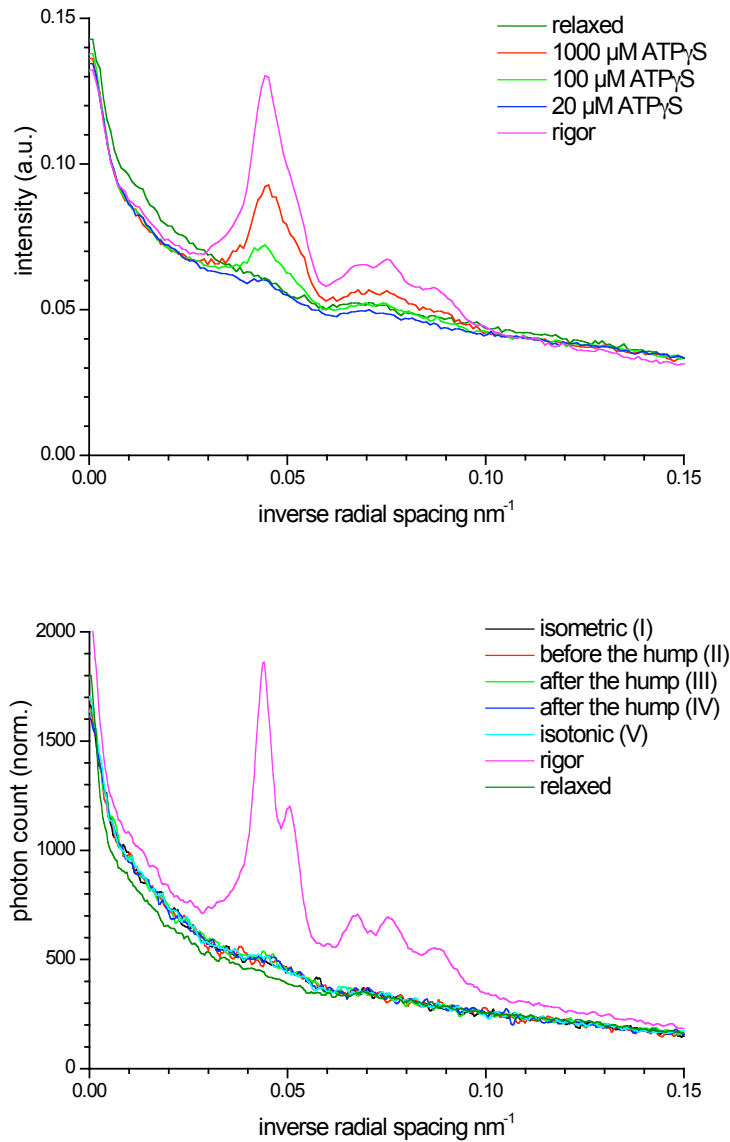
*Fig. 23: Radial profiles of ALL1, i.e., intensity distribution along the ALL1, obtained by integration in the axial direction within a strip ranging from 0.025 nm$^{-1}$ to 0.029 nm$^{-1}$ inverse radial spacing. Note, that the profiles are obtained from 2D diffraction patterns with no prior background subtraction. They, therefore, include a background, which gradually and asymptotically decreases in the direction of higher inverse radial spacing.*

Figure 24 compares the intensities of the first actin layer line (ALL1) and the sixth actin layer line (ALL6). The intensity values are obtained from the interval 0.039 to 0.06 nm$^{-1}$ of inverse radial spacing after subtraction of background and the component of the first

myosin layer line, as described in the Materials and methods part of this thesis (see also Fig. 17). Data recorded at the ESRF during the ramp-shaped releases of isometrically contracting fibers is shown in the left column, data recorded at the SRS on fibers incubated with different MgATPγS concentrations are shown in the right column of figure 24. In both columns, the intensities from patterns recorded under rigor and relaxing conditions are also shown for reference. The data are scaled and displayed such that for both, left and right hand graphs in each panel the difference between rigor and relaxing conditions are identical. This allows to compare changes observed during the ramp shaped releases with the changes seen when the fraction of nucleotide free, rigor cross-bridges was increased by lowering the concentration of MgATPγS.

The intensity of ALL1 for the activated fibers (Fig. 24, a, left panel) is overall somewhat higher than under relaxing conditions, as was shown before (Kraft et al., 2002). In contrast, the intensity of ALL1 is nearly 15-fold larger under rigor conditions. Accordingly, the MgATPγS titration shows an increasing intensity of ALL1 when MgATPγS concentration is reduced, consistent with an increasing number of nucleotide-free rigor-like myosin heads as MgATPγS-concentration is reduced. This very large increase in the ALL1 in rigor and when MgATPγS-concentration is low reflects the increasing lattice sampling on the ALL1, which at least in rabbit psoas is typical for rigor-like cross-bridge attachment. Compared to the large increase in intensity in rigor and at low MgATPγS concentration, only a very small increase in ALL1 intensity is seen between frame II and III during the ramp-shaped releases of the activated fibers. This increase in intensity between frame II and III becomes only detectable on an expanded intensity scale (see inset). It is just about 2% of the intensity in rigor. During the further release (time frames IV and V) the intensity of ALL1 decreases to finally reach a slightly lower intensity than during isometric steady state contraction. Overall, the changes of ALL1 during the release are very small. Nevertheless, the changes might indicate minor changes in the number of stereospecifically attached cross-bridges during the release.
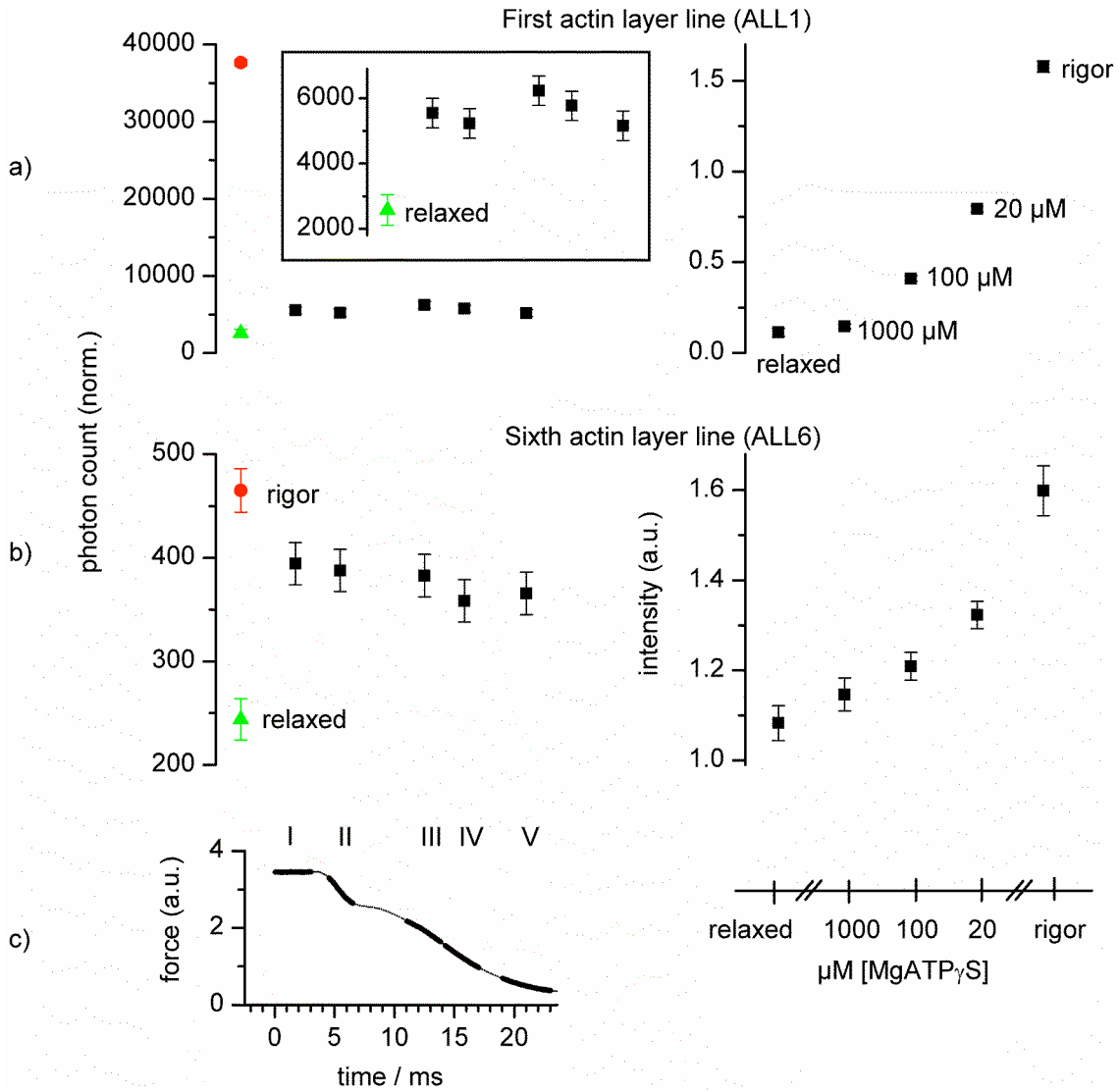
*Fig. 24: Intensity of first (a) and sixth (b) order actin based layer-line. Left column: Intensities of layer-lines in the time-resolved patterns recorded at the ESRF. Squares represent intensities of activated fibers before and during the ramp-shaped release. Data-points are plotted in the same way as in figure 22. Triangles represent mean intensities obtained from all time frames recorded under relaxing conditions; circles represent mean intensities recorded under rigor conditions. Error bars are obtained in the same way as in figure 22. Intensity values are recorded photon counts that have been normalized to different numbers of experiments during active contraction, in rigor and under relaxing condition (see methods). The inset in graph a) shows the intensities of ALL1 for the activated and relaxed fibers on an expanded scale. The time course is the same as in figure 22. Right column: Intensity data (figure legend continues)*

*(figure legend continued) of the same layer lines in patterns recorded under (from left to right) relaxing conditions, with 1000 μM MgATPγS, 100 μM MgATPγS, 20 μM MgATPγS, and in rigor. Error bars represent the standard error of the fit, calculated by the fitting software. Intensity values are in arbitrary units.*

## ALL6

The total integrated intensity of the sixth actin layer line (Fig. 24 b, left panel) was obtained after background subtraction for the area of the complete layer line as illustrated in figure 17 (area B). It is significantly higher during active contraction than under relaxing condition, as shown before (Huxley and Brown, 1967; Kraft et al., 2002). Under rigor conditions, the intensity is even higher. The total ALL6 intensity for the activated fibers shows a slight decrease in the course from time frame I to time frame V, away from the rigor intensity towards the relaxed intensity. With decreasing MgATPγS concentration and hence increasing proportion of myosin heads attached to actin in rigor-like conformation, an increase of the total ALL6 intensity is recorded (Fig. 24, b, right panel). The actually recorded slight decrease of total ALL6 intensity during the release stands, therefore, in contradiction to an increase in rigor-like myosin heads.
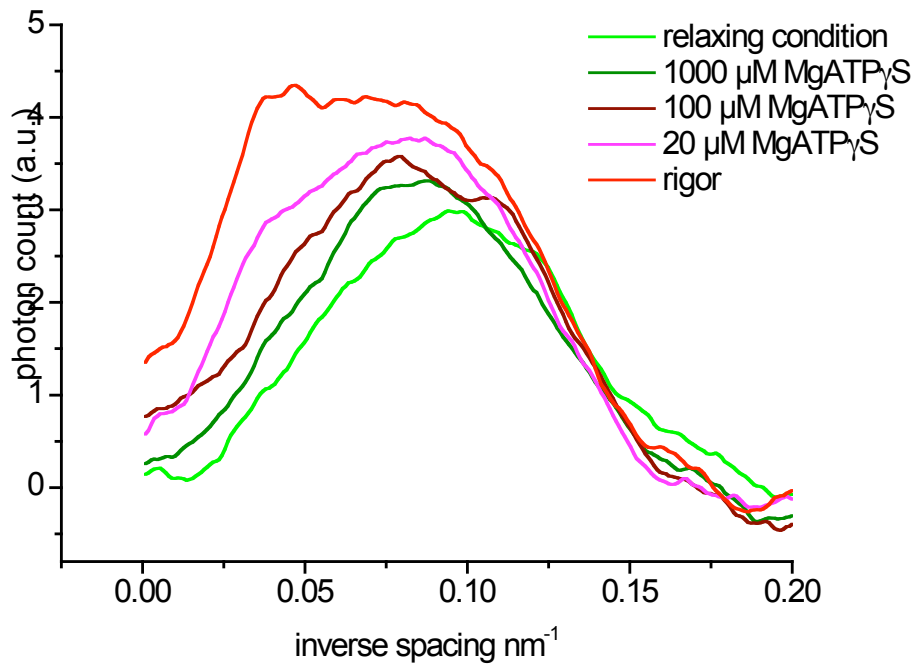
*Fig. 25: Intensity distribution along the ALL6 after background subtraction, from the static experiments with different MgATPγS concentrations and in rigor and relaxing condition. The series of intensity profiles show the sensitivity of the near-meridian part of the ALL6 intensity profile to different proportions of cross-bridges in a rigor-like conformation.*

To further investigate the discrepancy between the behavior of ALL1 and ALL6 during the ramp-shaped release, the profile of ALL6 in the radial direction, i.e. in the direction parallel to the equator, was analyzed. Different proportions of rigor-like cross-bridges versus weakly bound cross-bridges, as obtained with the MgATPγS titration, produce different ALL6 profiles (see Fig. 25). With more rigor-like cross-bridges the maximum of the profiles moves nearer to the meridian, as was observed earlier (Kraft et al., 2002). The part of ALL6 nearer to the meridian (particularly for inverse spacings up to 0.08 nm$^{-1}$) is intensified, while the shape of the profile for inverse spacings > 0.10 nm$^{-1}$ seems mostly unaffected by the different proportions of rigor versus weakly bound cross-bridges. Figure 25 clearly indicates that there is a positive correlation between the proportion of cross-bridges with rigor-like conformation and the near-meridian intensity of ALL6, at least within the interval from 0.02 nm$^{-1}$ to 0.08 nm$^{-1}$ inverse radial spacing.
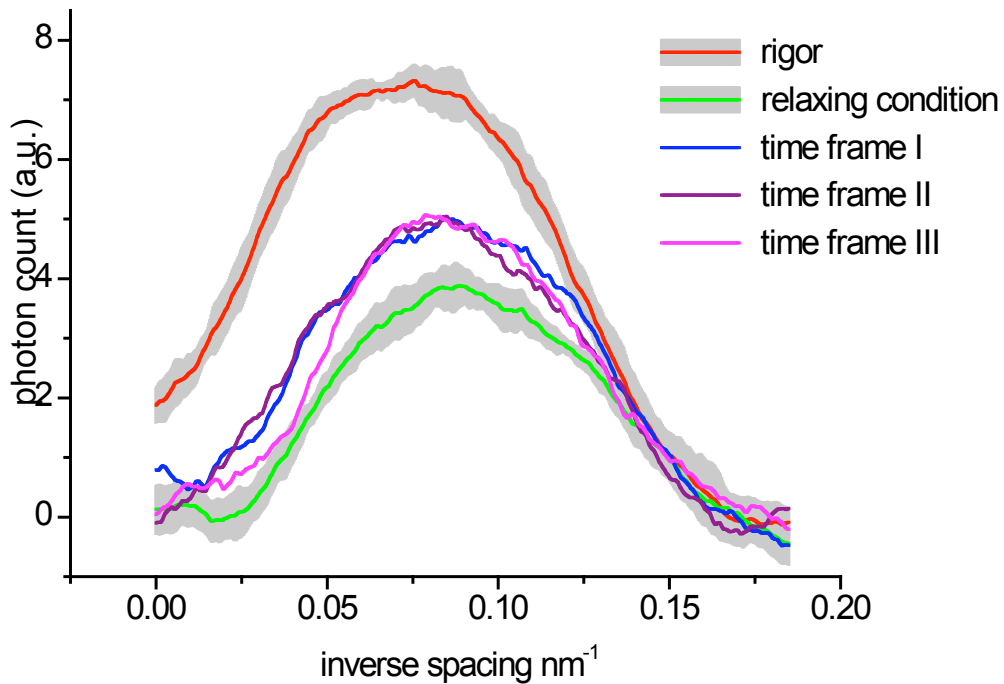
*Fig. 26: Time resolved patterns - background subtracted profiles of ALL6 in rigor and relaxing conditions as well as for the time frames I, II and III of the activated fibers subjected to ramp-shaped releases. The solid lines for rigor and relaxed conditions represent the average of all seven profiles recorded in the different time frames without imposed releases. The half width of the gray bands is the root-mean-square of the difference of the individual profiles from the average profile.*

Diffraction patterns recorded from fibers in the time-resolved experiments performed at the ESRF yielded the same characteristic difference in the ALL6 profile for rigor and relaxing conditions (figure 26) as shown for the patterns recorded at the SRS (figure 25). The profile under rigor condition has a maximum nearer to the meridian and substantially higher intensities in the near-meridian part, particularly for inverse spacing up to 0.08 nm$^{-1}$.

As the patterns for rigor and relaxing conditions were recorded in seven different time frames but without any length-change, the recording noise of the profile could be estimated from the variability of the seven individual profiles. Figure 25 visualizes the amount of recording noise by gray bands encompassing the average profiles for rigor and relaxing conditions.

For the activated fibers different profiles were recorded in time frames I to V (figure 26 - time frames IV and V omitted for clarity) before and during the ramp-shape length release. These profiles show distinct differences depending on the time frame they were taken in. While the profiles for time frame I and II follow essentially the same course, the profile of time frame III shows smaller intensities for inverse spacings up to 0.08 $nm^{-1}$, contrary to the course that would have been expected if the proportion of rigor-like cross-bridges had been higher during time frame III.

Integrated intensity-values of the background-subtracted ALL6 profiles were obtained for inverse radial spacing ranging from 0.02 to 0.08 $nm^{-1}$. This interval was chosen because the MgATPγS titration (figure 25) showed a positive correlation between the proportion of rigor-like cross-bridges and intensity for every value on the inverse spacing axis in this interval. Table 1 shows the integrated intensity-values for the time frames I to V of the activated fibers. The integrated intensity drops substantially from time frame II to time frame III. This coincides with the end of the pause in the tension drop during the ramp-shaped length release (compare figure 22 b), the time at which redistribution of cross-bridges to later states in the cross-bridge cycle was shown to have come to an end (Brenner, 1991).

| Time frame no. | Integrated intensity (a.u.) |
| --- | --- |
| I | 71.93296 |
| II | 75.79543 |
| III | 65.47161 |
| IV | 61.80461 |
| V | 70.74816 |

*Table 1: Intensity of the ALL6 profiles for time frames I to V integrated within the interval from 0.02 to 0.08 $nm^{-1}$ expressed in arbitrary units.*

# Discussion

## *Tension trace indicates structural transition during ramp-shaped releases*

During isometric contraction, transitions within different structural states of the individual cross-bridges occur asynchronously with high rates. By applying a rapid release to activated fibers, a temporary synchronization of these transitions can be achieved (Huxley and Simmons, 1973). During the short ramp-shaped releases of our experiments, the cross-bridges gradually redistributed among different structural states as the muscle fibers shortened. The mechanical maneuver of the release initiates a synchronized transition between different structural states of the cross-bridge. States that are later in the power stroke are preferentially populated by the release. This is because strongly attached cross-bridges become distorted in the direction of fiber shortening by the sliding of the filaments past each other during the shortening. According to Hill, 1974, such distortion in shortening direction is expected to change forward and reverse rate constants of the transitions between the different states of the power stroke such that equilibria of the state occupancies are shifted towards the later states in the power stroke.

In our experiments, tension of the fibers was recorded before and during the ramp-shaped release (figure 2 b). The observed pause in the tension decrease from time frame II to time frame III during the release indicates this redistribution of cross-bridges among at least two structural states during the release, according to the A-B transition described in Brenner, 1991. A substantial population of later states in the power stroke is therefore expected in time frame III.

In later time frames further changes in cross-bridge distribution among different states of the power stroke are expected, because now also (i) some cross-bridges will leave the strong binding states by ending their power stroke and (ii) some cross-bridges will newly enter the early states of the power stroke (Huxley and Simmons, 1971, Huxley and Simmons, 1973). This has been especially indicated in the modeling work of Eisenberg et al., 1980, and Chen and Brenner, 1993. Thus, comparison of frames II and III most exclusively reflects redistribution among strongly bound states of the power stroke with least complications by cross-bridges turnover, i.e., by transitions from

strong binding states back to weak binding states or by weak binding cross-bridges entering strong binding states.

## *Two-dimensional X-ray diffraction patterns show no appearance of rigor features after the pause in the tension decrease during ramp-shaped releases*

If in the redistribution occurring during the ramp-shaped release rigor-like states were preferentially populated, rigor features should be detectable or become more prominent in the 2D-X-ray diffraction patterns. It is known that rigor patterns differ substantially from relaxed and activated patterns (Huxley and Brown, 1967, Huxley, 1968, Kraft et al., 2002). This enhancement of rigor like features should be readily detected as we showed with the change in 2D patterns when MgATPγS concentration is reduced and thus the fraction of nucleotide free rigor cross-bridges increases (see figure 20). To our surprise, however, neither of the patterns recorded in time frames II to V shows much of an appearance of rigor features (figure 21), although late states in the power stroke are increasingly populated during the release.

As a reference, diffraction patterns were recorded from muscle fibers for which we could change the fraction of cross-bridges in a rigor conformation. MgATPγS is a very slowly hydrolyzed ATP-analog. Using sufficiently low but different MgATPγS concentrations, different ratios of nucleotide free rigor cross-bridges versus weak-binding MgATPγS cross-bridges can be obtained (Kraft et al., 2002). The static patterns in figure 20 show a gradual increase in rigor features with the decrease of MgATPγS concentration. In particular, an appearance of lattice sampling on the ALL1 and a strong overall increase in ALL1 intensity is visible. No comparable appearance of such rigor features is visible in the patterns recorded from activated fibers during the ramp-shaped release (see e.g. time frame III versus time frame II in figure 21).

To quantitatively investigate a putative appearance of rigor features during the release, the following indicators were chosen, because they are sensitive to rigor-like cross-bridges: (i) the ratio of the equatorial 1,1 and 1,0 intensities ($I_{1,1}/I_{1,0}$), (ii) the intensity of the first actin layer line (ALL1), and (iii) the intensity of the sixth actin layer line (ALL6).

## Redistribution of masses between myosin and actin filaments

The equatorial 1,0 reflection is produced by diffraction from the 1,0 order lattice plane in the hexagonal matrix of the myofilaments (see figure 10). This lattice plane comprises exclusively myosin filaments, whereas, the equatorial 1,1 reflection is produced by the 1,1 lattice plane that includes both myosin and actin filaments (figure 10). The ratio $I_{1,1}/I_{1,0}$ represents a measure for additional mass near the actin filaments (Brenner et al., 1984). It is also sensitive to the amount of overlap between the two types of filaments in the sarcomere, as well as to lattice disorder of the second kind (Vainstein, 1966). Lattice disorder of the first kind affects both $I_{1,0}$ and $I_{1,1}$ equally and is canceled out in the $I_{1,1}/I_{1,0}$ ratio, whereas the disorder of the second kind has a stronger effect on $I_{1,1}$.

During shortening the amount of overlap of the actin and myosin filaments rises and the lattice disorder decreases as increasingly longer parts of the actin filaments are ordered into the hexagonal lattice. Note that by their anchoring in the square lattice of the Z-disks, actin filaments outside the overlap are displaced from their hexagonal lattice within the overlap area. For static experiments at different sarcomere lengths it was previously shown that $I_{1,1}/I_{1,0}$ increases ~7% per 0.1 μm increase in filament overlap (Brenner, unpublished). Thus, both effects could produce only a slight rise in the ratio $I_{1,1}/I_{1,0}$ since in our experiments the pause in tension drop during the releases occurs at filament sliding of about 5-10 nm/h.s. (Brenner, 1991). Note that the overall length change of the fiber is larger than the length change at sarcomere level. This is due to compliant ends when the fibers are attached to the motor and force transducer. Thus, the correct amplitude of filament sliding is only obtained by measurement of sarcomere length, e.g. by laser light diffraction (see Brenner, 1991).

Thus, the step-wise increase in $I_{1,1}/I_{1,0}$ of about 6% observed between time frame II and time frame III very likely indicates a mass shift from the myosin to the actin filaments during this time-span. This is supported by the fact that this step change coincides with the time of the transition in the tension trace and $I_{1,1}/I_{1,0}$ does not change substantially before and after this transition, while a change in $I_{1,1}/I_{1,0}$ due to filament overlap should be a steady change throughout the ramp-shaped release. Unless the observed change in $I_{1,1}/I_{1,0}$ is caused by a change in the number of myosin heads stereospecifically attached to actin during the release, the noted mass shift must be due to conformational changes of the myosin heads themselves.

## *Number of stereospecifically attached cross-bridges*

Compared to the 15-fold difference from relaxed to rigor intensity of the investigated part of the ALL1, only a slight increase from time frame I to time frame III is observed (Fig. 24 a). This increase is about 2% of the intensity increase when relaxed fibers are put into rigor, i.e., all cross-bridges assume a rigor conformation. All the ALL1 intensities of all five time frames are much nearer to the intensity of relaxed fibers than the rigor intensity, as is typical for isometric steady state contraction (Kraft et al., 2002). This means that if there is an accumulation of rigor-like cross-bridges, it can only be a very slight one. The intensity distribution along the ALL1 is practically independent of axial disorder, but sensitive to transversal lattice disorder, whereas the total ALL1 intensity is not affected by lattice disorder (Koubassova and Tsaturyan, 2002). As we integrated the most intense part of the ALL1 (inverse radial spacing 0.039 nm$^{-1}$ to 0.06 nm$^{-1}$), substantial effects of decreasing lattice disorder during the release are not to be expected. According to Koubassova and Tsaturyan, 2002, lattice disorder influences the sharpness of the sampling peaks on ALL1. Increased lattice disorder "smoothes out" the sampling on the profile of ALL1, whereas decreased lattice disorder increases the sampling peaks and decreases the minima between them. As the intensity distribution of ALL1 in the integrated interval comprises at least two sampling peaks, it can serve as a reliable indicator of the number of stereospecifically attached myosin heads, although slight influences from lattice disorder cannot be ruled out completely. We limited the area of integration to the most intense parts because close to the meridian (inverse radial spacing $<$ 0.039 nm$^{-1}$) a meridional reflection originating from troponin overlaps the ALL1 and would therefore lead to misleading changes in observed intensity.

Assuming that the total intensity of ALL1 is proportional to the square of the number of myosin heads stereospecifically attached to actin, an increase in the in the number of stereospecifically attached heads from time frame I to III of about 1.4% and from time frame II to III of about 4.5% could have occured. Bear in mind though, that the error margins for the observed intensities are of about nearly the same range. So the observed increase of stereospecifically attached myosin heads is hardly significant. The data, though, indicate that detachment of a larger number of cross-bridges does not occur before time frame IV.

## *Structural changes of the cross-bridges*

For an (at least transient) accumulation of rigor-like cross-bridges an increase in total intensity of the sixth actin layer line (ALL6) would be expected, as demonstrated by the increasing ALL6 with decreasing MgATPγS concentration (see figure 24 b, right). Even though the registered decrease in total intensity from time frame I to time frame V is not statistically significant, it still is contrary to a putative accumulation of rigor-like cross-bridges during the imposed ramp-shaped release.

ALL6, however, is very sensitive to structural changes of the cross-bridge. ALL6 intensity profiles obtained from the static patterns at different MgATPγS concentrations (figure 25, Kraft et al., 2002) as well as model calculations (Koubassova and Tsaturyan, 2002) show that with increasing proportion of stereospecifically bound myosin heads in rigor-like conformation the form of the intensity profile along the ALL6 changes. This change is particularly prominent at the shoulder of the ALL6 profile nearer to the meridian (inverse spacing ranging from 0.02 to 0.08 $nm^{-1}$), where the intensity rises with increasing proportion of rigor-like heads (see figure 25). The integrated intensity in this interval, therefore, serves as an indicator for the proportion of myosin heads in rigor-like conformation. Hence, it is of interest to investigate this value also for the different time frames in the time resolved experiments. The intensity values for the activated fibers for time frames I to V are displayed in table 1. We are, of course, particularly interested in the change occurring from time frame II to time frame III in the ramp-shaped releases, as we have already demonstrated that during this period a major redistribution between different structural states occurs.

The question arises, whether the observed large change in the measured intensity (integrated in the above interval) from time frame II (75.79543) to time frame III (65.47161) during active contraction (see table 1) is significant or purely attributed to chance resulting from the recording noise. Therefore, the difference of the integrated intensity from time frame II and time frame III was compared to the amount of scatter in integrated intensities, namely the ones recorded in the same time frames when the fibers were in relaxing and rigor conditions. With these two latter conditions, no length changes were performed during the experimental protocol. Consequently, the scatter in intensity among the different time frames of one condition depicts the degree of noise of the recording. Standard deviations of the integrated intensity of 4.09 and of 4.63 under relaxed conditions and under rigor conditions, respectively, were found.

With this data, as a measure of recording scatter, we investigate statistically the question whether the change in intensity from time frame II to time frame III is significant. Our hypothesis is that the difference between the integrated intensity value for time frame II and the integrated intensity value for time frame III is significant and not accidental. Our null hypothesis is that the two measured intensities are random samples of the same population, i.e. that the true intensities do not differ.

We calculated an estimate for the standard deviation of the population of the activated condition from the standard deviations of the integrated intensities recorded under relaxed and rigor conditions. An estimate of 4.47 was obtained by interpolation, weighted by the integrated intensity values for relaxed and rigor condition.

With this estimate for the standard deviation of the population, a two-sided Gaussian test can be applied for testing our above stated hypothesis. The Gaussian test implies that the test statistic used, i.e.,

$$z = \frac{x_1 - x_2}{\sqrt{2}\sigma}$$

follows a normal distribution, where $x_1$ and $x_2$ are measured values and $\sigma$ is the common standard deviation of both measured values. With the above data and test statistic, the p-value was calculated to be 0.103. The p-value represents the probability that, given the null hypothesis is true (i.e., that the two intensities measured for time frame II and III belong to the same population), the two measured values differ as much as observed in our data or even more.

Assuming the true intensities within the selected ranges of time frame II and time frame III are identical, but are measured with a noise represented by the above standard deviation, then the measured difference would be exclusively attributed to the recording noise. In this case, the probability that the measured or a larger difference in intensity would be just accidental is 0.103.

Alternatively, we can also argue that a one-sided test would be appropriate. From increasing the proportion of rigor like cross-bridges we would originally expect an increase of the integrated intensity of the ALL6 in the investigated interval from time frame II to time frame III, as is the case with the different MgATPγS concentrations (see figure 25). So, we could state as the null hypothesis that the true integrated intensity for time frame III is equal or higher than the one for time frame II. In this case, the p-value obtained from the integrated intensities and the standard deviation estimated

from the relaxing and rigor condition is 0.0515. This means that, given the null hypothesis is true, only a ~5% probability exists to observe the actually recorded or an even larger decrease from time frame II to time frame III.

We could even restrict our criterion by further reducing the inverse spacing interval for intensity integration to 0.03 to 0.07 $nm^{-1}$. This results in a p-value for the one-sided test of 0.0295, which is actually lower than the typical 5% confidence level for hypothesis testing. Thus, with the one-sided test we can reject the null hypothesis (i.e. that the true intensity in this interval remains constant or increases from time frame II to time frame III) with a confidence level of 5%.

Thus, we can state with high certainty that the recorded profile of ALL6 is not showing any signs of an accumulation of rigor-like conformational states of the myosin heads. In our case, though, the statistical test is somewhat limited, as it is based on only one measured value (the difference between the integrated intensities for time frame II and III). Nevertheless, we can quite well argue that the probability to detect the observed difference in the profiles between time frame II and III just by chance is extremely low, if in reality both profiles were identical or the intensity for time frame III were even higher than for time frame II, as expected for accumulation of rigor cross-bridges. The measured ALL6 profiles, therefore, most likely argue against a substantial increase in the proportion of rigor-like cross-bridges during the release of the activated muscle fibers.

Since ALL6, however, is very sensitive to even small structural changes of stereospecifically attached cross-bridges (Koubassova and Tsaturyan, 2002), our data rather support a concept that the pause in tension drop during the releases is the result of accumulation of stereospecifically attached cross-bridges in a state of the power stroke, which is both different from the structural state in the power stroke that is mostly occupied during isometric steady state contraction, and also different from rigor or rigor-like states (i.e. the AM state and AMD states obtained upon addition of MgADP to rigor fibers).

The near-meridian part of ALL6 is enhanced by diffracting mass, which follows the helical periodicity of F-actin at larger diameters. The orientation of the neck region of the myosin heads, therefore, affects mostly this part of ALL6. A fixed orientation of the neck region produces high near-meridian intensity of ALL6, irrespective of its particular bent. This was demonstrated earlier by Kraft et al., 2002 using truncated S1 which includes only the motor domain of the myosin head and N-ethyl-maleimide (NEM)-

modified S1 which includes both the motor domain and the neck region of the myosin head. Actin decorated with truncated S1 and actin decorated with NEM-S1 mimics states with disoriented and uniformly oriented neck regions, respectively. The intensity maximum of ALL6 on diffraction images produced from the latter is seen to be nearer to the meridian. In addition, the "anti-rigor" conformation described in Koubassova and Tsaturyan, 2002, which is characterized by a 70° tilt of the neck region of the myosin head, also produces higher intensity of the ALL6 near to the meridian, in the same way the rigor conformation of the myosin head does. The decrease in near-meridian intensity of ALL6 observed in our experiments is, therefore, neither consistent with an accumulation of cross-bridges in rigor-like nor anti-rigor-like states. Instead, our data rather indicate a mixture of different neck orientations or a predominance of a myosin head conformation that produces an ALL6 profile with low intensity near the meridian. A mixture with a substantial proportion of rigor-like or anti-rigor-like myosin head conformations can be excluded, though, as this would show up as an increase in near-meridian intensity of ALL6 as in the case of the MgATPγS titration (figure 25). Thus, accumulation in an up to now structurally unknown state seems a likely possibility.

## *Consequences*

Before delving into the critical analysis of the consequences, I would like to recapitulate briefly. The finding, that no rigor cross-bridges are accumulated during the release, follows from the described line of reasoning: (i) We observed from the intensity of ALL1 that the number of stereospecifically attached myosin heads surely does not decrease until time frame III. There is even a slight, but insignificant increase in time frame III compared to time frame I and II. (ii) The step-wise change in $I_{1,1}/I_{1,0}$ and the force trace indicate a redistribution within different conformational states of the cross-bridge at the transition from time frame II to time frame III. (iii) The intensity distribution along ALL6 indicates an increased population of a conformational state in time frame III that is different from the rigor and even "anti-rigor" conformation of the cross-bridge.

Two questions that finally arise from the above line of argument are: (i) Which is the structural state of the cross-bridge accumulated during the ramp-shaped release and to which biochemical state does it correspond? (ii) What is the role of the rigor state of the

cross-bridge during the release and possibly during active force development when it obviously was not accumulated in time frame III of the release?

To tackle the first question, our data strongly suggests that the conformational state accumulated in time frame III cannot be a rigor-like state. Therefore, the biochemical states AM as well as the last A·M·ADP (obtained by addition of MgADP to rigor fibers) have to be excluded, because the latter also shows rigor-like features in the X-ray diffraction pattern (own unpublished results). One could hypothesize that the last A·M·ADP state is possibly short lived. In this case ADP dissociation has to occur at a high rate and there should be a number of different A·M·ADP states with only the last one expressing rigor-like features on the diffraction pattern.

The state accumulated during the ramp-shaped release also does not correspond to the "anti-rigor" conformation, which was proposed as a possible model for the conformation of the cross-bridges before exertion of the power stroke. The accumulated state could correspond to a cross-bridge conformation already strongly attached to actin but before the release of $P_i$, i.e. an A·M·ADP·$P_i$ state (compare figure 13 - kinetic scheme), or an early state after $P_i$ release, which does not yet produce lattice sampling in the diffraction pattern. A comparison to work done by colleagues from our lab (Kraft et al., 2005), where $P_i$ was substituted by the phosphate analogue aluminum fluoride ($AlF_4$) seems to be promising, as $AlF_4$ was employed to produce two different A·M·ADP·$P_i$ analogue states, a weak binding and a strong binding one. Diffraction patterns recorded from muscle fibers predominantly in the strong binding A·M·ADP·$AlF_4$-II state show no lattice sampling and also decreased intensity on the shoulder of the ALL6 profile nearer to the meridian. This A·M·ADP·$AlF_4$-II state is interpreted as a corresponding analogue to a strongly attached A·M·ADP·$P_i$ state. This state, therefore, seems to be a promising candidate for the state accumulated in time frame III of our ramp-shaped release.

It is also unlikely that the effect seen on the ALL6 in time frame III is produced by disorder resulting from a mixture of structural states, consisting of cross-bridges producing rigor-like diffraction patterns and/or cross-bridges producing diffraction patterns as in relaxing condition. The recorded decrease in near-meridian intensity of the ALL6 and, therefore, reduction in radial width of the profile can not be reproduced by any mixture of these states. Otherwise it could have been mimicked by some MgATPγS concentration. MgATPγS titration, however, produces profiles with increasing radial width when going from relaxing towards rigor condition (figure 25). It

can also be excluded that the recorded smaller radial width results from interference between different structural states, because this would require that these different structural states are distributed along the fiber axis in a repeating pattern, which is not likely to be true. They are rather expected to be distributed randomly along the fiber axis and therefore their individual participations in the diffraction pattern add up in absolute intensity values. The recorded decrease in radial width of ALL6 from time frame II to time frame III could therefore only be produced by the predominance of a structural state of the cross-bridge, which shows the adequate feature in the diffraction pattern, i.e. a narrower radial profile of the ALL6. A further characterization of this structural state of the cross-bridge could be done by means of molecular modeling.

Concerning the second of the two above questions, i.e., about the role of the rigor state, we already demonstrated that the rigor state or other states that produce rigor-like diffraction patterns are not accumulated in time frame III of the ramp-shaped release. It is, however, not very surprising not to see accumulation of rigor cross-bridges, i.e. nucleotide free cross-bridges, during ramp shaped releases. This is because of the high forward rate constant for binding of ATP to the nucleotide free myosin head and the subsequent fast detachment of the cross-bridge, i.e. the transition from the AM-state to the M·ATP-state in the cross-bridge cycle. This rate constant is estimated to be in the order of $10^6$ $M^{-1}s^{-1}$ (e.g. Somlyo et al., 1988). With the ATP concentration in active muscle in the range of 1 mM, the rate constant for the detachment is in the magnitude of $10^3$ $s^{-1}$. The AM-state is therefore very short lived, and not expected to accumulate even during releases. Hence, the rigor state seems to be only a short lived state and is very little populated during the power stroke.

Altogether, with the methods employed no evidence could be found that rigor-like conformational cross-bridge states are accumulated substantially during force generation, even when muscle fibers are released to shift the cross-bridge population in favor of states toward the end of the power stroke. Our data, however, do show a redistribution of cross-bridge states during the ramp-shaped release toward states that are structurally different from states that are predominantly occupied during isometric steady state contraction.

## *Outlook*

Further studies and comparison to different AlF$_4$ states could offer a promising approach to narrow in on a more detailled determination of the structural and biochemical characteristics of the state accumulated in time frame III of the ramp-shaped releases. A more detailed analysis of the diffraction patterns under different mechanical and chemical conditions of the muscle fibers would require, though, light sources of even higher brilliance and better time resolution than it was the case in the time our time-resolved experiments at the ESRF were conducted (April 2003).

Based on theoretical background provided by Vainstein, 1966, that has already been applied successfully by e.g. Gu et al., 2002, and Koubassova and Tsaturyan, 2002, molecular modeling could be employed to search for cross-bridge conformations that fit the recorded diffraction patterns and thus to possibly identify candidates for the conformational state accumulated in time frame III of the ramp-shaped release.

In the last few years also X-ray microscopy has been improved. Temporary techniques (Miao and Sayre, 2000; Pfeifer et al., ) coherent X-ray radiation of high brilliance could allow resolution on a nanometer scale. In this technique the phase problem is solved by so called oversampling, whereby the image could be calculated by specific information stored in the diffraction patterns. So far, no reference to experiments performed on living tissue could be found in the literature. Future applications of this technique on muscle fibers seem to be promising, though.

# References

Alberts, B., A. Johnson, J. Lewis, M. Raff, K. Roberts, and P. Walter. 2002. Molecular Biology of the Cell. Garland Publishing.

Banga, I., and A. Szent-Gyorgyi. 1942. Preparation and properties of myosin A and B. *Studies from the Institute of Medical Chemistry, University of Szeged* 1:5-15.

Bloom, W., and D.W. Fawcett. 1968. Muscular tissue. *In* A Textbook of Histology. Raviola E, editor. Saunders, Philadelphia. 273.

Bordas, J., G.P. Diakun, F.G. Diaz, J.E. Harries, R.A. Lewis, J. Lowy, G.R. Mant, M.L. Martin-Fernandez, and E. Towns-Andrews. 1993. Two-dimensional time-resolved X-ray diffraction studies of live isometrically contracting frog sartorius muscle. *J Muscle Res Cell Motil* 14(3):311-324.

Bordas, J., A. Svensson, M. Rothery, J. Lowy, G.P. Diakun, and P. Boesecke. 1999. Extensibility and symmetry of actin filaments in contracting muscles. *Biophys J* 77(6):3197-3207.

Brenner, B. 1980. Effect of free sarcoplasmatic Ca(2+) concentration on maximum unloaded shortening velocity: measurements on single glycerinated rabbit psoas muscle fibres. *Journal of Muscle Research and Cell Motility* 1:409-428.

Brenner, B. 1983. Technique for stabilizing the striation pattern in maximally calcium-activated skinned rabbit psoas fibers. *Biophys J* 41(1):99-102.

Brenner, B. 1986a. The cross-bridge cycle in muscle. Mechanical, biochemical, and structural studies on single skinned rabbit psoas fibers to characterize cross-bridge kinetics in muscle for correlation with the actomyosin-ATPase in solution. *Basic Res Cardiol* 81 Suppl 1:1-15.

Brenner, B. 1986b. Zum molekularen Mechanismus der Muskelkontraktion. Mechanische, biochemische und röntgenstrukturanalytische Untersuchungen am isolierten kontraktilen Apparat von Skelettmuskelfasern. Eberhard-Karls-Universität Tübingen.

Brenner, B. 1991. Rapid dissociation and reassociation of actomyosin cross-bridges during force generation: a newly observed facet of cross-bridge action in muscle. *Proc Natl Acad Sci U S A* 88(23):10490-10494.

Brenner, B., and J.M. Chalovich. 1999. Kinetics of thin filament activation probed by fluorescence of N-((2-(Iodoacetoxy)ethyl)-N-methyl)amino-7-nitrobenz-2-oxa-1, 3-diazole-labeled troponin I incorporated into skinned fibers of rabbit psoas muscle: implications for regulation of muscle contraction. *Biophys J* 77(5):2692-2708.

Brenner, B., J.M. Chalovich, and L.C. Yu. 1995. Distinct molecular processes associated with isometric force generation and rapid tension recovery after quick release. *Biophys J* 68(4 Suppl):106S-111S.

Brenner, B., and L.C. Yu. 1993. Structural changes in the actomyosin cross-bridges associated with force generation. *Proc Natl Acad Sci U S A* 90(11):5252-5256.

Brenner, B., L.C. Yu, and R.J. Podolsky. 1984. X-ray diffraction evidence for cross-bridge formation in relaxed muscle fibers at various ionic strengths. *Biophys J* 46(3):299-306.

Chalovich, J.M., P.B. Chock, and E. Eisenberg. 1981. Mechanism of action of troponin. tropomyosin. Inhibition of actomyosin ATPase activity without inhibition of myosin binding to actin. *J Biol Chem* 256(2):575-578.

Chalovich, J.M., L.E. Greene, and E. Eisenberg. 1983. Crosslinked myosin subfragment 1: a stable analogue of the subfragment-1.ATP complex. *Proc Natl Acad Sci U S A* 80(16):4909-4913.

Chen, Y.D., and B. Brenner. 1993. On the regeneration of the actin-myosin power stroke in contracting muscle. *Proc Natl Acad Sci U S A* 90(11):5148-5152.

Eisenberg, E., T.L. Hill, and Y. Chen. 1980. Cross-bridge model of muscle contraction. Quantitative analysis. *Biophys J* 29(2):195-227.

Fisher, A.J., C.A. Smith, J.B. Thoden, R. Smith, K. Sutoh, H.M. Holden, and I. Rayment. 1995. X-ray structures of the myosin motor domain of Dictyostelium discoideum complexed with MgADP.BeFx and MgADP.AlF4. *Biochemistry* 34(28):8960-8972.

Ford, L.E., A.F. Huxley, and R.M. Simmons. 1977. Tension Responses To Sudden Length Change In Stimulated Frog Muscle Fibres Near Slack Length. *J. Physiol.* 269:441-515.

Geeves, M.A., and K.C. Holmes. 1999. Structural mechanism of muscle contraction. *Annu Rev Biochem* 68:687-728.

Green, D.W., V.M. Ingram, and M.F. Perutz. 1954. The structure of haemoglobin IV. Sign determination by the isomorphous replacement method. *Proc. Roy. Soc, A* 225:287-307.

Greene, L.E., and E. Eisenberg. 1980. Cooperative binding of myosin subfragment-1 to the actin-troponin-tropomyosin complex. *Proc Natl Acad Sci U S A* 77(5):2616-2620.

Gu, J., S. Xu, and L.C. Yu. 2002. A model of cross-bridge attachment to actin in the A*M*ATP state based on x-ray diffraction from permeabilized rabbit psoas muscle. *Biophys J* 82(4):2123-2133.

Hanson, J., and H.E. Huxley. 1953. Structural basis of the cross-striations in muscle. *Nature* 172:530-532.

Harford, J., and J. Squire. 1997. Time-resolved diffraction studies of muscle using synchrotron radiation. *Rep.Prog.Phys.* 60:1723-1787.

Haselgrove, J.C. 1975. X-ray evidence for conformational changes in the myosin filaments of vertebrate striated muscle. *J Mol Biol* 92(1):113-143.

Hill, T.L. 1974. Theoretical formalism for the sliding filament model of contraction of striated muscle. Part I. *Prog Biophys Mol Biol* 28:267-340.

Holmes, K.C., D. Popp, W. Gebhard, and W. Kabsch. 1990. Atomic model of the actin filament. *Nature* 347(6288):44-49.

Huxley, A.F. 1974. Muscular contraction. *J Physiol* 243(1):1-43.

Huxley, A.F., and R. Niedergerke. 1954. Interference microscopy of living muscle fibres. *Nature* 173:971-974.

Huxley, A.F., and R.M. Simmons. 1971. Proposed mechanism of force generation in striated muscle. *Nature* 233(5321):533-538.

Huxley, A.F., and R.M. Simmons. 1973. Mechanical transients and the origin of muscular force. *Cold Spring Harb Symp Quant Biol* 37:669-680.

Huxley, H.E. 1953a. Electron microscope studies of the organization of the filaments in striated muscle. *Biochim Biophys Acta* 12:387-394.

Huxley, H.E. 1953b. X-ray analysis and the problem of muscle. *Proc R Soc Lond B Biol Sci* 141(902):59-62.

Huxley, H.E. 1957. The double array of filaments in cross striated muscle. *J Biophys Biochem Cytol* 3:631-647.

Huxley, H.E. 1968. Structural difference between resting and rigor muscle; evidence from intensity changes in the lowangle equatorial x-ray diagram. *J Mol Biol* 37(3):507-520.

Huxley, H.E., and W. Brown. 1967. The low-angle x-ray diagram of vertebrate striated muscle and its behaviour during contraction and rigor. *J Mol Biol* 30(2):383-434.

Huxley, H.E., A.R. Faruqi, M. Kress, J. Bordas, and M.H. Koch. 1982. Time-resolved X-ray diffraction studies of the myosin layer-line reflections during muscle contraction. *J Mol Biol* 158(4):637-684.

Huxley, H.E., and J. Hanson. 1954. Changes in the cross striations of muscle during contraction and stretch and their interpretation. *Nature* 173:973-976.

Kabsch, W., H.G. Mannherz, D. Suck, E.F. Pai, and K.C. Holmes. 1990. Atomic structure of the actin:DNase I complex. *Nature* 347(6288):37-44.

Knupp, C., and J. Squire. 2004. HELIX: A helical diffraction simulation program. *J Appl Cryst* 37:832 - 835.

Koubassova, N.A., and A.K. Tsaturyan. 2002. Direct modeling of x-ray diffraction pattern from skeletal muscle in rigor. *Biophys J* 83(2):1082-1097.

Kraft, T., J.M. Chalovich, L.C. Yu, and B. Brenner. 1995. Parallel inhibition of active force and relaxed fiber stiffness by caldesmon fragments at physiological ionic strength and temperature conditions: additional evidence that weak cross-bridge binding to actin is an essential intermediate for force generation. *Biophys J* 68(6):2404-2418.

Kraft, T., E. Mahlmann, T. Mattei, and B. Brenner. 2005. Initiation of the power stroke in muscle: insights from the phosphate analog AlF4. *Proc Natl Acad Sci U S A* 102(39):13861-13866. Epub 12005 Sep 13820.

Kraft, T., T. Mattei, A. Radocaj, B. Piep, C. Nocula, M. Furch, and B. Brenner. 2002. Structural features of cross-bridges in isometrically contracting skeletal muscle. *Biophys J* 82(5):2536-2547.

Kraft, T., S. Xu, B. Brenner, and L.C. Yu. 1999. The effect of thin filament activation on the attachment of weak binding cross-bridges: A two-dimensional x-ray diffraction study on single muscle fibers. *Biophys J* 76(3):1494-1513.

Kuhn, H.J., K. Guth, B. Drexler, W. Berberich, and J.C. Ruegg. 1979. Investigation of the temperature dependence of the cross bridge parameters for attachment, force generation and detachment as deduced from mechano-chemical studies in glycerinated single fibres from the dorsal longitudinal muscle of Lethocerus maximus. *Biophys Struct Mech* 6(1):1-29.

Lewis, R.A., A. Berry, C.J. Hall, W.I. Helsby, and B.T. Parker. 1999. RAPID detector system: first user data. oct ed. 97-102.

Lewis, R.A., C.J. Hall, W. Helsby, A. Jones, B. Parker, and J. Sheldon. 1995. 10-MHz photon counting detector system for time-resolved x-ray diffraction. *In* Proc. SPIE Vol. 2521, p. 290-300, Time-Resolved Electron and X-Ray Diffraction, Peter M. Rentzepis; Ed. 290-300.

Lewis, R.A., W.I. Helsby, A.O. Jones, C.J. Hall, B. Parker, J. Sheldon, P. Clifford, M. Hillen, I. Sumner, and N.S. Fore. 1997. The "RAPID" high rate large area X-ray detector system. *Nuclear Instruments and Methods in Physics Research Section A: Accelerators, Spectrometers, Detectors and Associated Equipment* 392(1-3):32.

Linari, M., G. Piazzesi, I. Dobbie, N. Koubassova, M. Reconditi, T. Narayanan, O. Diat, M. Irving, and V. Lombardi. 2000. Interference fine structure and sarcomere length dependence of the axial x-ray pattern from active single muscle fibers. *Proc Natl Acad Sci U S A* 97(13):7226-7231.

Lorenz, M., D. Popp, and K.C. Holmes. 1993. Refinement of the F-actin model against X-ray fiber diffraction data by the use of a directed mutation algorithm. *J Mol Biol* 234(3):826-836.

Lymn, R.W., and E.W. Taylor. 1971. Mechanism of adenosine triphosphate hydrolysis by actomyosin. *Biochemistry* 10(25):4617-4624.

Miao, J., and D. Sayre. 2000. On possible extensions of X-ray crystallography through diffraction pattern oversampling. *Acta Chryst* A 56:596-605.

Milligan, R.A., and P.F. Flicker. 1987. Structural relationships of actin, myosin, and tropomyosin revealed by cryo-electron microscopy. *J Cell Biol* 105(1):29-39.

Milligan, R.A., M. Whittaker, and D. Safer. 1990. Molecular structure of F-actin and location of surface binding sites. *Nature* 348(6298):217-221.

Needham, J., A. Kleinzeller, M. Miall, M. Dainty, D.M. Needham, and A.S.C. Lawrence. 1942. Is muscle contraction essentially an enzyme-substrate combination? *Nature* 150:46-49.

Pfeifer, M.A., G.J. Williams, I.A. Vartanyants, R. Harder, and I.K. Robinson. Three-dimensional mapping of a deformation field inside a nanocrystal.

Rapp, G., K. Guth, Y. Maeda, K.J. Poole, and R.S. Goody. 1991. Time-resolved X-ray diffraction studies on stretch-activated insect flight muscle. *J Muscle Res Cell Motil* 12(2):208-215.

Rayment, I., H.M. Holden, M. Whittaker, C.B. Yohn, M. Lorenz, K.C. Holmes, and R.A. Milligan. 1993a. Structure of the actin-myosin complex and its implications for muscle contraction. *Science* 261(5117):58-65.

Rayment, I., W.R. Rypniewski, K. Schmidt-Base, R. Smith, D.R. Tomchick, M.M. Benning, D.A. Winkelmann, G. Wesenberg, and H.M. Holden. 1993b. Three-dimensional structure of myosin subfragment-1: a molecular motor. *Science* 261(5117):50-58.

Reedy, M.K., K.C. Holmes, and R.T. Tregear. 1965. Induced changes in orientation of the cross-bridges of glycerinated insect flight muscle. *Nature* 207:1276-1280.

Smith, C.A., and I. Rayment. 1996. X-ray structure of the magnesium(II).ADP.vanadate complex of the Dictyostelium discoideum myosin motor domain to 1.9 A resolution. *Biochemistry* 35(17):5404-5417.

Somlyo, A.V., Y.E. Goldman, T. Fujimori, M. Bond, D.R. Trentham, and A.P. Somlyo. 1988. Cross-bridge kinetics, cooperativity, and negatively strained cross-bridges in vertebrate smooth muscle. A laser-flash photolysis study. *J Gen Physiol* 91(2):165-192.

Squire, J.M. 1981. The structural basis of muscular contraction. Plenum Press, New York, London.

Squire, J.M., and C. Knupp. 2004. MusLABEL: a program to model striated muscle A-band lattices, to explore crossbridge interaction geometries and to simulate muscle diffraction patterns. *J Muscle Res Cell Motil* 25(4-5):423-438.

Stein, L.A., R.P. Schwarz, Jr., P.B. Chock, and E. Eisenberg. 1979. Mechanism of actomyosin adenosine triphosphatase. Evidence that adenosine 5'-triphosphate hydrolysis can occur without dissociation of the actomyosin complex. *Biochemistry* 18(18):3895-3909.

Straub, F.B. 1942. Actin. *Studies from the Institute of Medical Chemistry, University of Szeged* 2:3-15.

Szent-Gyorgyi, A. 1942. The contraction of myosin threads. *Studies from the Institute of Medical Chemistry, University of Szeged* 1:17-26.

Szent-Gyorgyi, A. 1944. Studies on muscle. *Acta Physiologica Scandinavica* 9(Suppl. XXV).

Tamura, T., J. Wakayama, T. Fujisawa, N. Yagi, and H. Iwamoto. 2004. Intensity of X-ray reflections from skeletal muscle thin filaments partially occupied with myosin heads: effect of cooperative binding. *J Muscle Res Cell Motil* 25(4-5):329-335.

Vainstein, B.K. 1966. Diffraction of X-rays by chain molecules. Elsevier Publishing Company.

Xu, S., S. Malinchik, D. Gilroy, T. Kraft, B. Brenner, and L.C. Yu. 1997. X-ray diffraction studies of cross-bridges weakly bound to actin in relaxed skinned fibers of rabbit psoas muscle. *Biophys J* 73(5):2292-2303.

Yu, L.C., and B. Brenner. 1989. Structures of actomyosin crossbridges in relaxed and rigor muscle fibers. *Biophys J* 55(3):441-453.

# Appendix

## *Origin fit functions*

In order to obtain total intensities of overlapping peaks in one-dimensional profiles, I fitted functions containing the background and the appropriate number of Gaussian peaks to the intensity data. The computer application ORIGIN (OriginLab Corporation, Northampton, MA) was used the curve fitting.

**expdec1and2peaksArea**

No. of parameters 9

Names of parameters: y0,A1,A2,A3,t1,xc1,xc2,w1,w2

Independent variable: x

Dependend variable: y

$y = y0 + A1*\exp(-x/t1) + (A2/(w1*\text{sqrt}(PI/2)))*\exp(-2*((x-xc1)/w1)^2) + (A3/(w2*\text{sqrt}(PI/2)))*\exp(-2*((x-xc2)/w2)^2)$

Meaning of the parameters:

y0 offset

A1 amplitude of the exponential decay

A2 area of the first peak

A3 area of the second peak

t1 exponential decay constant

xc1 position of the first peak

xc2 position of the second peak

w1 width of the first peak

w2 width of the second peak

**expdec1and4peaksArea**

No. of parameters 15

Names of parameters: y0,A1,A2,A3,A4,A5,t1,xc1,xc2,xc3,xc4,w1,w2,w3,w4

Independent variable: x

Dependend variable: y

$y = y_0 + A_1 \cdot \exp(-x/t_1) + (A_2/(w_1 \cdot \sqrt{PI/2})) \cdot \exp(-2 \cdot ((x-xc_1)/w_1)^2) +$

$(A_3/(w_2 \cdot \sqrt{PI/2})) \cdot \exp(-2 \cdot ((x-xc_2)/w_2)^2) +$

$(A_4/(w_3 \cdot \sqrt{PI/2})) \cdot \exp(-2 \cdot ((x-xc_3)/w_3)^2) +$

$(A_5/(w_4 \cdot \sqrt{PI/2})) \cdot \exp(-2 \cdot ((x-xc_4)/w_4)^2)$

Meaning of the parameters:

y0 offset

A1 amplitude of the exponential decay

A2 area of the first peak

A3 area of the second peak

A4 area of the third peak

A5 area of the fourth peak

t1 exponential decay constant

xc1 position of the first peak

xc2 position of the second peak

xc3 position of the third peak

xc4 position of the fourth peak

w1 width of the first peak

w2 width of the second peak

w3 width of the third peak

w4 width of the fourth peak

## *X-ray diffraction in a nutshell*

The following text is a hand-out to a lab-seminar I gave in October 2004. It summarizes the basics of the underlying theory to X-ray diffraction, features of diffraction patterns expected from different parameters that characterize a helix, and some technical aspects. Including this information in the main text would have distracted from the main points of the thesis. Therefore I decided to add it as supplemental information in an appendix to my thesis.

# X-RAY DIFFRACTION IN A NUTSHELL

## by Ante Radocaj

1. What we want to achieve? Information about the molecular configuration and interaction
2. One way of doing it is x-ray diffraction
3. Why? Investigate functional muscle fibers
4. How does diffraction work?
5. Double slit (use coherent beam of light, resolution wavelength of used light)
6. Molecular structure 0.1 nm
7. Spectrum of light
8. What's synchrotron radiation? (accelerated electrons produce X-rays) (storage ring, electrons, bending magnet, deflection)
9. Arrangement specimen detector
10. Short exposure time pattern + other patterns
11. Diffraction theory (Fourier-transform, convolution)
12. More difficult arrangement of scattering masses: helices and discontinuous helices
13. Remind what our patterns look like

With our efforts, we wish to achieve information about the change in the conformation of myosin-heads during shortening of muscle fibers. What states are occupied? Are there any rigor-like states? And if so, what could be their percentage in the population?

We use x-ray diffraction to approach these questions, because it allows us to investigate functional muscle fibers, which can be activated, develop force and shorten themselves.

To start to explain the possibilities of X-ray diffraction, allow me to demonstrate the effect of diffraction using a very simple experiment that everyone should remember from high school.



wave fronts

coherent light source

double slit

2 sine waves in phase constructive interference

2 sine waves out of phase destructive interference
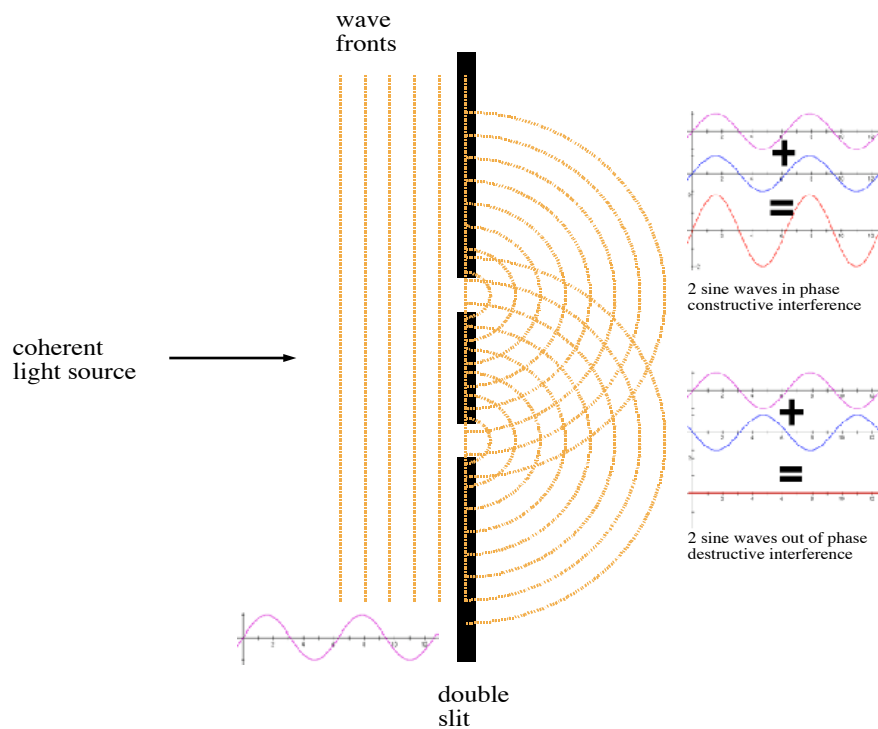
Fig. 1

The double slit experiment is performed by pointing a beam of coherent light to a non-transparent screen that allows the light only to pass through two narrow apertures. That what is observed on a wall positioned far away from the double slit opposite the light source is an illuminated strip of varying brightness. It is the diffraction pattern of the sample with the very simple structure of just two slits. Diffraction patterns of samples with more complicated structures will be discussed later in this paper.

By decreasing the distance between the two apertures of the double slit the light reflections on the wall spread out, i.e. the distance between two intensity maxima increases. And by increasing the distance of the apertures, the distance of the intensity maxima decreases. The distances are inversely proportional. The observed intensity maxima and minima on the wall can be explained by interference of the light emitted from one aperture and the light emitted from the other aperture. In the above image there are two point sources emitting light in circular waves. The waves add up the same way waves on the surface of a pond do. Waves that are in phase build up to a wave of twice the amplitude and waves that are in opposite phase annihilate themselves.

condition for maximum:

$$\delta = d \sin \theta = n \lambda$$

d: spacing od double slit
δ: difference of phase
θ: difraction angle
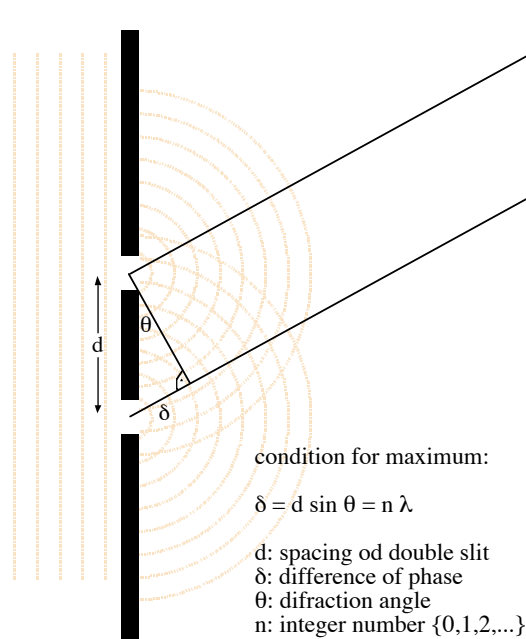n: integer number {0,1,2,...}

Fig. 2

Waves propagating in a direction with the angle θ to the axis are in phase, if the phase distance δ between them is an integer multiple of the wavelength λ (see image and equation above).

Using the above equation, the distance of the apertures of the double slit can be calculated by measuring the distance between the intensity maxima on the wall, and knowing the distance from the double slit to the wall and the wavelength of the light. So, the beam of coherent light can be used to investigate the property of the double slit. For the calculation to be effective, the wavelength should be in the same order of magnitude as the structure of the investigated object (the sample, here the double slit).

To investigate objects with structures smaller than the wavelength of visible light in the same way, we have to use electromagnetic waves of shorter wavelengths, i.e. higher frequencies.
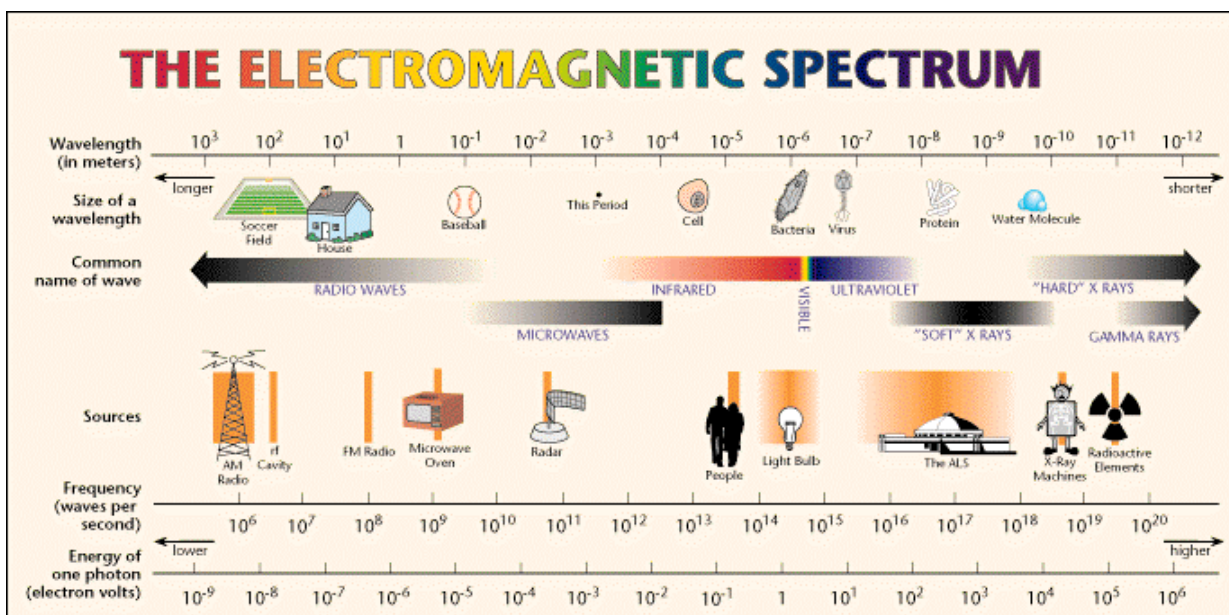


Fig. 3

As illustrated in the above diagram (Fig. 3) structures on a molecular scale could be resolved using X-rays. Synchrotrons generate coherent X-ray beams with exactly defined frequencies and high flux. Accelerated charged particles emit electromagnetic radiation. The electrons in the storage ring are kept in their track using bending magnets. As a side effect of their deflection in the bending magnets, synchrotron radiation, in the form of X-rays, emitted tangentially to the electron path is produced. For even higher efficiency of produced X-ray beams insertion devices (wigglers or undulators) are employed. The European Synchrotron Radiation Facility (ESRF) in Grenoble has 32 of these beamlines. We used beamline ID2 that is specifically equipped for fiber diffraction.
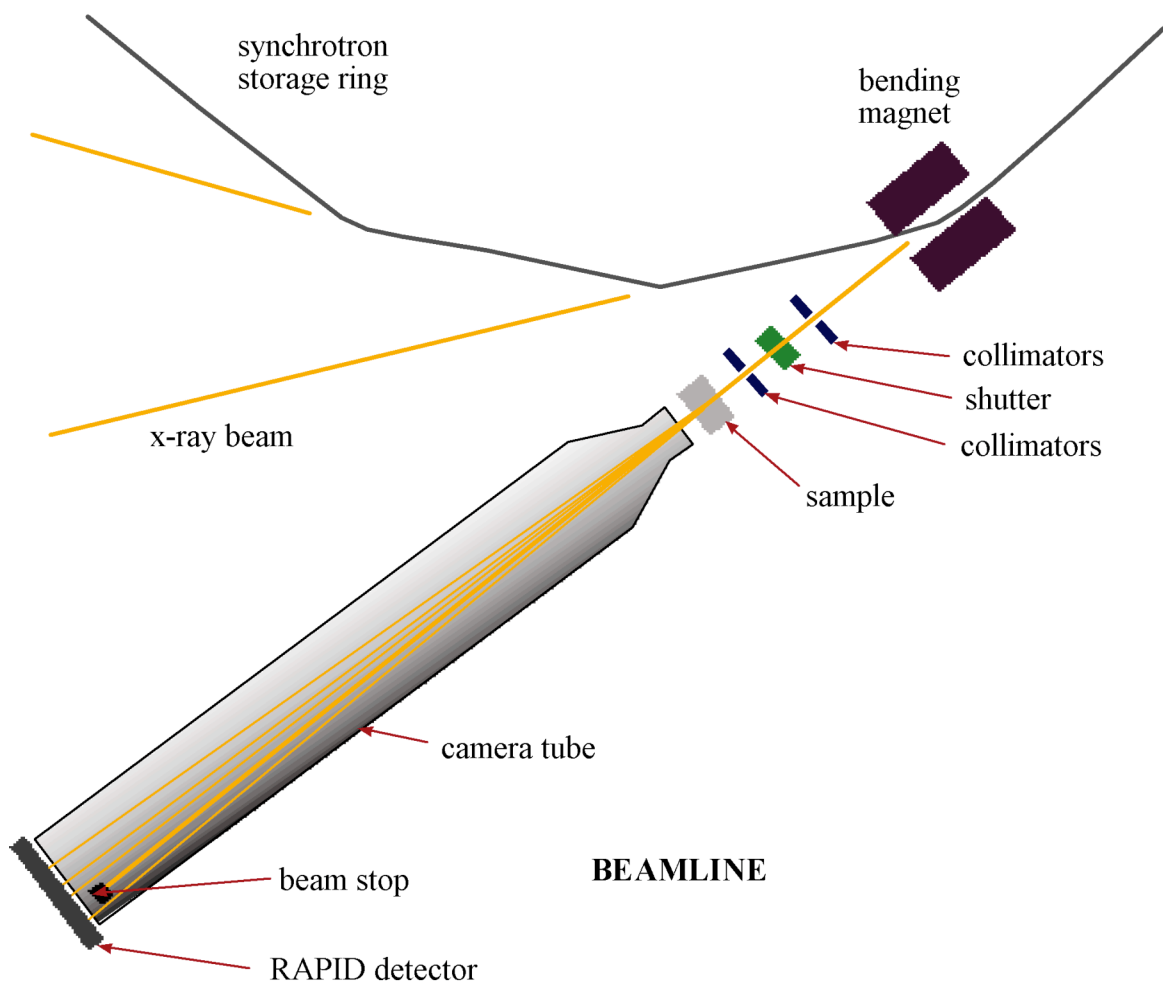
Fig. 4

The above drawing (Fig. 4) shows the arrangement of the equipment in the beamline as we used it in April 2003 at the ESRF.

Source characteristics for beamline ID2:

| undulator on a high ß section | segment A (U42) | segment B (U26) | segment C (U24) |
|---|---|---|---|
| magnet period: | 42 mm | 26 mm | 24.6 mm |
| X-ray wavelength range: | 0.05 - 0.15 nm | 0.1 nm | 0.1 nm |
| source size: | 0.945 x 0.0186 mm$^2$ (HxV)FWHM | | |
| source divergence: | 0.025 x 0.0075 mrad$^2$ (HxV)FWHM | | |
| flux at sample position (12.5 keV): | 7.0 10$^{12}$ ph/s at 100mA | 8.0 10$^{12}$ ph/s at 100mA | 1.7 10$^{13}$ ph/s at 100mA |
| beam size at 55 m: | 0.37 x 0.21 mm$^2$ (ideal mirror) | | |
| beam divergence at 55 m: | 0.038 x 0.015 mrad$^2$ (HxV) | | |

Small angle diffraction patterns were recorded using the 2D RAPID detector - a photon counting device - permitting sufficient output even with extremely short exposure times, as 2 ms.
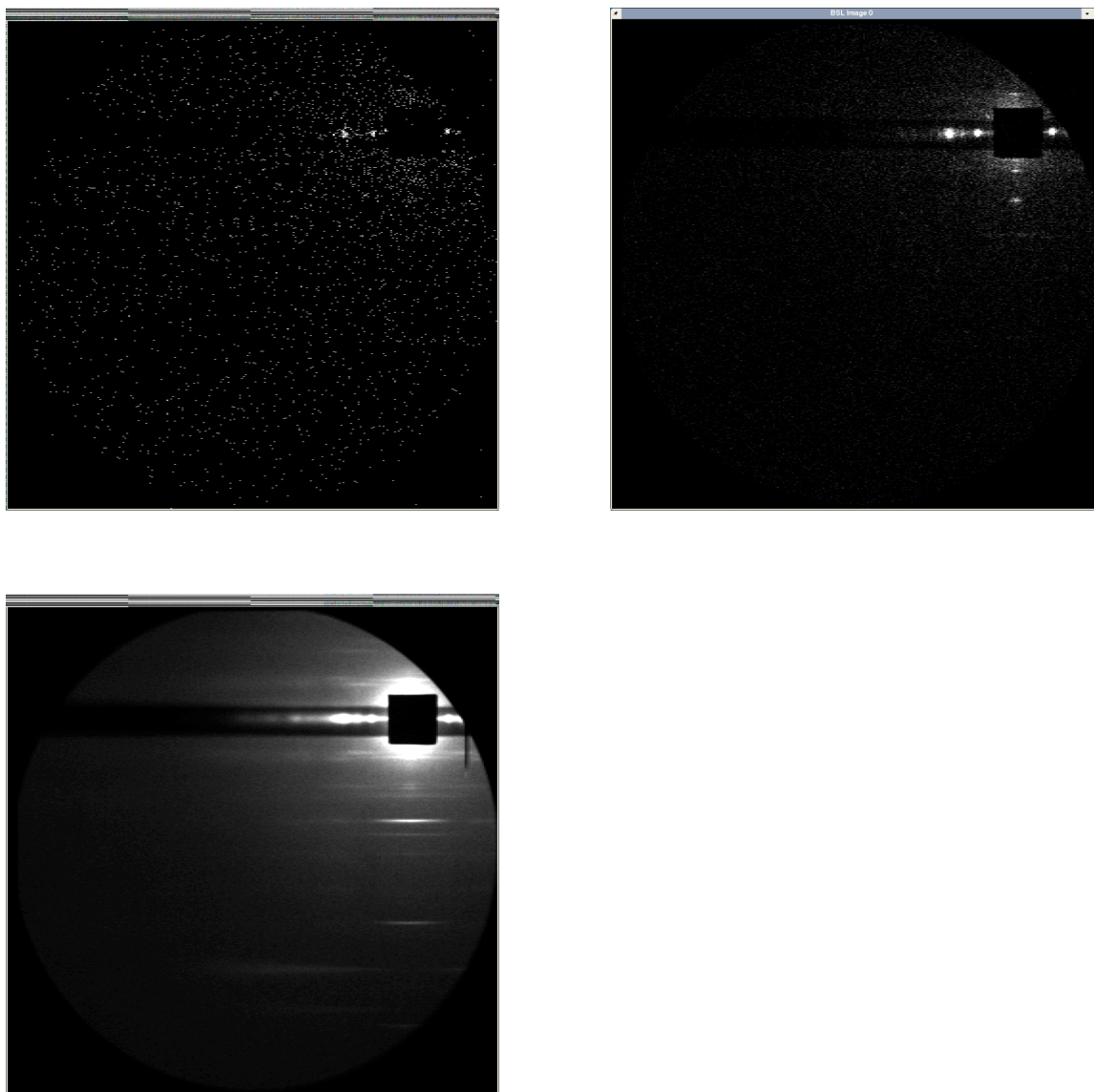


Fig. 5

The first picture in figure 5 shows a recording of a diffraction pattern by the RAPID detector with an exposure time of only 2 ms. One can actually see the single photons which hit the detector during this interval. The smooth diffraction patterns, we are doing our analysis with, are actually a sum of hundreds of single recorded patterns. The second picture consists of 15 accumulated frames with a total exposure time of 30 ms, and the third picture is an addition of about 1000 frames with a total exposure time of about 2.7 seconds. The dotted pictures with the discernible photons are a nice proof of the wave-particle duality and Heisenberg's uncertainty principle. Each single photon is actually passing all the possible paths and interfering with itself to be measured finally at one distinct position in space.

It's time to go back and ask ourselves, what kind of structure within the sample could produce such a complicated diffraction pattern. As it's not a double slot, it should be something more elaborate. The observed diffraction pattern of known samples can be calculated by a mathematical algorithm called discrete Fourier-transform. It's incorporated in many expert systems, like Mathematica, Origin and Maple V in form of the Fast Fourier-Transform (FFT).

Let's work our way up step by step from simple structures of samples to structures whose diffraction patterns look more like our recorded ones.
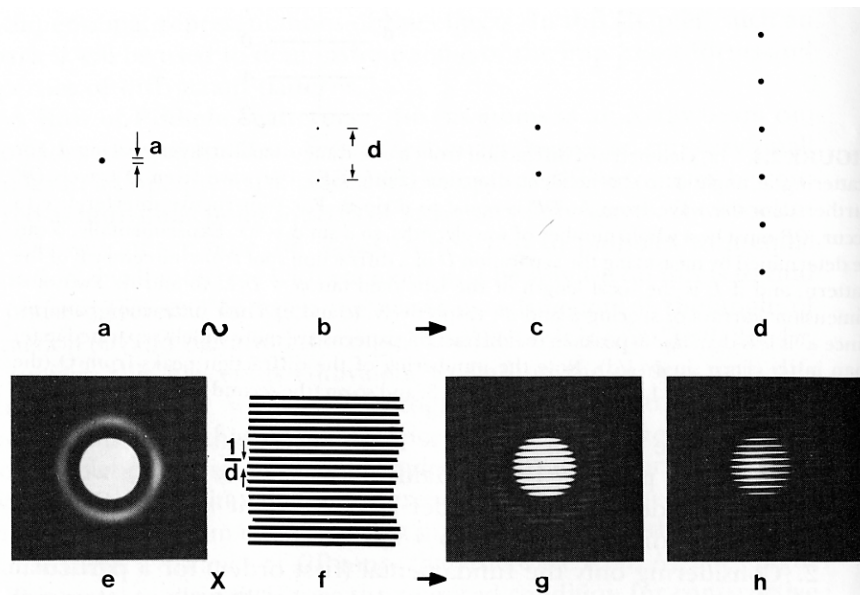


Fig. 6

According to the convolution theorem that results from the theory of the Fourier-transform, the diffraction pattern of a convolution of two sample structures is the intensity product of the two resulting diffraction patterns (and vice-versa). The diffraction pattern of a large hole (a) is an airy disk (e) and the diffraction pattern of two tiny holes (point sources) is a striped pattern (f). So, the diffraction pattern of two large holes is a pattern as (g). Adding up more holes to the row just makes the stripes in the pattern thinner and sharper. The distance between the stripes in the pattern is inversely proportional to the distance between the holes.
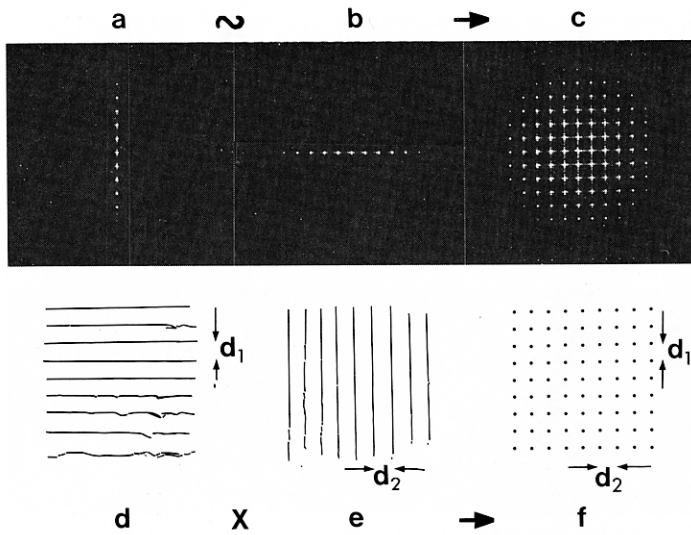
Fig. 7

The convolution theorem is valid the other way around, too. The diffraction pattern of an intensity multiplication of two samples is the convolution of the patterns of the two samples, resulting in the diffraction pattern (c) of a gird of holes.

The diffraction pattern of a three dimensional helix can be calculated using simple means of Fourier-transform and convolution. See figure 8.
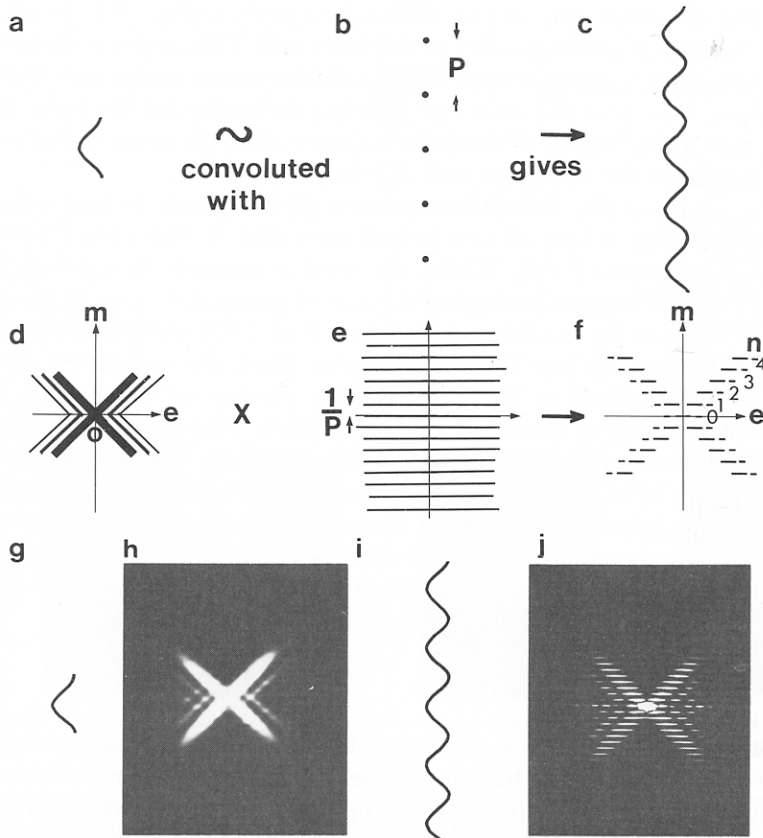


Fig. 8

Muscle proteins, such as actin, troponin, tropomysin and myosin, are configured to form helices. Figure 9 shows a helix in which all the subunits or monomers (black circles) are equivalent. P is the pitch of the helix, R the repeat (the distance from one subunit to the next at the same angular position in the helix) and p is the axial translation of the subunits.
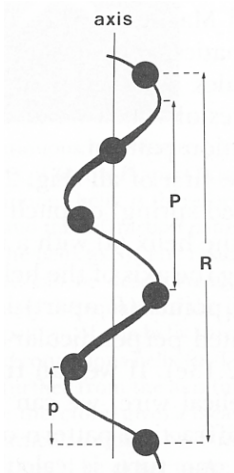


Fig. 9

Helical polymers can be represented by a helical chain of circles. The diffraction pattern of such a discontinuous helix can be deduced as in figure 10.
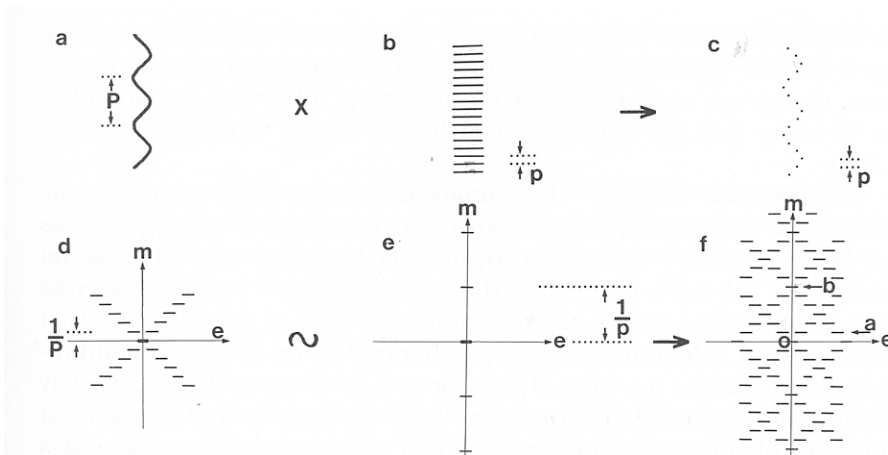


Fig. 10

A discontinuous helix is the product of a continuous one and a set of parallel planes perpendicular to the axis of the helix (a, b, c). The resulting diffraction pattern is shown in (f). The helix cross in (d) is convoluted with an array of dots on the meridian, so that the helix cross repeats itself in a distance proportional to 1/p.

Helices with a nonintegral number of subunits per turn produce a bit more complicated diffraction patterns, as the layer lines in adjacent helix crossed do not coincide. Nevertheless, a lot of information about the discontinuous helix can be gained by analysis of the diffraction pattern.
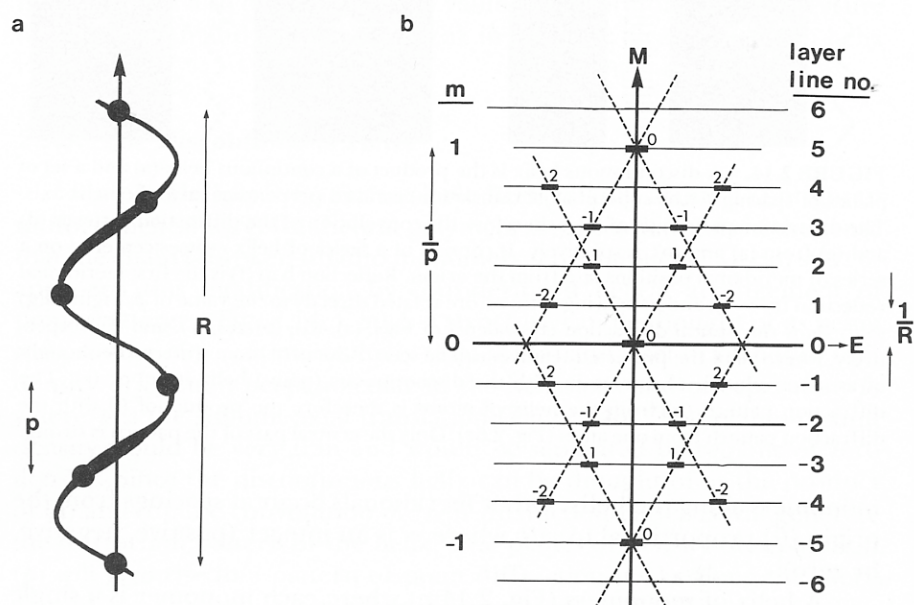
Fig. 11

The repeat of the helical polymer can be calculated from the inverse spacing of the layer lines and the translation of the subunits from the inverse spacing of the first meridional reflection. In this particular example, there are 5 translations per repeat. The ratio of the pitch to the diameter of the helix can be deducted from the angle of the helix crosses.

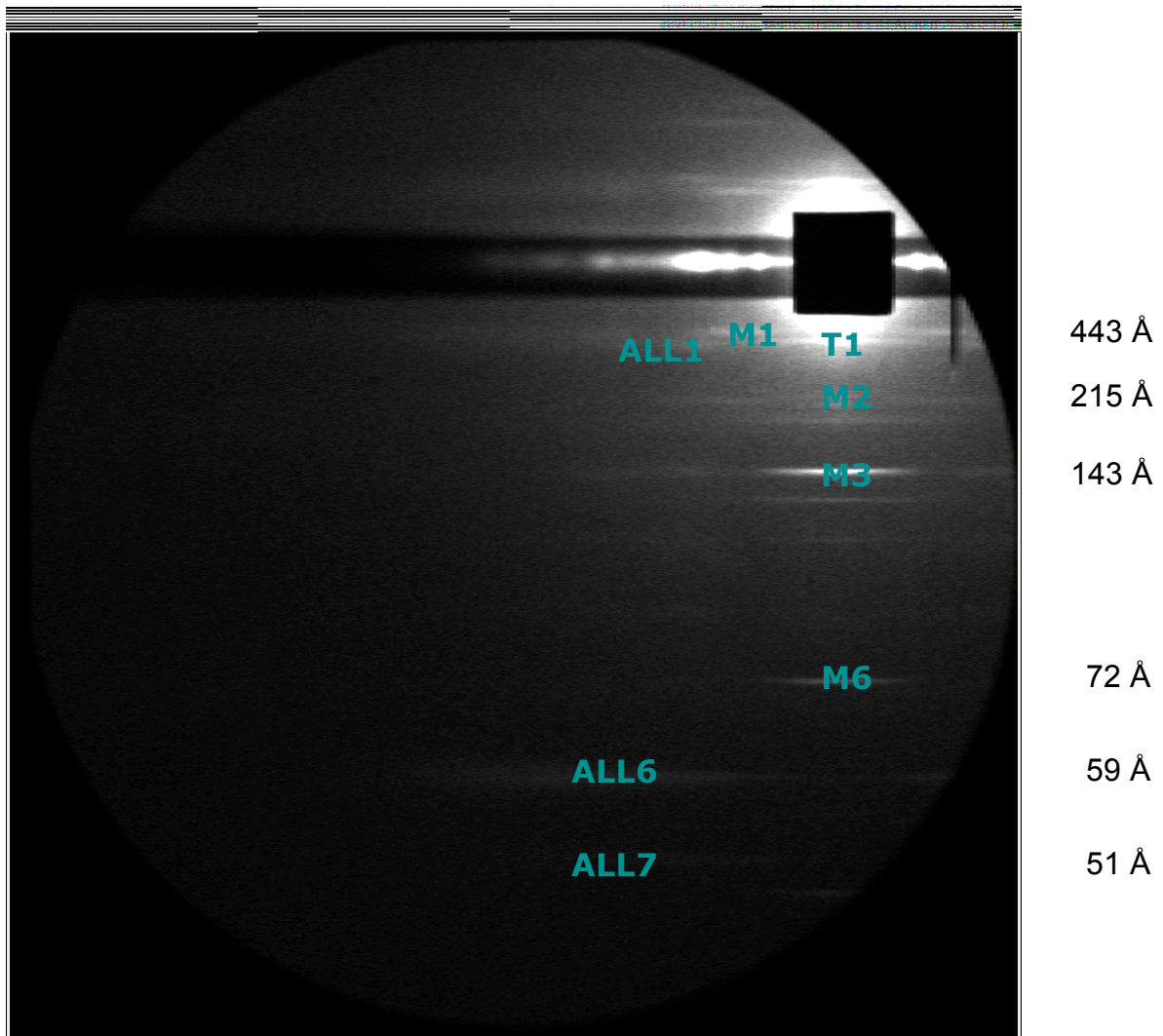So, let's compare the theory to our experimental results.



Fig. 12

The inverse spacing of the meridional reflection of the myosin structure M3 gives the periodicity of the myosin heads (~14,3 nm) on either end of the myosin filament. The intensity of each layer line varies with the degree of order and the sharpness of the corresponding macromolecular structure. From the intensity of M3 conclusions about the occupation of tail-up and tail-down states of the myosin-heads can be made. The intensity of the actin layer lines gives information about the number of occupied binding sites on the actin filament and the resulting disorder of its structure. Surely, a lot of other conclusion can be made, but I don't feel competent enough to comment about them.

Outside sources used for this presentation:
- John Squire, The structural basis of muscular contraction
- Web sites of the ESRF Grenoble, SRS Daresbury and ALS Berkley

Thanks to all the "inside sources"!

# Acknowledgements

My special gratitude goes to Bernhard and Terry who "pulled me back in" to science and persuaded me to finish my PhD in our lab in Hanover. The numerous beamtimes we had in Daresbury and the two in Grenoble were always fascinating and kept my interest awake over all these years. Thanks for giving me this wonderful opportunity to expand my knowledge and experience.



The two photos were taken during our beamtime at the ESRF in Grenoble in April 2003. They show Bernhard and Thomas discussing some technical aspects (left photo) and Terry diligently and joyfully preparing muscle fibers for the experiments (right photo).

I am very thankful to Prof. Walter Müller who took up the task of being my official supervisor and the link from the Medical School to the University of Hanover.

I thank all the past and present members of our lab I had the pleasure to work with and learn from and I congratulate them for having an excellent and friendly collaboration and teamwork. It would take up too much space to mention the names of all the people I am grateful to, but I just want to point out Eva and Birgit who are responsible for the essential work, without which none of this would have been possible.

I am also very obliged to all the friendly and helpful staff members at the beamlines in Daresbury and Grenoble, especially to Thomas Weiss and Bill Helsby who closely collaborated on the project my thesis is based on.

Last but not least, I thank my faithful and hard-working assistant Zdenka Petricko. She kept the business running back in Ulm, while I spent the time going after my scientific pursuit in Hanover.

This project was funded by DFG, EU (Large Facility Program), ESRF Grenoble, and EMBL Grenoble Outstation.

# Curriculum vitae

| | |
|---|---|
| First name | Ante |
| Last name | Radocaj |
| Date of birth | May 18, 1962 |
| Place of birth | Sibenik, Croatia |
| Citizenship | German |
| Address | Helstorfer Str. 2, G 1606, 30625 Hannover, Germany |

**Education**

| | |
|---|---|
| 2003 - present | PhD student, Department of Molecular and Cell Physiology, Hannover Medical School, Germany |
| 1983 - 1989 | Undergraduate and graduate studies in physics, University of Karlsruhe, Germany<br><br>Diploma thesis: Messung und mathematische Beschreibung von Kraftwechselwirkungen bei der Bewegung von Objekten durch eine künstliche Hand, Karlsruhe, 1988. - 194 S.,  Institute for Process Control and Robotics, University of Karlsruhe, Germany |
| 1982 - 1983 | Undergraduate studies in physics, ETH Zurich, Switzerland |
| 1968 - 1981 | Elementary and high school, Germany |

**Professional experience**

| | |
|---|---|
| 1992 - 2003 | Scientific collaboration with the Department of Molecular and Cell Physiology, Hannover Medical School, during beam times at the synchrotrons in Daresbury and Grenoble |
| 1994 - 2003 | Self-employed translator, proprietor of a translation-agency |

**Published papers**

Kraft, T., T. Mattei, A. Radocaj, B. Piep, C. Nocula, M. Furch, and B. Brenner. 2002. Structural features of cross-bridges in isometrically contracting skeletal muscle. Biophys J 82(5):2536-2547.

Lorkovic, H., U. Jäger, and A. Radocaj. 1995. Comparison of the effects of Ca2+ and those of Mg2+ and La3+ on endplate currents in mouse interosseus muscles. Comp Biochem Physiol A Physiol 111(4):597-602.

Lorkovic, H., U. Jäger, and A. Radocaj. 1994. Fast and Slow Desensitization in Mouse Endplate. Periodicum Biologorum 96(1):3-12.

**Published abstracts**

Kraft, T., M. Mattei, C. Nocula, A. Radocaj, M. Furch, D.J. Manstein, and B. Brenner. 1999. Effects of myosin-subfragment-1 and truncated S-1 binding on actin layer-line profiles of single fibers from rabbit psoas. Biophys J 76/1:A34.

Brenner, B., T. Mattei, A. Radocaj, and T. Kraft. 2000. Kinetics and structural properties of cross-bridges during isotonic steady state contraction. Biophys J 78(1):134a.

Brenner, B., R. Stehle, T. Mattei, A. Radocaj, and T. Kraft. 2000. Cross-bridge attachment during isotonic steady state contraction: Kinetic and structural studies. Pflug Arch 439(6):R433.

Kraft, T., T. Mattei, A. Radocaj, and B. Brenner. 2000. Actin layer line profiles of single skinned fibers of rabbit psoas muscle during isometric contraction, relaxation and rigor at 20°C. Biophys J 78(1):228A.

Kraft, T., M. Mattei, A. Radocaj, C. Nocula, and B. Brenner. 2000. 2D-X-ray diffraction on single muscle fibers: a tool for studying the molecular mechanism of muscle contraction. Am. Cryst. Assoc. 27 (2):46.

Kraft, T., M. Mattei, A. Radocaj, C. Nocula, B. Piep, M. Furch, and B. Brenner. 2000. Force generating cross-bridges in isometrically contracting skeletal muscle are structurally different from rigor-like cross-bridges. Pflug Arch 439 (6):R408.

Radocaj, A., T. Weiss, W. Helsby, B. Brenner, and T. Kraft. 2006. Investigation of structural transitions of force generating cross-bridges during ramp-shaped releases using time resolved 2D-X-ray diffraction. Biophys J 90.

Radocaj, A., T. Weiss, W. Helsby, T. Kraft, and B. Brenner. 2006. 2D-X-ray diffraction study of structural properties of force generating cross-bridges during ramp-shaped releases. J Muscle Res Cell Motil 27:485.